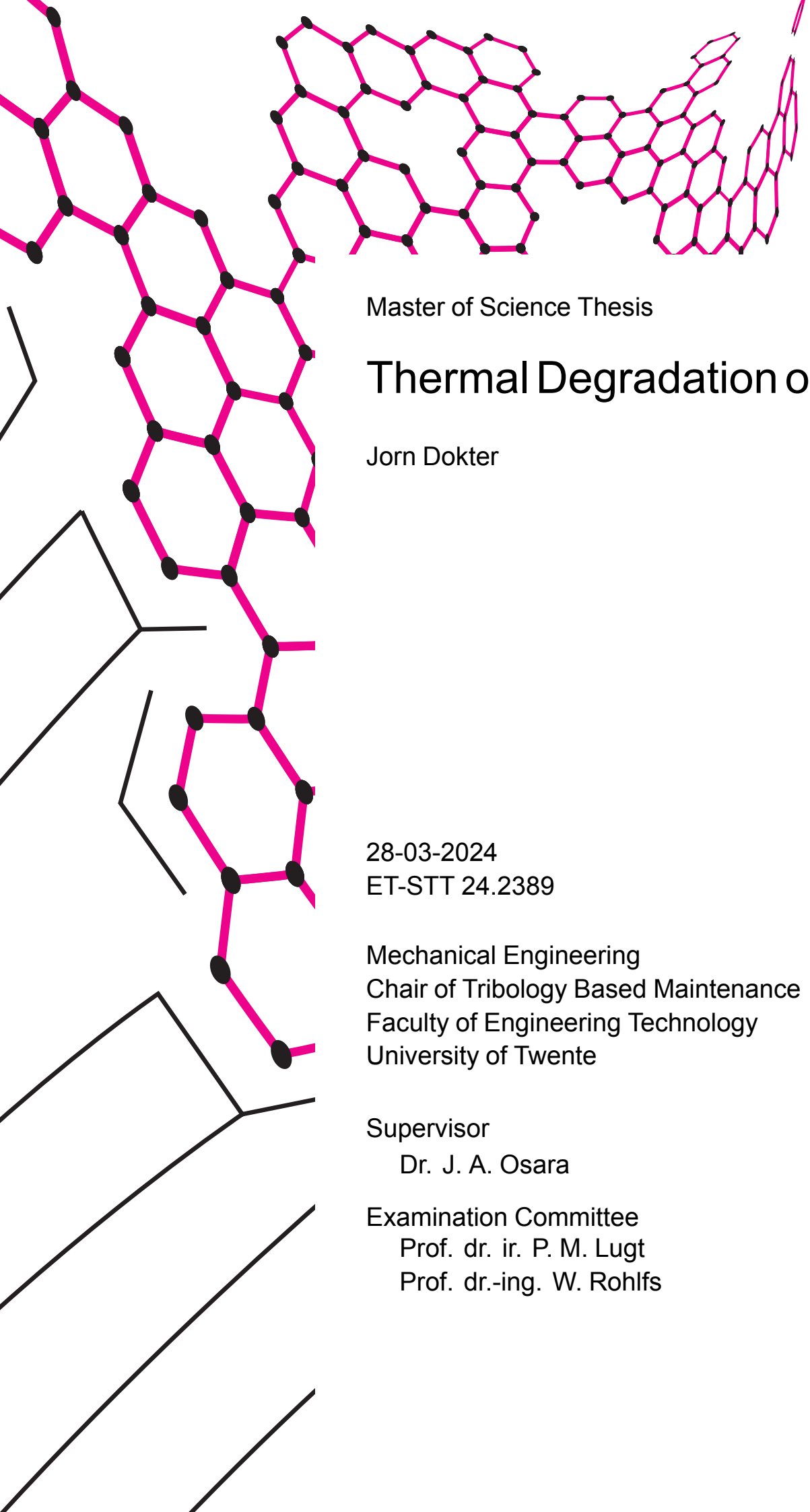

Master of Science Thesis

Thermal Degradation of Grease

Jorn Dokter

28-03-2024
ET-STT 24.2389

Mechanical Engineering
Chair of Tribology Based Maintenance
Faculty of Engineering Technology
University of Twente

Supervisor
Dr. J. A. Osara

Examination Committee
Prof. dr. ir. P. M. Lugt
Prof. dr.-ing. W. Rohlfs

Acknowledgements

I want to thank Jude Osara for his amazing support and enthusiasm as day-to-day supervisor. Furthermore, I want to thank Piet Lugt for his role as supervisor, Norbert Bader for preparing the oven for use and Christopher Balfe for his critical technical support. I lastly want to thank Femke Hogenberk for sharing her expertise on grease.

Abstract

The thermal degradation of lubricating grease is investigated using a temperature-only thermodynamic model. This model is derived from first principles in accordance with existing models to include heat storage, heat transfer and evaporation mechanisms via their respective entropies.

As grease churning in a bearing experiences high amounts of thermal degradation, the thermodynamic model is utilised to characterise the thermal entropy generation. These entropies are then used to define a novel three-phase approach to characterise churning behaviour. These three phases are: the initiation phase, continuation phase and termination phase. The churning measure ϕ is introduced and applied to experimental data, where it was found to be able to quantitatively characterise peak- and plateau-type churning behaviour.

The same temperature-only model is applied to greases thermally aged for 10, 20 and 30 days at 130°C in a nitrogen atmosphere. The greases tested are Li/M (lithium soap/mineral base oil), Li/SS (lithium soap/semi-synthetic base oil) and PU/E (polyurea/synthetic ester base oil). Critical rheological, thermo-physical and mechanical properties are measured on fresh and aged grease samples: bleed capacity measure, heat capacity, storage modulus, thermal strain coefficient and yield stress.

The Degradation-Entropy Generation methods are applied to find degradation coefficients that characterise the thermal degradation with an accuracy of $R^2 > 0.99$. The impacts of all three active thermal mechanisms on the degradation of greases are investigated and quantified. All three mechanisms are shown critical for accurately modelling thermal degradation. The tested greases are ranked in thermal degradation resistance using their degradation coefficients.

CONTENTS

Acknowledgements **1**

Abstract **3**

1 Introduction **7**
1.1 Introduction . . . 7
1.1.1 Degradation mechanisms of grease . . . 7
1.1.1.1 Mechanical degradation . . . 7
1.1.1.2 Chemical degradation . . . 8
1.1.1.3 Thermal degradation . . . 8
1.1.2 Grease degradation during churning . . . 9
1.1.3 Thermodynamic characterisation of grease degradation . . . 9
1.1.4 Modelling grease degradation through Degradation-Entropy Generation . 10
1.1.5 Grease material properties . . . 10
1.2 Research questions . . . 11
1.3 Novelty of research . . . 11
1.4 A review of the Degradation-Entropy Generation theorem . . . 12
1.5 A review of relevant thermodynamics . . . 12
1.6 Outline of thesis . . . 15

2 Theoretical foundation **17**
2.1 Proposed thermodynamic model . . . 17
2.1.1 Energy balance with evaporation . . . 17
2.1.2 The generation of entropy in an open system . . . 19
2.1.3 Application of the Degradation-Entropy Generation (DEG) method . . . 19
2.1.4 Definition of the function . . . 20
2.1.5 Calculation of the degradation coefficients . . . 20

3 Thermal degradation during churning in grease-lubricated bearings **23**
3.1 Introduction . . . 23
3.2 Grease churning in a bearing . . . 23
3.3 Thermodynamic characterisation of grease during churning . . . 24
3.3.1 Thermal model of the churning rig . . . 25
3.3.1.1 Heat storage entropy . . . 25
3.3.1.2 Heat transfer . . . 25
3.3.2 Entropy generation during churning . . . 28
3.3.2.1 Isolation of churning phase from raw temperature data . . . 29
3.3.2.2 Entropy accumulated during churning . . . 29
3.4 Characterisation of churning using a novel three phase approach . . . 31
3.4.1 Quantifying the three phases using the heat storage entropy S_T . . . 31
3.4.2 Cumulative entropy during phases . . . 32
3.5 Churning measure . . . 33

3.5.1 Definition of the churning measure ϕ . . . 33
3.5.2 Upper and lower bound of the churning measure . . . 33
3.5.3 Characterising grease type using ϕ . . . 34
3.6 Applying the churning measure to additional experimental data . . . 34
3.6.1 Calculating the churning measure . . . 35
3.6.2 Grouping all the greases . . . 36

4 Experimental methods — Grease ageing in an oven 39
4.1 Grease samples . . . 39
4.2 Grease properties (used as degradation measures) and their measurements . . . 39
4.2.1 Measuring the latent heat of evaporation of base oil . . . 40
4.2.2 Measuring IR-spectrum . . . 41
4.2.3 Measuring bleed capacity measure . . . 41
4.2.4 Measuring the specific heat capacity . . . 42
4.2.5 Measuring the storage modulus . . . 43
4.2.6 Measuring the thermal strain coefficient . . . 43
4.2.7 Measuring the yield stress . . . 44
4.3 Grease ageing . . . 44
4.3.1 Vacuum oven . . . 44
4.3.2 Sample preparation . . . 45
4.3.3 Ageing intervals and temperature . . . 47

5 Experimental results 49
5.1 Ageing . . . 49
5.1.1 Oven temperature profiles and time intervals . . . 50
5.1.2 Visual inspection of the samples . . . 50
5.1.3 Mass change due to evaporation . . . 51
5.2 Latent heat of evaporation (LHE) of base oil . . . 52
5.3 Oxidation check via IR-spectra . . . 53
5.4 Grease properties/degradation measures . . . 54
5.4.1 Bleed capacity measure d_b . . . 54
5.4.2 Specific heat capacity c . . . 55
5.4.3 Storage modulus G' . . . 55
5.4.4 Thermal strain coefficient α_γ . . . 56
5.4.5 Yield stress τ_y . . . 56

6 Thermal model of grease heating in an oven 57
6.1 Transient material properties . . . 57
6.1.1 Transient specific heat capacity . . . 58
6.1.2 Transient mass and mass change . . . 58
6.2 Heat transfer model . . . 60
6.3 Estimation of grease sample temperature . . . 64
6.3.1 Solution to the transient grease temperature . . . 64
6.3.2 Numerical simulation of the grease temperature . . . 66

7 Grease degradation model 69
7.1 Thermal energy dissipated during ageing . . . 69
7.1.1 Energy by mechanism/source . . . 69
7.1.2 Dissipated energy . . . 70
7.2 Entropy generation during thermal ageing . . . 70
7.2.1 Entropy by mechanism/source . . . 71
7.2.2 Entropy generated . . . 72

7.3 The Degradation-Entropy Generation (DEG) model . . . 73
7.3.1 Degradation impact of active mechanisms: the DEG coefficients . . . 73
7.3.2 Mechanism significance analysis . . . 75
7.3.3 Thermal degradation resistance: Grease ranking . . . 75

8 Summary, conclusions and recommendations **79**
8.1 Thermal degradation of grease . . . 79
8.1.1 During churning in a bearing . . . 79
8.1.2 In an oven: the DEG model . . . 80
8.2 Conclusion . . . 81
8.3 Recommendations . . . 83

References **85**

A Finding the latent heat of grease base oil **89**
A.1 Introduction . . . 89
A.2 Analysis . . . 89
A.2.1 Compensation for changing gas density . . . 89
A.2.2 Non-isothermal evaporation . . . 91

B A comparison of different ways of modelling entropy **93**
B.1 The various ways of calculating system properties . . . 93
B.1.1 Linear interpolation of material properties . . . 93
B.1.2 Non-linear interpolation . . . 94
B.1.3 Thermal resistance . . . 94
B.2 Comparing system properties . . . 96
B.3 Comparing the resulting entropy calculations . . . 96

C Tabulated values **97**

Chapter 1

Introduction

1.1 Introduction

Bearings are some of the most commonly used machine components. Most rolling element bearings are lubricated using grease, making grease one of the most important lubricants in use. Stationary grease is a solid at ambient temperatures. This gives it self-sealing properties, keeps contaminants out and lubricating oil in. Grease releases its lubricating oil slowly (under normal operating conditions), which causes the contacts to run under starved elastohydrodynamic lubrication (EHL) conditions, leading to favourable tribological conditions [1–3].

Grease is often applied as a semi-permanent lubrication solution. This means the bearings often outlive the lubricating grease. The life of the bearing is determined by the grease life. Due to the long life span, infrequent maintenance, and (often) difficulty in accessing the location of grease application, it is often difficult to gauge when fresh grease is needed [1–3]. Research into methods to predict the extent of grease degradation is therefore of particular interest.

Lubricating grease consists of three components: a base lubricating oil, a thickener and additives [1–3]. A common ratio for a general-purpose grease is 85% base oil, 10% thickener and 5% additives and fillers [3]. The thickener creates a fibrous matrix, with voids filled with base oil, contained by Van der Waals and capillary forces [1].

Grease life is typified by three phases: the churning phase, bleed phase and the steady long-term continuous degradation phase [1]. Shear stress, decreasing oil content, high temperatures and chemical reactions (via oxidation) degrade the grease over time, reducing the lubrication effectiveness. This literature study focuses on understanding these mechanisms and characterising the extent of degradation.

1.1.1 Degradation mechanisms of grease

There are three primary grease degradation mechanisms: mechanical, chemical and thermal degradation [4]. Of these three mechanisms, mechanical and chemical degradation are the most intensively studied [1, 5].

At low temperatures, mechanical degradation is considered dominant. At elevated temperatures, chemical and thermal degradation become dominant. Chemical degradation is primarily driven by oxidation. The mechanisms behind thermal degradation — the degradation effects due to elevated temperatures — are not fully understood.

1.1.1.1 Mechanical degradation

Mechanical degradation is defined as the permanent degradation caused by applied forces (shear and over-rolling) by solid boundaries. Grease is a viscoelastic substance [1], so thixotropic effects are not considered mechanical degradation [5]. Mechanical degradation is a relevant

factor whenever greases experience stresses [1,6] and occurs at high rates during the churning phase [7].

A study into greases worked by a Couette ageing machine found two phases of degradation in fresh grease samples [6]. In the first phase, grease deteriorated rapidly as the thickener fibres aligned in the shear direction. The second phase was characterised by slow deterioration as the fibres started to break apart into small fragments.

It was found that mechanical ageing of grease reduced the bleed capability and permeability of grease [8], and decreased its consistency [6, 9]. At lower levels of mechanical degradation, bleed capability did not change, but the grease did experience a reduction in consistency [10].

1.1.1.2 Chemical degradation

Chemical degradation is primarily driven by oxidation of base oil and thickener. To prevent oxidation, most greases have antioxidants as additives. These protect the grease by neutralising free radicals or decomposing reaction products of oxidation into less reactive compounds [1].

Before grease oxidises, it first goes through the induction phase. The induction time is the time it takes to deplete almost all (about 99%) of the antioxidants. During the induction phase, grease properties are not expected to change significantly. The induction time depends on the amount of energy supplied to the grease and the induction time follows first-order kinetics via an Arrhenius relation with temperature [11–14].

The oxidation of grease is often studied in the context of the kinetic model proposed by Naldu et al. [15]. This model describes the oxidation of base oil in three steps: oil oxidises to form low molecular weight (LMW) products or evaporate, LMW products react further into high molecular weight (HMW) products or evaporate, and finally, HMW products react into sludge and varnish compounds.

These reaction pathways are studied further and compiled by Lugt [1]. Four phases are described: initiation phase, propagation phase, chain branching phase and termination phase. As the name suggests, the initiation phase starts the cascade of reactions and the products resulting from this phase are critical to continue the oxidation reactions.

The initiation phase can be induced by heat, exposure to ultraviolet light, hydroxy radicals or catalysing metal ions. This phase creates hydroperoxide groups that decompose to fuel the other oxidation reactions. At temperatures below 100°C, these hydroperoxide groups are stable and little oxidation occurs. Thickeners such as metal soaps or polyurea also oxidise, resulting in ketones, acids or polymerised HMW products [1].

The results of these oxidation reactions are reduced equilibrium film thickness and re-flow ability [16, 17], loss of mechanical stability, oil retention and changes in storage modulus and loss modulus [1].

1.1.1.3 Thermal degradation

Thermal degradation is considered to be the degradation of grease due to elevated temperatures. This does not include the effects of chemical degradation and concerns the temperature-only effects. The effects of temperature alone are not extensively studied, as neither the widely referenced book on grease lubrication by Lugt [1] and the literature review on grease degradation by Rezasoltani and Khonsari [5] detail its effects. Yet, grease experiences very high temperatures during its churning phase [7] and some greases are used in high-temperature applications.

A possible reason thermal degradation is rarely studied is because it is dominant in the same temperature ranges as chemical degradation when in the presence of oxygen. To empirically study the sole effect of high temperatures, grease should be aged in an oxygen-free environment. There are few studies into the effects of temperature alone on the degradation of grease,

though steps were made by Osara and Bryant [18] to characterise grease degradation using only thermal entropies.

The rheological properties of grease depend on temperature: at higher temperatures, the yield stress, storage modulus (G') and loss modulus (G") rapidly decrease and grease starts to exhibit flow behaviour [19, 20].

Keeping grease at elevated temperatures for long time spans results in permanent changes in its material properties. High temperature changes the storage modulus, loss modulus and yield stress [20–22]. High temperatures cause the fibrous microstructure to break down, with the severity increased at higher temperatures. High temperatures also reduce the ability to recover from stress [20] and increases evaporation [15, 23]. Evaporation is less significant however when the bearings are well sealed.

1.1.2 Grease degradation during churning

At the start of bearing operation, the grease churns in the bearing between the rolling elements, cages and rings. In Sections 1.1.1.1 and 1.1.1.3, the high stresses and temperatures that are experienced during the churning phase are briefly mentioned. These temperatures can reach up to 130°C and these temperatures can remain for several hours, depending on experimental conditions [7]. The extent of these stresses and temperatures during churning are partially characteristic for each grease, as is the length of the churning phase [7]. These notable conditions point to high rates of mechanical and thermal degradation, as well as oxidation.

Chatra and Lugt [7] identified two types of greases based on churning behaviour: peak and plateau-type greases. Peak-type greases experience high temperatures and stresses for only a short time (i.e. they peak) and plateau-type greases maintain high temperatures and stresses for a longer time (i.e., they plateau).

The churning phase depends on some amount of critical energy that must be supplied to finish churning, after which the churning phase ends. This critical energy was found to depend highly on churning conditions like grease type and rotation speed during churning [24].

Chatra [24] further indicated that whether a grease is a peak or plateau type is determined by its microstructural flexibility. This is the ability of the grease to redirect its fibres along the shear direction without significant breakage. This effect was also observed by Zhou et al. [6] when studying mechanical degradation. The extent of degradation is higher in the swept area (the region through which the rolling elements move) than in the unswept area. However, as the swept area is clear, the degraded grease mixes with less degraded grease in the unswept area, resulting in a more homogeneous mixture [25].

Peak-type greases were found to have less fragmentation of fibres than plateau types. Peak-type greases also experienced negligible changes in yield stress, while plateau types showed a significant reduction in yield stress [7, 24]. Bleed capacity increases for both grease types at the start of churning and after some time, reduces. Peak types maintain a higher bleed capacity after churning than plateau types [26]. This indicates a higher amount of degradation during churning for plateau types compared to peak types. Chatra et al also correlated energy dissipated in the grease with grease life using actual bearing tests. They found that the peak-type greases with lower energy dissipation had longer lives.

1.1.3 Thermodynamic characterisation of grease degradation

The effects of degradation on grease are most often understood through varying empirical tests. Mechanical degradation is studied using shear ageing machines, such as the Couette ageing test rig [6, 22] or the grease worker [10, 27]. For more severe mechanical degradation, the roll stability test can be used to age grease [24, 28]. More true-to-application test conditions are produced by the R0F+ test rig, which tests the grease in bearings, with adjustable axial and

radial load [7, 26], often at elevated temperatures to accelerate degradation. This method offers more controlled test conditions than in situ degradation studied by Lundberg and Höglund, who retrieved grease samples from rolling stock over a span of three years [29]. Chemical and thermal degradation are often studied by heating grease in a chamber, in either oxygen-rich or oxygen-starved environments, respectively [20–22].

In many of these degradation studies, energy put into the grease, either by heat or work, is used as the driving mechanism in degradation. Zhou et al. [6] used single-variable entropy generated (via mechanical shearing) to describe the reduction in viscosity. The grease worker by Meijer and Lugt [27] allows characterisation via either entropy or energy expended. Chatra et al. used energy to characterise the changes in tackiness and bleed rate [28] and the change in yield stress [24] during churning. Rezasoltani and Khonsari [13] used energy to investigate the induction time of grease.

Early works by Kuhn suggested a relation between rheological energy density and grease degradation [30] and later described the maximum degradation of grease as the maximum amount of energy that can be applied to the grease [31]. This was later described as a relation between changes in grease properties during degradation to the apparent rheological frictional energy density. Kuhn's rheological energy density is the ratio of applied friction energy to grease volume [32, 33]. Kuhn also proposed using the energy needed to reach a crossover point as a measure of mechanical degradation [34].

This approach was applied in a number of subsequent works. Acar et al. [35] related shear-induced degradation to activation energy, via critical deformation, as well as the point where grease starts to flow. Ahme et al. [36] similarly related the amount of work put into grease to the shear needed to reach flow behaviour. Akchurin [8] described the relation of the mechanical shear degradation of grease to bleed, where the friction energy density was used to generate a master curve.

1.1.4 Modelling grease degradation through Degradation-Entropy Generation

Of the many thermodynamic approaches to grease degradation, the most structured and accurate approach is the DEG method by Osara and Bryant [4].

The original DEG theorem was proposed by Bryant et al. [37], describing degradation via irreversible entropy generations due to active concurrent dissipative processes. The entropy generated within a system, described by the laws of thermodynamics, impacts a degradation measure. This measure could be a system property that represents its performance.

The DEG method has been successfully applied to various mechanisms and systems such as frictional wear, metal fatigue, and capacity fade of batteries [18, 38, 39]. Applying the DEG method to grease degradation has been very successful. Using DEG, cumulative shear stress was modelled as a function of shear and microstructural temperature [4] and as a function of grease temperature [18]. The induction time of grease has been modelled using reaction rates in a pressure differential scanning calorimeter [14]. The DEG methods have been able to describe these degradation mechanisms with near-perfect accuracy. Kuhn reinforced their energy density method, showing the similarity between energy density and entropy supply [34], and describing grease structural breakdown using entropy [40].

This accuracy, combined with the structured approach of the methodology and flexibility to describe degradation using the laws of thermodynamics, make this a promising way of describing grease degradation.

1.1.5 Grease material properties

To study grease degradation, many state-defining measures are used to characterise the extent of degradation. Many have already been mentioned. In addition, some important properties

of grease have been described using first principles of thermodynamics [41]. The mentioned degradation measures are:

1. Yield stress [20].
2. Viscosity [6, 42].
3. Consistency [9, 43].
4. Bleed rate/bleed capacity [8, 10].
5. Storage modulus [20, 21, 41].
6. Dynamic modulus [20, 21].
7. Heat capacity [41].
8. Thermal strain coefficient [41].
9. Thermal stress coefficient [41].
10. Chemical resistance [41].
11. Thermal decay coefficient [41].

A few of the above properties will be tested during the course of this investigation.

1.2 Research questions

Considering the literature on grease degradation, it becomes clear that thermal degradation is the least studied of the three grease degradation mechanisms. It is also found that thermal degradation plays an important role during the churning of grease in bearings.

Therefore, the following research questions are formulated to expand the knowledge on the thermal degradation of lubricating grease:

1. *What are the effects of thermal degradation, induced by temperature only, on grease thermo-physical and rheological properties such as specific heat capacity, thermal strain coefficients, bleed capacity, yield stress and storage modulus?*
   (a) *What are the effects of these properties on the thermal degradation resistance of grease?*
   (b) *How significant is evaporation in the thermal degradation of grease?*
2. *What are the effects of the peak and plateau temperature rise profiles on the degradation of grease during the churning phase?*
   (a) *Can temperature-only thermal degradation be used to characterise grease behaviour during churning?*
   (b) *What is the contribution of thermal degradation to the total degradation of grease during churning?*

1.3 Novelty of research

The degradation of grease via temperature only is not extensively studied. Osara and Bryant [18] showed that grease degradation due to temperature only can effectively be characterised by the DEG method. Their study only investigated one type of grease and used shear stress as the degradation measure. The heat, which resulted in the elevated temperatures, in that work was generated by mechanical shearing of the grease, which most likely also contributed to the measured degradation. The novelty this research includes:

- Characterising the churning of grease lubricated bearings using thermal entropies and using these thermal entropies to identify churning behaviour.

- Furthering the understanding of temperature-induced degradation by heating more samples of different greases in an oven in the absence of oxygen, while allowing evaporation to take place, and measuring the resulting degradation.
- Characterising grease degradation due to thermal mechanisms only by applying the Degradation-Entropy Generation theorem and using the results to provide insight into the thermal degradation resistance of various greases.

By measuring changes in the grease material properties [41], a novel way of describing degradation can be found. Because these material properties are based on thermodynamic principles, they are directly connected to the entropy generation of the DEG method. To characterise temperature-only degradation, the heat capacity, strain coefficient, yield stress and storage modulus will be investigated, before and after oven heating in the absence of oxygen and boundary work, while allowing evaporation to take place.

1.4 A review of the Degradation-Entropy Generation theorem

Bryant et al. [37] proposed a theorem to describe degradation using a thermodynamic characterisation of the system. This method correlates the entropy generation to changing (or degrading) properties of the system. The degradation is driven by irreversible dissipative processes, an example being the frictional wear of a contacting surface in relative motion.

Before applying the DEG methods, the definition of this method is recalled. Bryant et al. [37] defines:

- A *dissipative degradation process*, denoted by p_i, as the minimum group of dissipative sub-processes for which some non-negative amount of entropy is generated, i.e. $\dot{S}' \geq 0$.
- A *degradation mechanism* as a group of one or more *dissipative degradation processes* (p_i) that degrades a system.
- A *degradation measure*, denoted by $w = w\{p_i\}$, as a non-negative, non-decreasing continuous function, differentiable in one or more of its processes p_i, associated with a *degradation mechanism*.

These definitions are slightly paraphrased. Because the dissipative processes drive both the change in the degradation measure, according to $w = w\{p_i(\zeta_i^j)\}$, and the entropy, according to $S' = S'\{p_i(\zeta_i^j)\}$, Bryant et al. [37] found that entropy generation can be directly related to the degradation measures. Here, ζ_i^j are phenomenological variables, i numbers active processes and j numbers variables per process. This relation is as follows:

$$\dot{w}_i = B_i \dot{S}'_i, \qquad B_i = \frac{\partial w_i}{\partial S'_i} \tag{1.1}$$

This shows the change in a degradation measure to be proportional to the generated entropy, scaled by the degradation coefficient B_i. This coefficient represents how much a dissipative process contributes to the change of a degradation measure.

1.5 A review of relevant thermodynamics

The degradation of grease will be characterised using the DEG method. Therefore, the entropy generation of the active process the grease undergoes must be characterised. Using a characteristic/representative entropy generation is critical to the success and accuracy of the DEG methods, hence a first principles approach is considered here in enumerating existing models

for describing grease degradation. These models will facilitate the choice of the optimum model to be used.

Two works by Osara and Bryant [4, 39] and one by Osara et al. [41] utilise the Helmholtz free energy for thermodynamic characterisation, which is commonly interpreted as the "maximum work" available in a system. This is a logical entry point for wanting to know how degraded a system is: a low Helmholtz energy could suggest very degraded systems, as little useful work can be extracted from it (though a low Helmholtz energy is not exclusive to degraded systems). The Helmholtz fundamental relation is:

$$dF = -SdT - V\tau d\gamma + \frac{\mu}{M}dm. \tag{1.2}$$

Here, S is entropy, T is temperature, V is volume, τ is shear stress, γ is shear strain, μ is the chemical potential, M is molecular weight and m is mass.

$-SdT$ is termed micro-structuro-thermal (MST) energy. Shear stress and strain were conjugated to give the boundary work as $V\tau d\gamma$. Including the chemical processes $\mu dm/M$, this showed a relation for the change of Helmholtz potential when grease experiences energy changes. Including the entropy balance which introduces entropy generation and replaces the Clausius inequality, the expression for Helmholtz-based entropy generation was given as [4, 39, 41]

$$\delta S' = -\frac{SdT}{T} - \frac{V\tau d\gamma}{T} - \frac{\mu dm}{MT} - \frac{dF''}{T}, \tag{1.3}$$

where dF'' is the reversible Helmholtz energy. This model has been applied to grease degradation [4] and metal fatigue characterisation [39] in conjunction with the DEG theorem.

To model grease oxidation, Osara et al. [14] derived an enthalpy-based entropy generation as

$$\delta S' = \frac{TdS}{T} - \frac{Vdp}{T} - \frac{\sum_i \mu_i dN_i}{T} - \frac{dH''}{T}. \tag{1.4}$$

where H'' is the reversible enthalpy, S is entropy, T is temperature, V is volume, p is pressure, μ is chemical potential and N is the amount of active species.

Chatra et al. [26] investigated churning, which can be considered a process where mechanical and thermal degradation are present. Their work considered the total energy in the grease after the churning phase, to be the Helmholtz free energy density:

$$F_V(t) = -\int_0^t S_V \dot{T}\, dt' + \int_0^t \dot{W}_V\, dt', \tag{1.5}$$

where the first right-hand term is the MST energy and the second term is the work applied to the system. Both terms are density normalised. When these terms are difficult to determine, it is proposed that heat transfer entropy density might be enough to characterise degradation. This is equal to

$$S_{QV}(t) = \frac{1}{V}\int_0^t \frac{T - T_\infty}{TR_\theta}\, dt' \tag{1.6}$$

where R_θ is the equivalent thermal resistance. Another notable characterisation by Osara et al. [41] also employs the Helmholtz free energy to derive grease material properties. It formulates the Helmholtz energy total differential as a sum of partial differentials of the intensive variables:

$$dF = \frac{\partial F}{\partial T}dT + \frac{\partial F}{\partial \gamma}d\gamma + \frac{\partial F}{\partial N}dN \tag{1.7}$$

noting, via comparison with Equation 1.2, that

$$\left(\frac{\partial F}{\partial T}\right)_{\gamma,N} = -S, \qquad \left(\frac{\partial F}{\partial \gamma}\right)_{T,N} = -V\tau, \qquad \left(\frac{\partial F}{\partial N}\right)_{T,\gamma} = \mu. \tag{1.8}$$

This work showed a direct connection between important grease properties and the fundamental relations governing thermodynamic transformations. Helmholtz "free entropy" content, necessary to evaluate the MST energy (first right-hand side term in Equation 1.2), was given as

$$S = \underbrace{C \ln \frac{T}{T_0}}_{\text{thermal}} + \underbrace{V \alpha_\gamma G' \gamma}_{\text{thermo-mechanical}} - \underbrace{\lambda (N - N_0)}_{\text{chemical}} \tag{1.9}$$

introducing grease material properties: heat capacity C, thermal strain coefficient α_γ, the storage modulus G' and thermo-oxidation coefficient λ into the final entropy generation model.

Oftentimes, the mechanical load on a system can be difficult to evaluate/measure. For such cases, Osara and Bryant [18] formulated thermal entropy generation using the measured temperature profile only. This model combined the thermal energy balance with the second law's entropy balance to characterise temperature-only degradation of batteries, dynamically loaded structures (fatigue) and lubricating grease. For each of these systems, the generated entropy density was found to be

$$S'_V = \int_0^t \frac{\rho c \dot{T}}{T} dt - \frac{1}{V} \int_0^t \frac{T - T_\infty}{T R_\theta} \, dt. \tag{1.10}$$

The first term represents the heat storage density, where the heat capacity decomposes to $C/V = \rho c$. This directly links entropy generation to the temperature of the system, as the heat flux is $\dot{Q} = (T_\infty - T)/R_\theta$. The primary difference between this model and the earlier mentioned Helmholtz free energy based models (Equations 1.2 and 1.5) is that the latter includes, via Equation 1.9, other non-thermal material properties whereas the former (Equation 1.10) only includes the specific heat capacity.

Chatra et al. [26] investigated grease churning in a bearing, a process where mechanical and thermal degradation are present. Their work considered the total energy in the grease after the churning phase, to be the Helmholtz energy:

$$F_V(t) = -\int_0^t S_V \dot{T} \, dt' + \int_0^t \dot{W}_V \, dt', \tag{1.11}$$

which is simply the rate form of Equation 1.2, without change in composition ($dm = 0$) and the boundary work is represented by W_V. Again, here, the first right-hand term is the MST energy rate and the second term is the mechanical shear power applied to the system. Both terms were density normalised. The shear power imposed on the grease in a bearing is difficult to determine, so the authors proposed the use of heat transfer entropy density to characterise degradation (based on the above temperature-only model by Osara and Bryant [18] which showed a direct dependence of heat transfer entropy on the mechanical work entropy). The heat transfer entropy density, the second RHS term in Equation 1.10 was used, re-stated here as

$$S_{QV}(t) = \frac{1}{V} \int_0^t \frac{T - T_\infty}{T R_\theta} \, dt'. \tag{1.12}$$

A consistent correlation between grease life and S_{QV} was observed.

When regarding the various models that were found in literature, one distinction can be noted: for systems that experience boundary (external) work, Helmholtz free energy is often used. When heat transfer and chemical changes (e.g., oxidation) are involved, enthalpy is considered appropriate. For temperature-only transformations, the thermal energy/entropy balance is adequate.

In the current study into thermal degradation only, the temperature-only model presented by Osara and Bryant [18], shown in Equation 1.10, seems most appropriate. To also take evaporation into account, that model must be extended. To ensure consistency and robustness, the newly proposed model (which includes evaporation) will be derived from first principles. As mass changes over time, the entropy will not be volume corrected. The new model will be created with the derivation by Osara and Bryant [18] in mind.

1.6 Outline of thesis

In this thesis,

- Chapter 1 introduces the research problem, background and research questions;
- Chapter 2 derives the theoretical model to be used in quantifying grease degradation;
- Chapter 3 characterises the thermal mechanisms during grease churning in a bearing;
- Chapter 4 details the experimental methods;
- Chapter 5 presents the experimental results;
- Chapter 6 develops a thermal model for oven heating needed to determine grease temperature and other relevant parameters;
- Chapter 7 presents the detailed characterisation and quantification of thermal degradation of greases;
- Chapter 8 summarises the findings, answers the research questions, concludes and recommends future work.

Chapter 2

Theoretical foundation

2.1 Proposed thermodynamic model

The above models have primarily been applied to closed systems or consider an open system experiencing oxidation. The current study is limited to temperature-only degradation, without oxidation. Here, a semi-open system model is presented to enable inclusion of the thermal process of evaporation which is prevalent in open bearings, gears and other applications without seals, and is strongly driven by temperature.

2.1.1 Energy balance with evaporation

Consider the first law of thermodynamics for an open system [44]:

$$dU = TdS - \delta W + \sum_i \mu_i dN_i, \tag{2.1}$$

where δW is the work done by the system on the surroundings. This includes pressure-volume work, stress-strain work, and other work interactions. However, this investigation is limited to temperature-only thermodynamics, so the work done is neglected.

Furthermore, the system is assumed non-reactive. It will only experience evaporation, meaning the potential μ is equal to the enthalpy of evaporation L, also known as the latent heat of evaporation. Strictly speaking, base oil commonly consists of a cocktail of various hydrocarbons and volatile compounds. However, for simplicity, L will be seen as the latent heat of evaporation of the mixture.

With these considerations, the first law reduces to

$$dU = TdS + Ldm. \tag{2.2}$$

where the system mass $m = N/M$, with N as the number of moles of active species and M the molar mass. For a real (irreversible), closed system, the second law's entropy balance is

$$TdS = \delta Q + T\delta S'. \tag{2.3}$$

By regarding the evaporation as a compositional change, Equation 2.3 can be substituted into Equation 2.2 to obtain

$$dU = \delta Q + Ldm + T\delta S'. \tag{2.4}$$

where the last term represents energy dissipated in the grease. For a temperature-only system, the heat capacity [45, 46] for isochoric processes is

$$C_V = \left(\frac{\partial U}{\partial T}\right)_{V,N}, \tag{2.5}$$

where for solids $C_V \approx C_p$ and it is expected that the evaporation of base oil and volatiles change the grease volume by a negligible amount. For simplicity, the heat capacity will be denoted with $C = cm$, where c is the specific heat capacity and m is the system mass. Taking the integral with respect to temperature,

$$dU = cm\,dT \tag{2.6}$$

and substitution into Equation 2.4 yields

$$cm\,dT = \delta Q + L dm + T\delta S'. \tag{2.7}$$

Via the IUPAC convention of positive energy into a system, the heat flux is positive into the system (which in this study is the grease), assuming the system's temperature is lower than its environment (or heat source), i.e., $T < T_\infty$. The rate of heat flux can be calculated using the general thermal resistance R_θ network:

$$\dot{Q} = \frac{T_\infty - T}{R_\theta}. \tag{2.8}$$

The mass balance gives the rate of change of mass in a control volume as

$$\frac{dm}{dt} = \dot{m}_{in} - \dot{m}_{ex}, \tag{2.9}$$

where $\dot{m}_{in}$ is mass flow rate in and $\dot{m}_{ex}$ is mass flow out. In the case of evaporation, $\dot{m}_{in} = 0$ yielding $\dot{m} = -\dot{m}_{ex}$. Dropping the "ex" subscript and substituting Equations 2.8 and 2.9 into Equation 2.7 yields, in rate form,

$$cm\dot{T} = \frac{T_\infty - T}{R_\theta} - L\dot{m} + T\dot{S}'. \tag{2.10}$$

Similar to the heat flux term (Equation 2.8), the other energy terms will be categorised by their mechanisms. The internal energy rate of the system due only to the changes in temperature, positive for an increase in temperature only, known as the heat storage rate, is

$$\dot{E}_T = cm\dot{T}. \tag{2.11}$$

The energy change rate due to loss of matter via evaporation is:

$$\dot{E}_m = L\dot{m} \tag{2.12}$$

and the energy dissipation rate is

$$\dot{E}_d = T\dot{S}'. \tag{2.13}$$

By rearranging,

$$\dot{Q} = \dot{E}_T + \dot{E}_m - \dot{E}_d \tag{2.14}$$

is obtained, showing how heat flowing across the system boundary leads to a temperature rise of the system, the evaporation of volatile components and dissipation (loss) of energy. While the other mechanisms are measurable, energy dissipation cannot be directly measured but can be obtained from the other energy terms, after integrating with respect to time as

$$E_d = E_T + E_m - Q. \tag{2.15}$$

2.1.2 The generation of entropy in an open system

The entropy generation, like energy dissipation, cannot be directly measured but is obtainable from measurements of the other active mechanisms. Rearranging equation 2.10, entropy generation rate is:

$$\dot{S}' = \frac{cm}{T}\dot{T} - \frac{T_\infty - T}{TR_\theta} + \frac{L}{T}\dot{m}. \tag{2.16}$$

The rate of total entropy generated is a linear combination of three distinguishable mechanisms. These are heat storage entropy rate $\dot{S}_T$, heat transfer entropy rate $\dot{S}_Q$ and evaporation entropy rate $\dot{S}_m$:

$$\dot{S}_T = \frac{cm}{T}\dot{T}, \qquad \dot{S}_Q = \frac{T_\infty - T}{TR_\theta}, \qquad \dot{S}_m = \frac{L}{T}\dot{m} \tag{2.17}$$

With the rearrangement that yielded Equation 2.16, $\dot{S}_Q$ is negative for heat transfer into the grease. So, the total entropy generation rate becomes

$$\dot{S}' = \dot{S}_T - \dot{S}_Q + \dot{S}_m. \tag{2.18}$$

Then, the accumulated entropy generation can be obtained by integrating this expression with respect to time. The bounds of interest are from the reference state at $t = 0$ to some arbitrary time t. At the reference state, each entropy source is zero. The total entropy generated is the time integral of the entropy generation rate:

$$S'(t) = \int_0^t \dot{S}'\, dt \tag{2.19}$$

where $S'(0) = 0$. The accumulated entropy contributions from each source is then as follows: the accumulated entropy contribution via heat storage is

$$S_T(t) = \int_0^t \frac{cm}{T}\dot{T}\, dt, \tag{2.20}$$

the accumulated heat flux entropy is

$$S_Q(t) = \int_0^t \frac{T_\infty - T}{TR_\theta}\, dt, \tag{2.21}$$

and the accumulated evaporation entropy is

$$S_m(t) = \int_0^t \frac{L}{T}\dot{m}\, dt. \tag{2.22}$$

Finally, the total entropy generated at some arbitrary time t is

$$S'(t) = S_T(t) - S_Q(t) + S_m(t) \geq 0 \tag{2.23}$$

where the inequality indicates a universally non-negative entropy generation in accordance with the second law. Equation 2.23 is the entropy generation model used in this study.

2.1.3 Application of the DEG method

The DEG method described in Section 1.4 will be applied here. For the temperature-only characterisation these processes are: heat storage (T), heat transfer (Q) and evaporation (m). This means the processes are

$$p_i = \{p_T, p_Q, p_m\}. \tag{2.24}$$

Each of these processes is a function of one or more phenomenological variables $\zeta_i^j(t)$ which depend on time. These phenomenological variables are

$$\zeta_i^j(t) = \begin{cases} \{c, m, T, \dot{T}\} & i = T \\ \{T, T_\infty, R_\theta\} & i = Q \\ \{L, T, \dot{m}\} & i = m \end{cases} \tag{2.25}$$

which are the driving forces behind the dissipative processes.

2.1.4 Definition of the function

The DEG method relates the rate of change of a degradation measure to the rate of entropy generation:

$$\dot{w} = \sum_i B_i \dot{S}_i'. \tag{2.26}$$

Notation is shortened using the Einstein summation convention:

$$\dot{w} = B_i \dot{S}_i' \tag{2.27}$$

The current (degraded) value of the degradation measure can be found at time t by integrating the expression with respect to time:

$$\int_0^t \dot{w}\, dt = \int_0^t B_i \dot{S}_i'\, dt. \tag{2.28}$$

Time $t = 0$ is considered to be the reference state. For the application discussed here, the reference state is the conditions of the fresh grease. Therefore, it is defined that $w(0) = w_0$ and $S_i'(0) = 0$. Resolving the integral then yields

$$w(t) - w_0 = B_i S_i'(t). \tag{2.29}$$

One can bring w_0 to the right hand side to find

$$w(t) = B_i S_i'(t) + w_0, \tag{2.30}$$

the value of a degradation measure at any time $t \geq 0$. By considering that both the degradation measure and entropy generated are functions of time,

$$w(S_i') = B_i S_i' + w_0 \tag{2.31}$$

shows that the degradation measure can be found as a function of the generated entropy. Next, expanding Equation 2.31 by introducing the various degradation processes ($i = \{T, Q, m\}$) yields

$$w(S_T, S_Q, S_m) = B_T S_T + B_Q(-S_Q) + B_m S_m + w_0. \tag{2.32}$$

2.1.5 Calculation of the degradation coefficients

Equation 2.32 can be rewritten in matrix form. The index k, is used to denote the number of points for which the degradation measure is recorded, for a non-zero amount of entropy generated. Each of the k points then also has some generated entropy associated with it. This allows Equation 2.32, after bringing w_0 to the left-hand side, to be written in the following form:

$$(w_k - w_0 I_{k\times 1}) = S_{ki} B_i. \tag{2.33}$$

where $w_k - w_0 I_{k\times 1}$ means w_0 is subtracted from each measurement point w_k. Interestingly, for the case that the number of ageing intervals k is equal to the number of dissipative processes i, the entropy matrix is square. The degradation coefficients can then be found by

$$B_i = S_{ki}^{-1}(w_k - w_0 I_{k\times 1}). \tag{2.34}$$

This yields an exact solution for the coefficients. This leads to the proposition that for the best results of finding the degradation coefficients, the number of ageing intervals should be equal to or greater than the number of dissipative processes.

For the current system-process interaction — lubricating grease undergoing thermal degradation — there are three active processes: heat storage, heat transfer and evaporation, i.e., $i = \{T, Q, m\}$. Three ageing intervals are used in the oven experiments: 10 days, 20 days and 30 days, meaning $k = \{10, 20, 30\}$. The matrix system then becomes:

$$\begin{bmatrix} \Delta w_{10} \\ \Delta w_{20} \\ \Delta w_{30} \end{bmatrix} = \begin{bmatrix} S_{T10} & -S_{Q10} & S_{m10} \\ S_{T20} & -S_{Q20} & S_{m20} \\ S_{T30} & -S_{Q30} & S_{m30} \end{bmatrix} \begin{bmatrix} B_T \\ B_Q \\ B_m \end{bmatrix}. \tag{2.35}$$

Computing the inverse matrix according to Equation 2.34 will yield the degradation coefficients.

Chapter 3

Thermal degradation during churning in grease-lubricated bearings

3.1 Introduction

Section 1.1.2 already discussed the literature regarding the churning of grease in a bearing. It was noted that churning in grease lubricated bearings induces high temperatures, typically between 120°C and 150°C [7]. These temperatures, close to the dropping point of some greases, are accompanied by significant thermal degradation.

The thermodynamic model derived in Section 2.1.2 is applied here. Similar to the temperature-only approach by Osara and Bryant [18], the temperature behaviour can be correlated to the mechanical degradation. Applying the derived model might provide some interesting insights into the churning characteristics of greases in bearings.

This chapter will expatiate on churning, attempting to quantify this process using the entropy generation equations applied to the data provided by the authors of these studies, first presented by Chatra and Lugt [7]. This investigation into churning warrants a deeper look into the literature regarding the churning process, test setup and specifics of the models.

3.2 Grease churning in a bearing

Commonly, sealed-for-life-bearings are filled to 30%–40% of their free volume, where almost all grease is located in the un-swept area (as grease reservoirs) for the majority of its lifetime. When the bearings are filled for the first time, grease will end up in the raceways and in between the ball bearings. As the bearing starts to rotate, grease starts to re-distribute. Grease will be pushed sideways into the un-swept area, also known as channeling or clearing. Grease ending up in the un-swept area will form lubrication reservoirs. Some grease will have nowhere to go and will be pushed against the bearing seals or into grease located in the un-swept area, and therefore end up back on the raceway. The combination of this flow behaviour is called churning. Churning is typified by high viscous drag forces, resulting in high shear stresses and high temperatures [7, 24, 25, 28].

Studying the churning behaviour yielded two primary categories: peak-type greases and plateau-type greases [7]. The former is characterised by a short peak in temperature, while the latter is characterised by a sustained high temperature. The high temperature and shear mean a high rate of degradation, therefore greases that have a short churning period degrade to a lesser extent than greases that churn for a long time [7].

Chatra et al. [7] performed bearing tests using the R0F+ test rig [1], see Figure 3.1. This test rig has two test bearings and two support bearings placed on a common driven shaft. The test bearings were placed under 150 N radial load and driven at 15000 rpm. The test bearing used

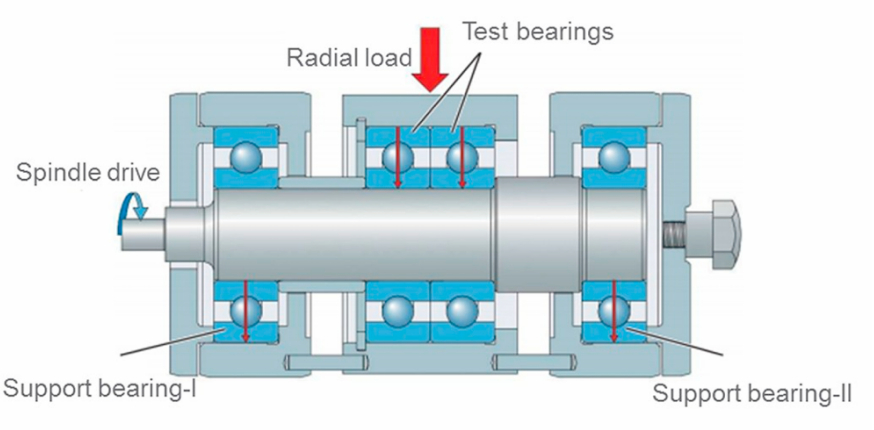

Figure 3.1: A schematic representation of the R0F+ bearing test rig [7].

Table 3.1: Some properties of the greases tested by Chatra et al. [28], obtained from Osara et al. [41]. The LPC2.5C grease is the same as the PE2.5C grease mentioned in Osara et al. [41].

Grease		LM2L	LM3L	LM3C	LPC2.5C
Thickener		Lithium	Lithium	Lithium	Poly urea
Base oil		Mineral	Mineral	Mineral	Ester
Viscosity (@ 40°C)	[mm^2/s]	100	100	98.9	72
Density	[kg/m^3]	900	900	900	960
Specific heat capacity	[J/kgK]	2566	2170	2088	1947

is the 6204-2Z/C3 Deep Groove Ball Bearings by SKF. A thermocouple was placed on the outer ring of the bearing. A diagram of the set up can be seen in Figure 3.1.

The data analysed in this chapter come from reference [28]. Greases studied include LM2L and LM3C, which are both peak type greases, and LM3L and LCP2.5C, which are both plateau types. The properties of these greases were investigated in Osara et al. [41], with the most relevant properties listed in Table 3.1.

3.3 Thermodynamic characterisation of grease during churning

As mentioned in Section 3.1, the thermodynamic model derived in Section 2.1.2 can be applied to the temperature data obtained during churning. Note that for thermal analysis, the thermal entropy is used and boundary (mechanical) work is excluded. The measured temperature data is plotted in Figure 3.2. For the sealed bearings used here, thermal energy changes are only due to temperature change via heat generation and heat transfer, without evaporation. The thermodynamic model for the total thermal entropy generated is in Equation 2.23, restated here as

$$S'(t) = S_T(t) + S_Q(t). \tag{3.1}$$

where $\dot{m} = 0$ to render $\dot{S}_m = 0$ and observing $T > T_\infty$, allowing the negative sign to be multiplied out ($-S_Q \to S_Q$). The accumulated heat storage entropy is, according to Equation 2.20,

$$S_T(t) = \int_0^t \frac{cm}{T}\dot{T}\, dt \tag{3.2}$$

and the total heat transfer entropy is, according to Equation 2.21,

$$S_Q(t) = \int_0^t \frac{T - T_\infty}{R_\theta}\, dt. \tag{3.3}$$

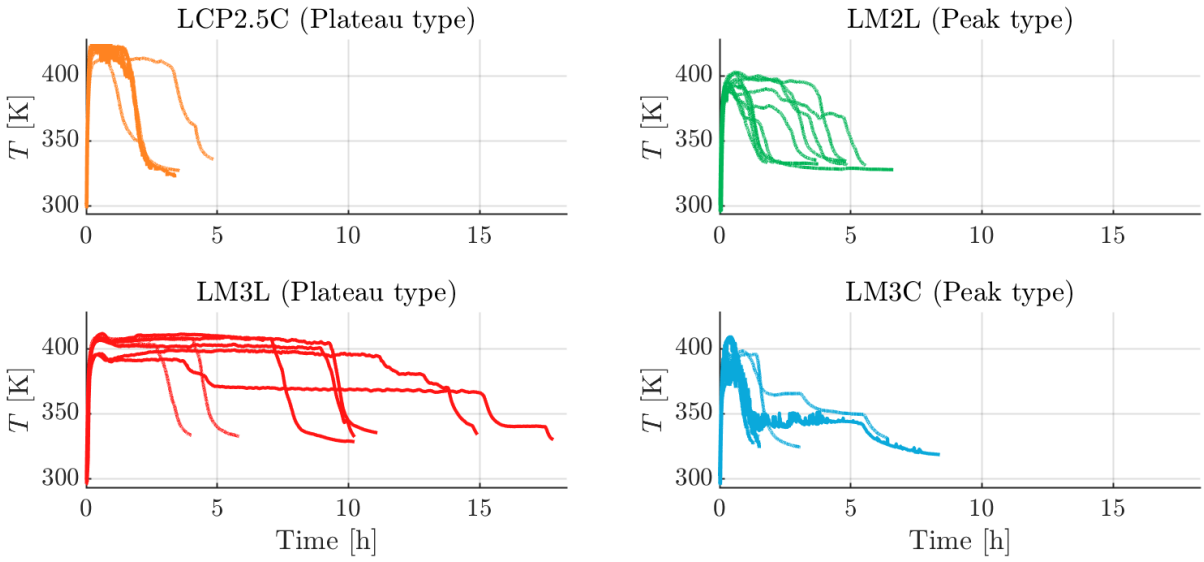

Figure 3.2: The bearing temperature measured during churning.

3.3.1 Thermal model of the churning rig

The heat storage entropy and heat transfer entropy are now adapted to this specific application.

3.3.1.1 Heat storage entropy

On the churning test rig is a thermocouple located on the outer ring of the bearing, see Figure 3.3. This means the actual temperature of the grease is not directly measured, but rather the temperature of the bearing which is assumed uniform with the grease temperature T. While the mass with which the bearings were filled is not directly stated, it is mentioned in Chatra et al. [7] that 30% of the free volume of the bearing was filled with grease. This means the mass of grease present is

$$m = 0.3 V_{\text{free}} \rho \tag{3.4}$$

and the free volume V_{free} of this specific bearing can be calculated by a rule of thumb provided by SKF [47]:

$$V_{\text{free}} = \frac{\pi}{4} w_b (d_o^2 - d_i^2) \cdot 10^{-3} - \frac{m_b}{7.8 \cdot 10^{-3}}. \tag{3.5}$$

where w_b is the bearing width, d_o outer diameter, d_i bore diameter and m_b is the bearing mass. It is important to note that for this rule of thumb, all dimensions are in millimetres and the free volume is in cubic centimetres. The bearing mass is in kilograms. Substituting Equation 3.4 and grease density ρ_{gr} in place of grease mass results in heat storage entropy of the grease during churning in a bearing

$$S_T = \int_0^t \frac{0.3 V_{\text{free}} c \rho_{gr}}{T} \dot{T} \, dt, \tag{3.6}$$

3.3.1.2 Heat transfer

The heat transfer entropy is dependent on the thermal resistance network from the inside of the bearing to the outside air, assuming a one-dimensional heat transfer. The total thermal resistance network can be found in Figure 3.3, which identifies conduction through housing

Table 3.2: Some constants for the calculation of the thermal resistance of the churning setup. (a) are obtained from the datasheet of 6204-2Z/C3 Deep Groove Ball Bearings by SKF and (b) is obtained from the churning rig.

Constant	Value	
r_2	23.5	mm (a)
r_3	31.0	mm (b)
w_b	14.0	mm (a)
k_b	443	W/mK [48]

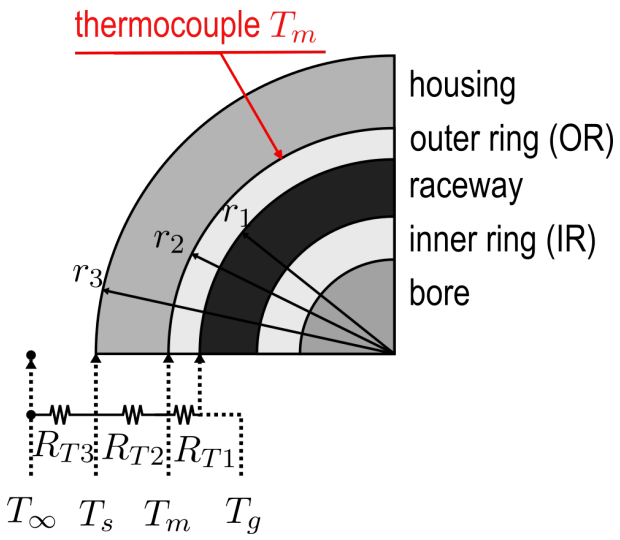

Figure 3.3: A schematic representation of the cross-section of the bearing and its position in the churning rig.

and convection at the surface of the housing as thermal resistances in series. The thermal resistance network from the bearing and grease (T) to the ambient air (T_∞) is

$$R_\theta = R_{T1} + R_{T2}. \tag{3.7}$$

R_{T1} is conductive thermal resistances and R_{T2} is a convective thermal resistance. Substituting the expressions for the resistances yields [48]

$$R_\theta = \frac{\ln\left(\frac{r_3}{r_2}\right)}{2\pi b k_b} + \frac{1}{2\pi r_3 w_b h}. \tag{3.8}$$

Here, r_3 is the housing radius, r_2 is outer ring or bearing radius, w_b is bearing width, k_b is the thermal conductivity of steel and h is the convective heat transfer coefficient. The values of these constants can be found in Table 3.2. R_{T1} is calculated using the bearing dimensions resulting in a value of 0.0787 K/W. This is negligibly small, so for simplicity, the thermal resistance is only based on the convection at the surface of the housing:

$$R_\theta = \frac{1}{2\pi r_3 w_b h}. \tag{3.9}$$

Using this thermal resistance, the resulting entropy transfer via heat, via Equation 2.21, is

$$S_Q(t) = \int_0^t \frac{T - T_\infty}{R_\theta}\, dt. \tag{3.10}$$

To improve the accuracy, the convective heat transfer coefficient h is regarded as a function of temperature. The reasoning for this, is that convection changes a lot over the 20°C to 150°C range found in the churning data. It is therefore considered insufficient to assume a constant value.

The main way dimensionless numbers depend on temperature is through the liquid's material properties. In this case, that liquid is air. The material properties are retrieved from standard tables [48] and interpolated using Matlab's [49] `makima` function. The temperature-dependent material properties can be found in Figure 3.4.

An airspeed of 0.1 m/s was assumed for a well-ventilated laboratory. The characteristic length is set equal to the diameter of the housing $L_c = 2r_3$. The Richardson number,

$$\mathrm{Ri} = \frac{\mathrm{Gr}}{\mathrm{Re}^2}, \tag{3.11}$$

then determines which convection type is dominant. Here, Gr is the Grashof number and Re is the Reynold's number. If Ri $<< 0.1$, force convection is dominant, if Ri $>> 10$ natural convection is dominant. In the range $0.1 \leq \mathrm{Ri} \leq 10$, the convection type is mixed [48]. Figure 3.5 shows the Richardson number for the expected range of surface temperatures.

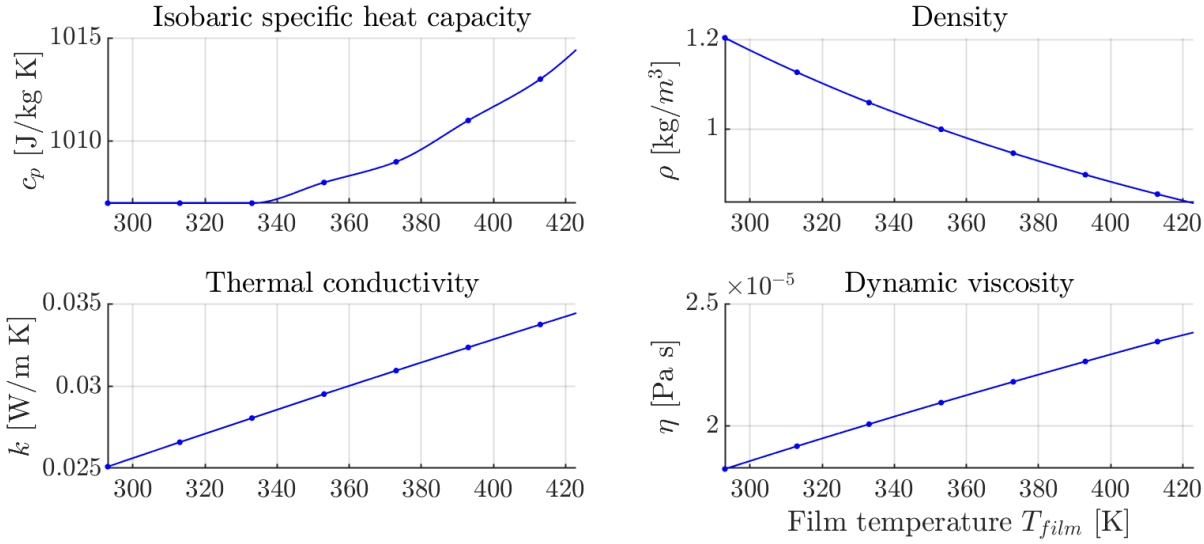

Figure 3.4: The properties of air, obtained from standard table [48] and interpolated using Matlab's [49] `makima` function. The control points are denoted by dots.

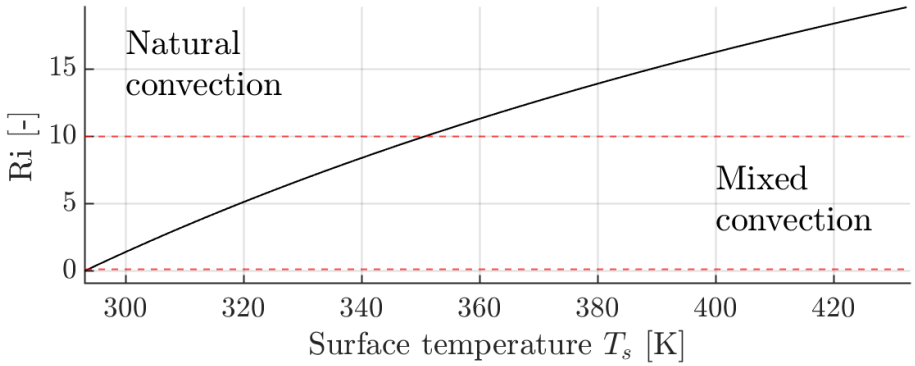

Figure 3.5: The Richardson number plotted over the range of expected surface temperature T_s. The Richardson number remains in the mixed convection region for low temperatures. At 350 K it crosses into where natural convection is dominant.

Figure 3.5 shows that the Richardson number does not truly fulfill the Ri $>> 10$ condition to consider natural convection dominant. Therefore, a formulation for mixed convection is used for the complete range. The mixed convection Nusselt number is [48]

$$\mathrm{Nu}_{mix} = \left(\mathrm{Nu}_{nat}^2 + \mathrm{Nu}_{for}^2\right)^{1/2} \tag{3.12}$$

where

$$\mathrm{Nu}_{nat} = \left(0.6 + \frac{0.387\mathrm{Ra}^{1/6}}{\left(1 + (0.559/\mathrm{Pr})^{9/16}\right)^{8/27}}\right)^2 \tag{3.13}$$

and

$$\mathrm{Nu}_{for} = 0.3 + \frac{0.62\mathrm{Re}^{1/2}\mathrm{Pr}^{1/3}}{\left(1 + (0.4/\mathrm{Pr})^{2/3}\right)^{1/4}}\left(1 + \left(\frac{\mathrm{Re}}{282000}\right)^{5/8}\right)^{4/5} \tag{3.14}$$

The convective heat transfer coefficient is then obtained by

$$h(T) = \frac{k_{air}(T)}{2r_3}\mathrm{Nu}_{mix}(T). \tag{3.15}$$

The Nusselt number and convective heat transfer coefficient are plotted against temperature in Figure 3.6. An earlier work by Chatra et. al. [26] also calculated the heat transfer entropy. This

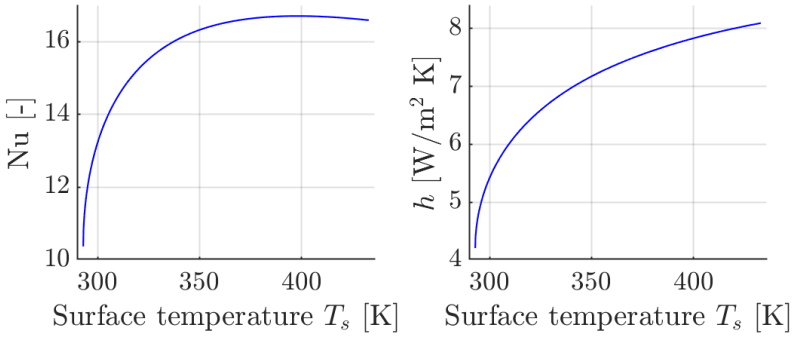

Figure 3.6: The Nusselt number and convective heat transfer coefficients plotted over the expected surface temperature range.

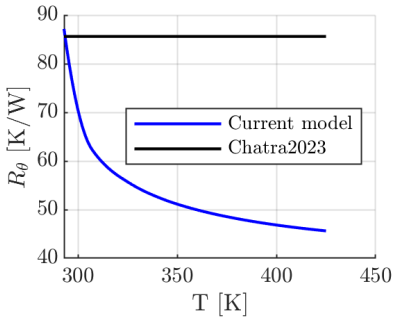

Figure 3.7: A comparison of the thermal resistance of the newly proposed heat transfer model and the model created by Chatra et. al. [26].

study calculated the thermal resistance as

$$R_\theta = \frac{1}{A_b h_{cr}}, \tag{3.16}$$

where A_b is the surface area of the bearing and h_{cr} the combined convection and radiation heat transfer coefficient. That study also made use of 6204–2Z/C3 Deep Groove Ball Bearings. A value of $h_{cr} = 11.3$ W/m^{2}K was found. When compared to the proposed model in Figure 3.7, the new heat transfer model yields a lower thermal resistance at high temperatures, meaning the current study will yield higher heat transfer entropy rates.

3.3.2 Entropy generation during churning

The thermal entropies will be calculated from the measured temperature profiles of the bearing.

3.3.2.1 Isolation of churning phase from raw temperature data

It should be noted that the data of experiments where churning was finished was used. Most experiments stop their recording long after the end of churning. So, before further analysis is done, churning-only data has to be extracted from the raw data. Here, churning is assumed to start at $t_0 = 0$, when the experiment starts. When churning is finished, temperature drops and remains constant at the steady state EHL temperature [7]. This will also be the last temperature measured after the experiment is stopped. So whether churning has finished can be measured by how close the temperature is to the final temperature T_f. This comes with the requirement that the maximum temperature T_{max} has been passed. The end of churning time

$$\left\{ t_{end} = t \left| \frac{T_{max} - T(t)}{T_{max} - T_f} > 0.95 \right. \right\}. \tag{3.17}$$

yields the churning-only temperature profiles plotted in Figure 3.8.

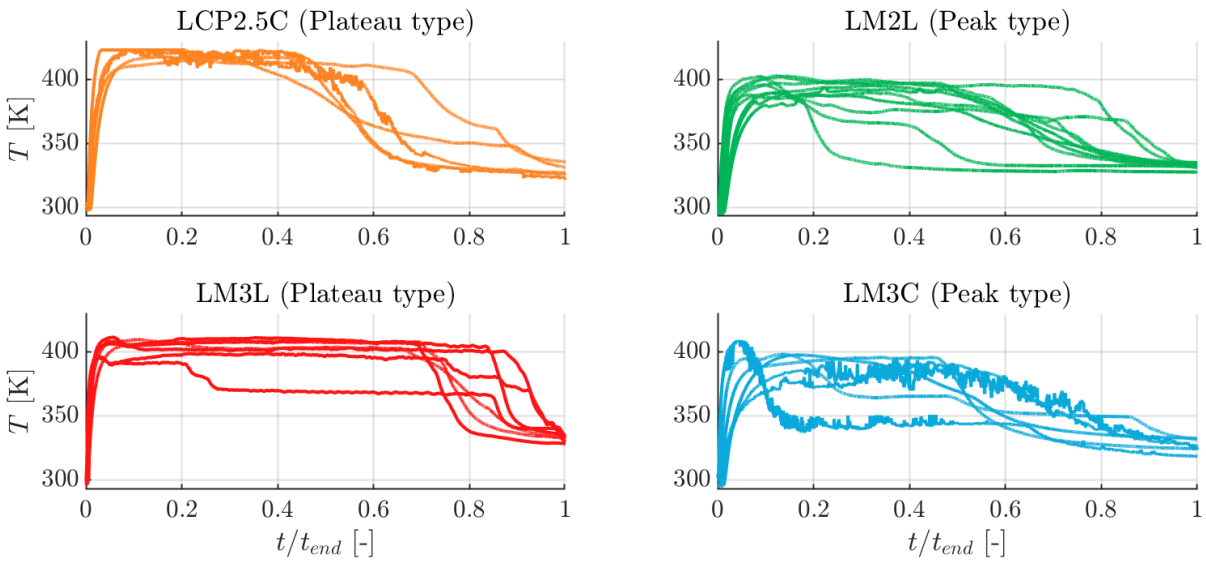

Figure 3.8: The temperature plotted against the progress towards the end of churning.

3.3.2.2 Entropy accumulated during churning

One way of characterise the entropy accumulated during churning is by comparing the two entropy sources: heat storage entropy $S_T(t)$ and heat transfer entropy $S_Q(t)$. This can be seen in Figure 3.9. It is evident that heat storage entropy, which primarily depends on temperature changes, has only a small range. The heat transfer entropy however steadily accumulates over time, as it scales with temperature difference with the environment and time.

By plotting these two sources, S_T and S_Q, against each other over the complete churning process may provide some insight into how each entropy source evolves during churning. The entropy profiles of Figure 3.9 seem to parallel the temperature curves of Figure 3.2, suggesting classification can be done in a similar way as done by Chatra and Lugt [7]. It should be noted that LCP2.5C is denoted as a plateau type, but it seems to consistently perform more ”peak-like” than half the experiments of LM2L, which is denoted a peak type.

Figure 3.10 shows that there is a distinction between the two churning types based on the accumulated heat transfer entropy. Some greases have low heat transfer entropy (LCP2.5C, LM2L and LM3C) and LM3L has much higher heat transfer entropy. Again considering that LCP2.5C seems to perform similarly to LM2L, one could consider this a sign that the comparison of the two entropies might be a good way to classify churning behaviour. Though this distinction is not strong enough to make classifications just yet.

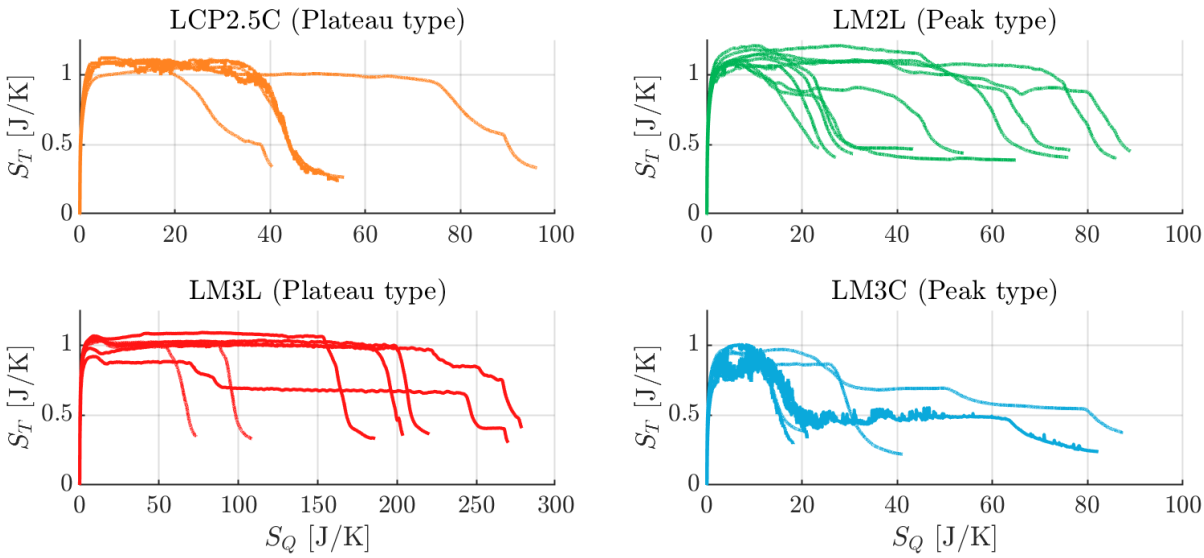

Figure 3.9: The heat storage entropy S_T and heat flux entropy S_Q during churning. Note the similarity of the shapes of the curves compared to the time-temperature data of Figure 3.2.

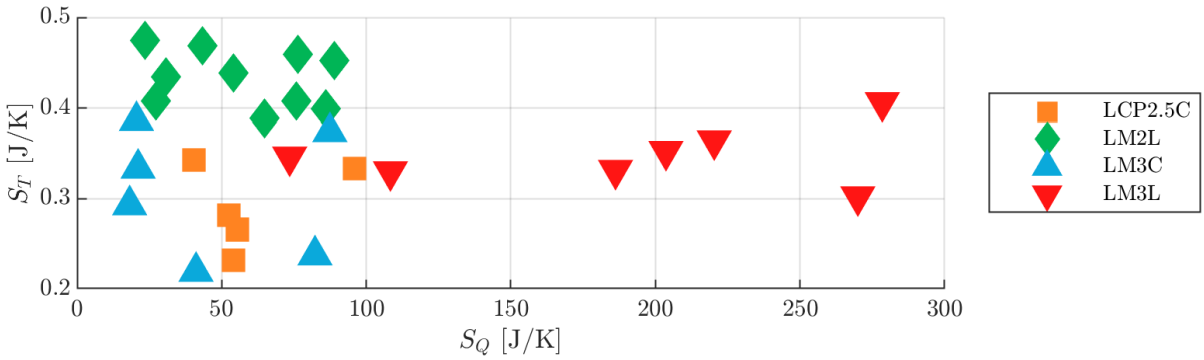

Figure 3.10: Discrete end-of-churning values of the entropy generation components S_T and S_Q.

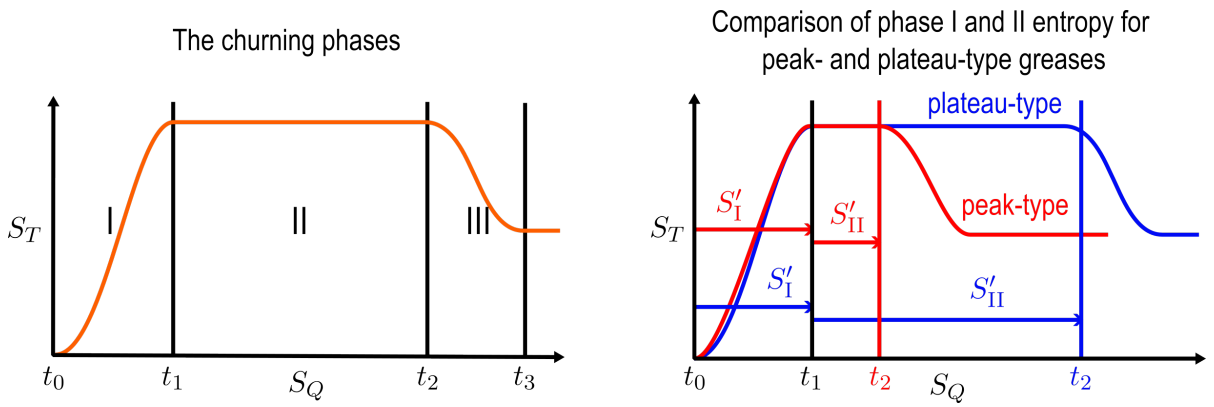

Figure 3.11: A schematic presentation of how churning can be separated into three phases on the left, and how these phases then result in different entropy generations for peak- and plateau-type.

3.4 Characterisation of churning using a novel three phase approach

Consider the schematic representation of a grease churning process in Figure 3.11. The left-hand figure demarcates the three phases:

- The initiation phase (phase I).
- The continuation phase (phase II).
- The termination phase (phase III).

The right-hand figure shows how different churning types will have different amounts of entropy generation in phase II compared to phase I.

3.4.1 Quantifying the three phases using the heat storage entropy S_T

The initiation phase will be defined as the period from t_0 until t_1. For most experiments t_0 will be simply equal to 0 s, i.e. when the bearing rig is started. When churning starts, the temperature starts to rise until it stabilises. First consider that

$$\dot{S}_T(t_0) = 0. \tag{3.18}$$

Then, the heat storage entropy maintains the following condition:

$$\dot{S}_T(t) > 0, \qquad t : \langle t_0, t_1 \rangle. \tag{3.19}$$

At the transition point between phase I and II, characterised by time t_1, the heat storage entropy stabilises at a constant temperature for the full range of phase II

$$\dot{S}_T(t) = 0, \qquad t : [t_1, t_2]\,. \tag{3.20}$$

The termination phase, phase III, is characterised by a drop in temperature and therefore a reduction of the heat storage entropy. This results in the condition

$$\dot{S}_T(t) < 0, \qquad t : \langle t_2, t_3 \rangle, \tag{3.21}$$

and finally ends at t_3 where

$$\dot{S}_T(t_3) = 0. \tag{3.22}$$

The final time was earlier defined in Equation 3.17. This is was based on the temperature of the grease, but can be redefined using $S_T(t)$. Similarly to the temperature definitions, a maximum heat storage entropy $S_{T\,max}$ and a final heat storage entropy $S_{T\,f}$ are defined. The final time is where the heat storage entropy is within 5% of its final EHL value:

$$\left\{ t_3 = t \left| \frac{S_{T\,max} - S_T(t)}{S_{T\,max} - S_{T\,f}} > 0.95 \right. \right\}. \tag{3.23}$$

3.4.2 Cumulative entropy during phases

The overall entropy generated during churning from t_0 to t_3 can be calculated using Equation 2.19:

$$S' = \int_{t_0}^{t_3} \dot{S}'(t)\, dt. \tag{3.24}$$

The entropy generated in each phase is the rate of entropy generation, integrated over their respective time durations. The entropy of phase I is

$$S'_{\mathrm{I}} = \int_{t_0}^{t_1} \dot{S}'(t)\, dt, \tag{3.25}$$

the entropy of phase II is

$$S'_{\mathrm{II}} = \int_{t_1}^{t_2} \dot{S}'(t)\, dt, \tag{3.26}$$

and finally, the entropy of phase III is

$$S'_{\mathrm{III}} = \int_{t_2}^{t_3} \dot{S}'(t)\, dt. \tag{3.27}$$

Figure 3.12 shows the entropy of each phase. It is notable that the entropy generated in phase I is far smaller than the entropy generated in phase II and III. Furthermore, the entropy of phase III is much higher for one of the LM3L runs than all others.

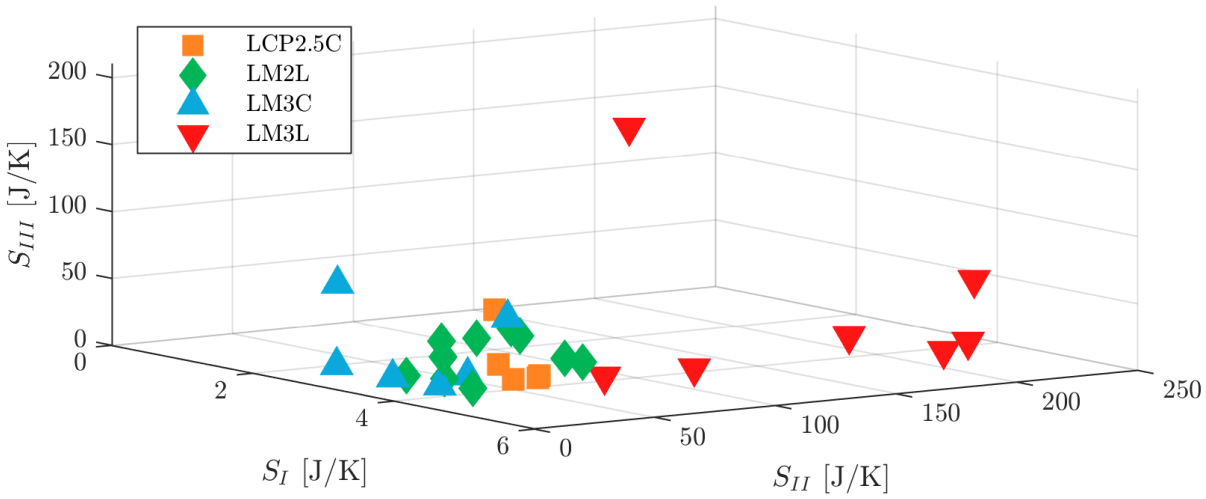

Figure 3.12: Entropy generated by phase (S'_I vs S'_{II} vs S'_{III}). The peak type greases (LM2L and LM3C) and the more contentious LCP2.5C have, relative to LM3L, a smaller phase II entropy.

3.5 Churning measure

In an effort to characterise the churning behaviour of grease, a single variable will be defined. This variable will be a measure of churning behaviour. The lower the churning measure, the more a grease behaves like a peak type. The larger the value, the more it behaves like a plateau type. This will place churning behaviour on a continuous axis, from best to worst.

3.5.1 Definition of the churning measure ϕ

Phase III contains the termination of the churning phase. The drop in temperature suggests churning is finished when entering this phase. If there is a classification of behaviour to be made, it might not entirely be productive to include phase III. This will yield no additional information about the churning behaviour of the grease. Then phases I and II are characteristic of the churning behaviour.

Figure 3.12 shows that the difference in magnitudes between phase I and phase II entropy generations is the most differentiating factor. One can then regard phase II as the determining factor in churning behaviour. The phase I entropy generation can then be used as a normalising factor between experiments. The churning measure ϕ is therefore defined as

$$\phi = \frac{S'_{\text{II}}}{S'_{\text{I}}}. \tag{3.28}$$

3.5.2 Upper and lower bound of the churning measure

For a grease that exhibits the ”perfect” churning behaviour, there would be a minimal amount of time spent at the plateau temperature. For a pure peak, there is only one instance where the entropy generation rate is equal to zero. This means phase I ends at the same time phase II starts: $t_1 = t_2$. From this follows that Equation 3.26 results in

$$S'_{\text{II}} = \int_{t_1}^{t_2} \dot{S}'(t)\, dt, \tag{3.29}$$

$$S'_{\text{II}} = \left[S'(t)\right]_{t_1}^{t_2} \tag{3.30}$$

With the condition that $t_1 = t_2$, it follows that $S'(t_1) = S'(t_2)$, meaning

$$S'_{\text{II}} = S'(t_2) - S'(t_1) = 0 \tag{3.31}$$

The lower bound, i.e. the churning measure for a perfect peak-type grease, is equal to

$$\phi = \frac{S'_{\text{II}}}{S'_{\text{I}}} = \frac{0}{S'_{\text{I}}} = 0 \tag{3.32}$$

The upper bound wholly depends on the length of the churning phase. This phase spans from t_1 to t_2. For the worst plateau-type grease, churning never ends. This means $t_2 \to \infty$ and

$$S'_{\text{II}} = \int_{t_1}^{\infty} \dot{S}'(t)\, dt, \tag{3.33}$$

$$S'_{\text{II}} = \left[S'(t)\right]_{t_1}^{\infty}. \tag{3.34}$$

By maintaining the criterion that $\dot{S}'(t) > 0$, as is the case at a constant temperature, it follows that for $t_2 \to \infty$, $S'(t_2) \to \infty$. This yields

$$S'_{\text{II}} = S'(t_2) - S'(t_1) \to \infty \tag{3.35}$$

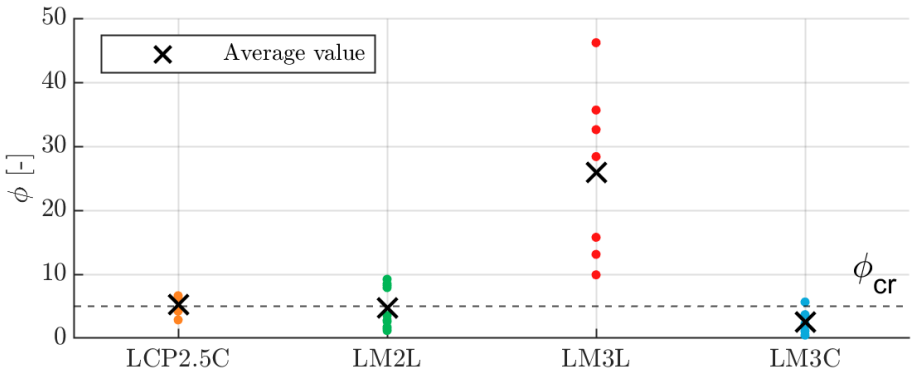

Figure 3.13: Grease churning measure ϕ for the four greases.

and means the churning measure is equal to

$$\phi = \frac{S'_{II}}{S'_{I}} \rightarrow \infty. \tag{3.36}$$

This leads to the conclusion that the churning measure

$$\phi : [0, \infty) . \tag{3.37}$$

3.5.3 Characterising grease type using ϕ

The next step will be to characterise the grease type using the churning measure. Qualitatively, LM2L and LM3C are characterised as peak-type greases and LM3L and LCP2.5C as plateau-type greases [7]. This is then quantitatively supported by calculating the ratio of the yield stress of churned grease to fresh grease.

Though the method presented here aims to somewhat fuzzy the hard limits between the grease types, by considering the churning measure as a continuous space, it is useful to see if the presented method agrees with previous works. Figure 3.13 shows box plots for the churning measures. Using the mean values of ϕ of these greases, we select a transition value of $\phi_{cr} = 5.0$. (Note that this choice is somewhat arbitrary, based on these four greases analysed, so a more robust mechanism should be used to define the boundary between peak and plateau behaviours). This classifies LCP2.5C and LM3L as plateau-types and LM2L and LM3C as peak types (when considering the mean of the data points).

However, the main goal of the churning measure is to make the characterisation more continuous and less categorical. Therefore, the critical churning measure should be regarded as a bridge between the original work by Chatra and Lugt [7]. Further characterisation is suggested to be done using the churning measure.

3.6 Applying the churning measure to additional experimental data

A work by Shetty et al. [50] investigated the dependence of film thickness during the bleed phase on the initial fill level of grease in deep-groove ball bearings. This investigation measured the film thickness throughout the churning process as well as the churning-induced temperature.

The time-temperature data will be subject to the same analysis as the other grease data. The results will be compared to the results from the previous analyses.

Table 3.3: The properties of the greases on which the additional data was collected, as presented by Shetty et al. [50]. The specific heat capacity of LM3C is used, obtained from the measurements done by Osara et al. [41].

Grease		LM3C-100	LM3C-460
Name in reference [50]		LiM-100-2.5	LiM-460-1.5
Thickener		Lithium	Lithium
Base oil		Mineral	Mineral
Viscosity (@ 40°C)	[mm^2/s]	102.8	474.5
Density	[kg/m^3]	891	902
Specific heat capacity	[J/kgK]	2088	2088

Table 3.4: The test conditions of the data used to build the churning measure model, by Chatra et al. [28], and the conditions of the example data, by Shetty et al. [50].

	RPM	Radial load
Chatra et al. [28]	15000	150 N
Shetty et al. [50]	4000	513 N

3.6.1 Calculating the churning measure

The grease samples are very similar to the earlier mentioned LM3C grease and they will be denoted as LM3C-100 (LiM-100-2.5) and LM3C-460 (LiM-460-1.5). An overview of their properties can be found in Table 3.3. The temperature-time evolution profiles are plotted in Figure 3.14. The data provided was discarded after 40 hours to ignore some secondary micro-churning behaviours.

No churning behaviour can be easily discerned from the data presented in Figure 3.14. However, comparatively, 30% filling experiences the most churning, then 15% and lastly 7.5%. This ranking is based on how quickly the temperature drops to the steady EHL temperature.

Because there is little known about the test rig employed, the same thermal resistance model as derived in Section 3.3.1.2 is used for this data. This yields the entropy generation presented in Figure 3.15.

An interesting difference between the churning behaviour of LM3C and the behaviour of LM3C-100 and LM3C-460, is that the peak temperatures vary. LM3C peaks at approximately 410 K, whereas LM3C-100 and LM3C-460 peak at 365 K and 380 K respectively.

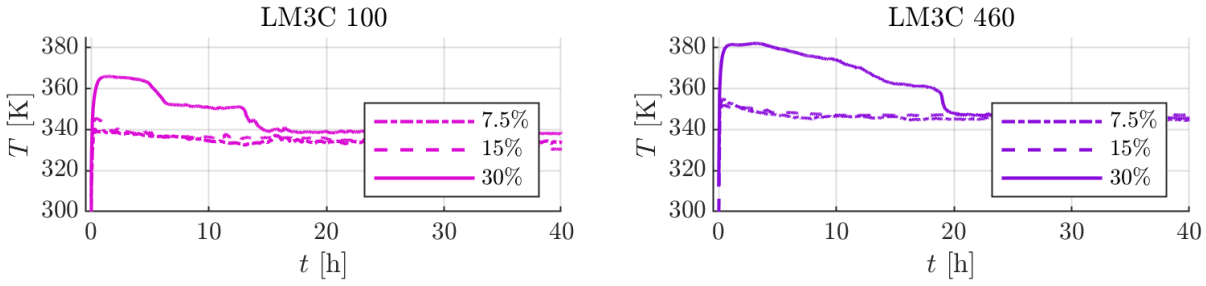

Figure 3.14: The temperature plotted over time. The percentages denote the fill level of the ball bearings.

These differences are due to the different experimental conditions . Table 3.4 shows that the RPM of the original datasets obtained on the ROF+ rig is much lower, 4000rpm compared to 15000rpm, and the radial load is much higher, 513 N compared to 150 N.

One can see very large differences between the churning behaviour of the various fill levels. The typical fill level of 30% shows behaviour similar to grease data from Chatra et al. [28]. Lower

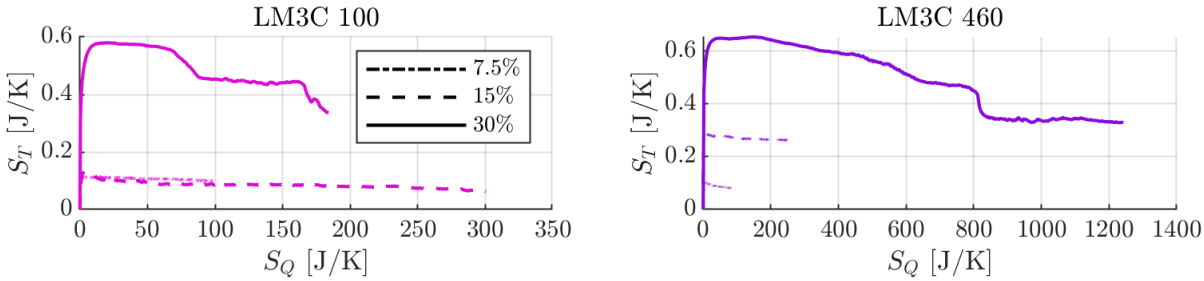

Figure 3.15: The heat storage entropy S_T plotted against the heat transfer entropy S_Q for the data provided by Shetty et al. [50].

fill levels show nearly no churning. Calculating the churning measure ϕ for the presented data results in Figure 3.16. This shows that below the commonly employed fill level of 30%, the grease experiences very small amounts of churning and therefore very low amounts of entropy generation.

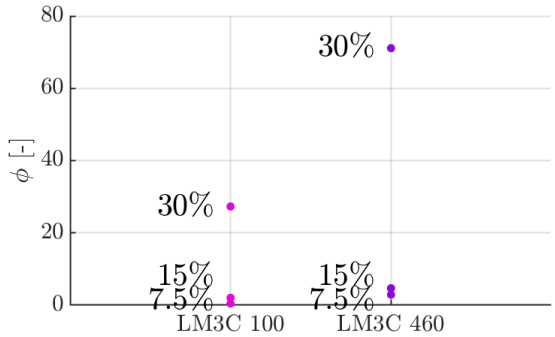

Figure 3.16: The churning measure from the data set provided by Shetty et al. [50]. The large difference between the churning measures of each grease is determined by the grease filling percentage in the bearings. Higher filling percentage corresponds to a higher ϕ, indicating more plateau-like performance.

3.6.2 Grouping all the greases

Figure 3.17 shows the churning measure side by side for the data obtained form Chatra and Lugt [7] and the data obtained from Shetty et al. [50]. This figure shows that the churning behaviour depends on the experimental conditions. The grease measures of LM3C 100 and LM3C 460 are separated based on the fill percentage of the bearing.

Based on the fill percentage, one could also say that these conditions are favourable for churning, as lower fill percentages mean a lower churning measure. This is as expected: if there is less grease in the bearing, less effort is required to clear the raceways of grease.

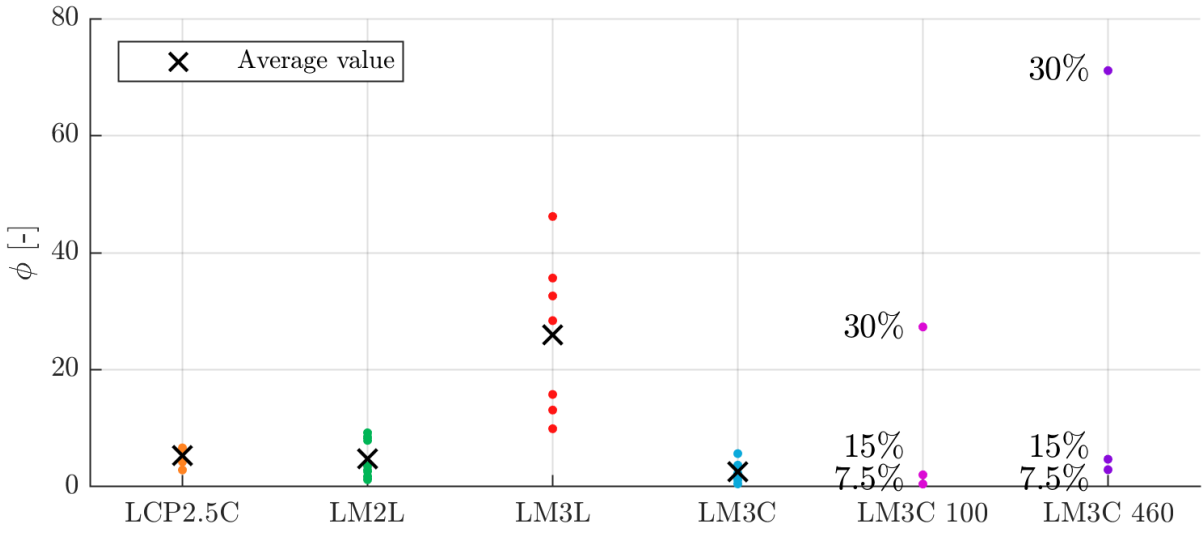

Figure 3.17: The churning measures ϕ of the the data provided by Chatra et al. [28] and Shetty et al. [50] compared.

Chapter 4

Experimental methods — Grease ageing in an oven

4.1 Grease samples

For this investigation into the thermal degradation of grease, three greases are investigated: Li/SS, Li/M and PU/E. The properties of these greases can be found in Table 4.1. The same greases were used by Hogenberk et al. [10] and Osara et al. [41].

4.2 Grease properties (used as degradation measures) and their measurements

To study the thermal degradation of grease, a set of five material properties are measured at various stages of thermal ageing — fresh greases, and greases aged for 10, 20 and 30 days. These properties are referred to as degradation measures. These degradation measures are:

- Bleed capacity measure.
- Specific heat capacity.
- Storage modulus.
- Thermal strain coefficient.
- Yield stress.

In addition to these properties, the latent heat of evaporation (LHE) of base oil has to be found to characterise evaporation. The IR-spectra will also be measured of each sample, to see if any oxidation occurs during ageing.

To ensure the most accurate results in the most time effective way, all measurements will be

Table 4.1: The greases tested in this study. These properties are collated from Hogenberk et al. [10] and Osara et al. [41], who studied the same greases.

Grease		Li/M	Li/SS	PU/E
Thickener		Lithium soap	Lithium soap	Polyurea
Base oil		Mineral	Semi-synthetic	Synthetic ester
NLGI grade		3.0	2.5	2.5
Density	[kg/m^3]	900	910	960
Viscosity (@ 40°C)	[mm^2/s]	99.9	41.9	70.0
Viscosity (@ 100°C)	[mm^2/s]	10.0	7.5	9.4
Drop point	[°C]	191	180	270
Oil separation	[%]	2.1	4.9	0.5

done twice. When there is a large discrepancy between the measured values, the measurement is repeated to identify the outlier.

4.2.1 Measuring the latent heat of evaporation of base oil

The LHE determines the energy needed to evaporate a unit amount of a liquid. The LHE is denoted by L, in either J/mol or J/kg. All mass measurements will be in kg, so the latter unit (J/kg) will be used from now on.

A method proposed by Dollimore et al. [51] utilises non-isothermal thermogravimetric analysis to characterise solid-state kinetics of thermal decomposition. In its current application, the thermal decomposition process is the evaporation of material. Chatterjee et al. [52] applied this method to find the LHE, which was then used to find the vapour pressure curves of hydroxy benzoic acid derivatives. Smook et al. [53] applied the same non-isothermal thermogravimetric method to study the oxidation stability of grease to great effect. All in all, the non-isothermal thermogravimetric analysis methodology seems a promising approach to find the LHE for the base oils of these greases.

Because this method deserves some more extensive explanation, the details of how this method is set up and applied can be found in Appendix A. The rest of this section will summarise.

The fundamental relation for non-isothermal decomposition is [51]

$$\frac{d\alpha}{dT} = \frac{A_{Arr}}{\dot{T}} e^{-\frac{E_a}{R_s T}} f(\alpha). \tag{4.1}$$

α is the ratio of evaporated material. The reaction mechanism function, $f(\alpha)$, depends on the kind of mechanism present. Because evaporation behaves like a first-order kinematic process [54], the process can be modelled using a first-order decay, rendering the function as

$$f(\alpha) = 1 - \alpha. \tag{4.2}$$

Lastly, E_a is the activation energy, which takes the value of the latent heat L for the evaporation process [23]. The final equation is

$$\frac{\dot{T}}{1-\alpha}\frac{d\alpha}{dT} = A_{Arr} e^{-\frac{L}{R_s T}}, \tag{4.3}$$

where the left-hand side of the equation is known. The unknowns of the right-hand side of the equation (L and A_{Arr}) can be found by fitting a linear equation to the left-hand side in Arrhenius space.

By increasing the temperature, the evaporation rate also accelerates. The slope of the rising portion of this curve, plotted in logarithmic space, is equal to $-L/R_s T$ from which LHE can be obtained.

Procedure The following procedure is performed on the TA Instruments TGA 550, a picture of which can be seen in Figure 4.1.

1. Obtain base oil from the grease sample using a centrifuge (or any other method of choice).
2. Tare the TGA baskets.
3. Load approximately 20 mg of base oil into the TGA basket.
4. Measure the temperature and mass of the sample. Vary the temperature according to:
   (a) Equilibrate at 40°C.
   (b) Ramp temperature to 200°C at a rate of 10.0°C/min.
   (c) Ramp temperature from 200°C to 400°C at a rate of 2.00°C/min.

4.2.2 Measuring IR-spectrum

The IR-spectra show the ratio of absorbed infrared radiation over a range of wavelengths. The location of each peak is characteristic of a certain molecular group and all these groups together can qualitatively characterise the composition of a grease [5]. Oxidation can be observed using IR, as oxidation will result in the appearance of new peaks or widening of existing peaks as compounds are broken down into LMW or polymerised into HMW molecules [15]. Evaporation would result in no change in the IR-spectra.

Procedure The following procedure is performed on a PerkinElmer Spectrum 100, a picture of which can be found in Figure 4.2.

1. Clean the measurement crystal.
2. Place a small volume of sample on the measurement crystal.
3. Enclose a small amount of sample using the press, applying 150 N.
4. Perform the IR spectrum scan from wave numbers 650 $1/\text{cm}$ to 4000 $1/\text{cm}$, with 16 repetitions.

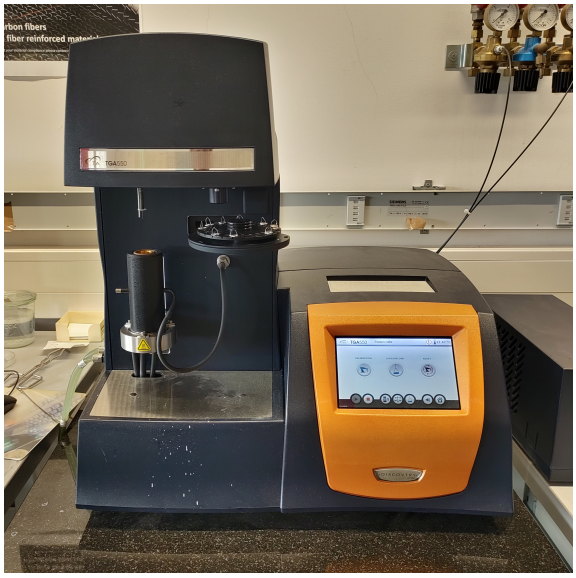

Figure 4.1: TA Instruments TGA 550.

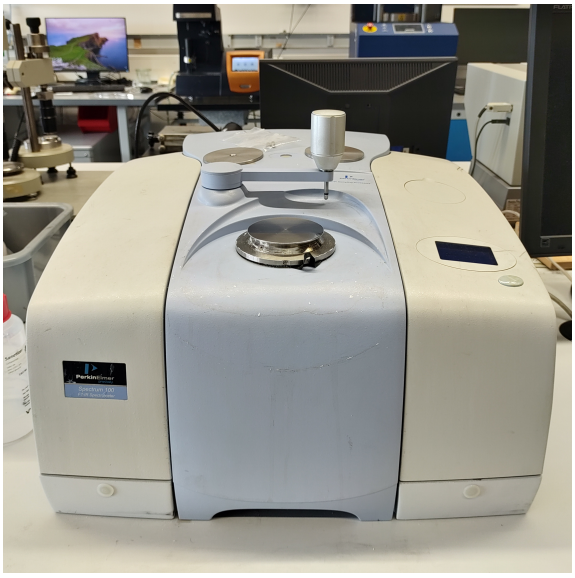

Figure 4.2: PerkinElmer Spectrum 100.

4.2.3 Measuring bleed capacity measure

The bleed capacity measure describes the ability of the grease to bleed its base oil. The following method is adapted from Hogeberk et al. [10], who used the SKF Grease Test Kit to measure the bleed capacity measure. The test kit provides a plastic disc that allows a consistently sized grease puck to be deposited on a piece of blotting paper. As the grease sits on the paper, oil starts to permeate through the paper fibres, creating a stain. To speed up this process, the experiment is done on a hot plate. The size of this stain gives an qualitative measure of the bleed capacity of the grease.

The resulting oil stain will have an elliptical shape, so both the major and minor dimensions are measured, and bleed capacity measure is then calculated according to

$$d_b = \sqrt{d_{\text{major}} d_{\text{minor}}}. \tag{4.4}$$

Procedure The following procedure is performed using a SKF Grease Test Kit, a picture of the setup can be found in Figure 4.3.

1. Use the template to place a puck of grease at the centre of the blotting paper.
2. Place the blotting paper onto a hot plate at 55°C for 2 h.
3. Remove the grease puck and measure the major and minor diameter of the elliptical oil stain.

4.2.4 Measuring the specific heat capacity

The specific heat capacity relates the temperature rise of the material to the heat energy input:

$$c = \frac{\Delta Q}{m \Delta T}. \tag{4.5}$$

By slowly raising the temperature of the sample and measuring the total energy needed to bring about this temperature rise, the specific heat capacity can be determined. To prevent both evaporation and oxidation during the experiment, closed-lid pans are used. The procedure is adapted from Osara et al. [41].

Procedure The following procedure is performed on the Netzsch DSC 214 Polyma, a picture of which can be seen in Figure 4.4.

1. Fill the crucible with between 10 and 20 mg of the sample.
2. Seal the crucible using a press.
3. Place the sealed crucible in the DSC.
4. Apply heat and measure the temperature according to:
   (a) Equilibrate the sample at 40°C.
   (b) Raise the temperature from room temperature to 40°C, at a rate of 0.5°C/min.
   (c) Maintain 40°C for 2 min.
   (d) Raise the temperature from 40°C to 60°C, at a rate of 0.5°C/min.
   (e) Reduce the temperature from 60°C to room temperature at a rate of 10°C/min.

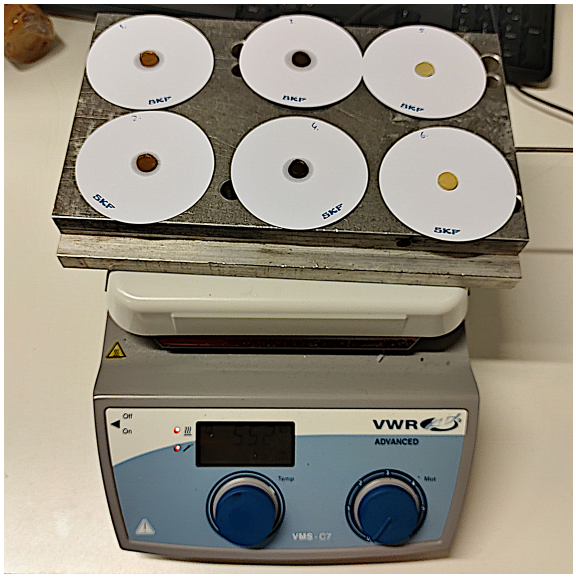

Figure 4.3: The heating plate with blotting paper and grease samples, the latter two being part of the SKF Grease Test Kit.

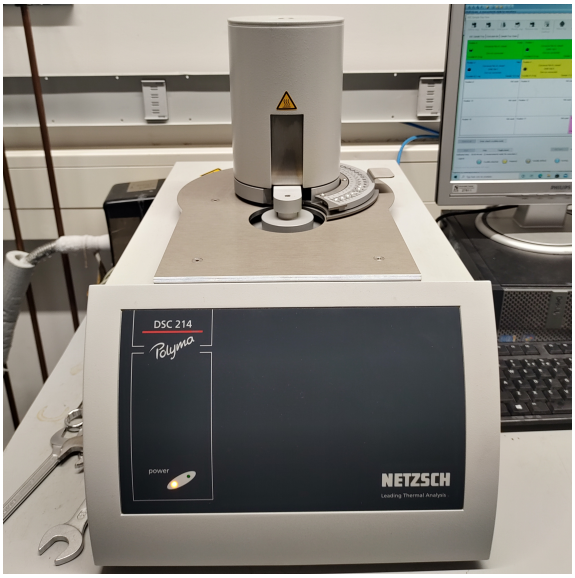

Figure 4.4: Netzsch DSC 214 Polyma.

4.2.5 Measuring the storage modulus

The storage modulus is a part of the dynamic modulus which determines the material's response to low-frequency loading and is commonly associated with the elastic response of viscoelastic materials. The storage modulus can be obtained by shearing grease with low oscillatory stresses, where the storage modulus is the average measurement of this experiment.

Procedure The following procedure is performed on a Thermal Instruments HR20, which can be seen in Figure 4.5.

1. Load approximately 0.5 mL of grease onto the lower rheometer plate.
2. Lower the plate down to a height of 575 µm and trim off the excess grease.
3. Lower the plate down to a gap of 525 µm.
4. Raise the temperature of the rheometer to 40°C at a rate of 0.5°C/min.
5. Pre-shear the grease at a rate of 10 s^{-1} for 30 s.
6. Allow the grease to rest for 30 min.
7. Apply an oscillatory shear stress of 10 Pa at 1 Hz for 2 h.

4.2.6 Measuring the thermal strain coefficient

The thermal strain coefficient α_γ connects a rise in temperature to the shear strain response of the grease [41]. The thermal strain coefficient can be determined by measuring the strain evolution as a function of temperature rise. The slope of the relationship between strain and temperature then determines the thermal strain coefficient.

The thermal strain coefficient is closely related to the thermal stress coefficient β,

$$\beta = \alpha_\gamma G', \tag{4.6}$$

which determines the stress induced by a temperature rise. Only the thermal strain coefficient is measured, as one could calculate the thermal stress coefficient using the measured storage modulus.

Figure 4.5: Thermal Instruments HR20.

Procedure The following procedure is performed on a Thermal Instruments HR20, which can be seen in Figure 4.5, using parallel plates with a diameter of 25.0 mm.

1. Load approximately 0.5 mL of grease onto the lower rheometer plate.
2. Lower the plate down to a height of 575 µm and trim off the excess grease.
3. Lower the plate down to a gap of 525 µm.
4. Ramp the temperature from room temperature to 40°C at a rate of 1.0°C/min.
5. Pre-shear the grease at a rate of 100 s^{-1} for 60 s.
6. Allow the grease to settle for 30 min at a starting temperature of 40°C.
7. Raise the temperature of the grease from 40°C to 100°C, at a rate of 1.0°C/min while applying a low oscillatory shear stress of 0.1 Pa at a frequency of 1 Hz.

4.2.7 Measuring the yield stress

The yield stress, in visco-elastic materials, defines the transition from the elastic regime to the viscous regime. This point can be found by ramping up the strain to find where the material's behaviour drastically changes. The exact value of the yields stress depends on the method employed.

The method proposed by Cyriac et al. [55], which is also used by Osara et al. [41], is used to measure the yield stress. This method defines the yield stress as the point where the stress-strain response of the grease deviates from linearity. The algorithm creates a spline between all measurement points. Then, a linear fit is made on said interpolated points. While $R^2 < 0.995$, the point with the highest strain is removed and the fit is remade. Once $R^2 \geq 0.995$, the yield stress is the stress corresponding to the highest strain.

Procedure The following procedure is performed on a Thermal Instruments HR20, which can be seen in Figure 4.5, using parallel plates with a diameter of 25.0 mm.

1. Load approximately 0.5 mL of grease onto the lower rheometer plate.
2. Lower the plate down to a height of 575 µm and trim off the excess grease.
3. Lower the plate down to a gap of 525 µm.
4. Ramp the temperature from room temperature to 40°C at a rate of 1.0°C/min.
5. Pre-shear the grease at a rate of 100 s^{-1} for 30 s.
6. Allow the grease to rest for 30 min.
7. Perform a logarithmic oscillatory strain sweep from 0.001% - 1000%.

4.3 Grease ageing

To study the thermal degradation of grease, the grease samples should be kept at an elevated temperature for an extended period of time. However, at high temperatures, grease is at risk of oxidation. The grease samples are therefore aged in a nitrogen atmosphere, preventing oxidation and allowing evaporation to occur, as the samples can be aged uncovered. The grease samples will be aged for 10 days, 20 days and 30 days, at a temperature of approximately 130°C (403 K).

4.3.1 Vacuum oven

The vacuum oven is an air-tight electric oven which is connected to a vacuum pump. This allows all the air to be pumped out of the oven to create a vacuum inside the oven. The oven is also hooked up to a nitrogen gas line. After pulling a vacuum, the oven can be flushed with nitrogen gas, creating an inert non-oxidising environment for the grease. A picture of the vacuum oven and some important hardware connected to it are in Figure 4.6.

The oven temperature is recorded using a Voltcraft DL-240K thermocouple reader, which is connected to a K-type thermocouple. Due to the very long ageing interval projected, the temperature is measured every 90 seconds. At that rate, the internal storage of the thermocouple is

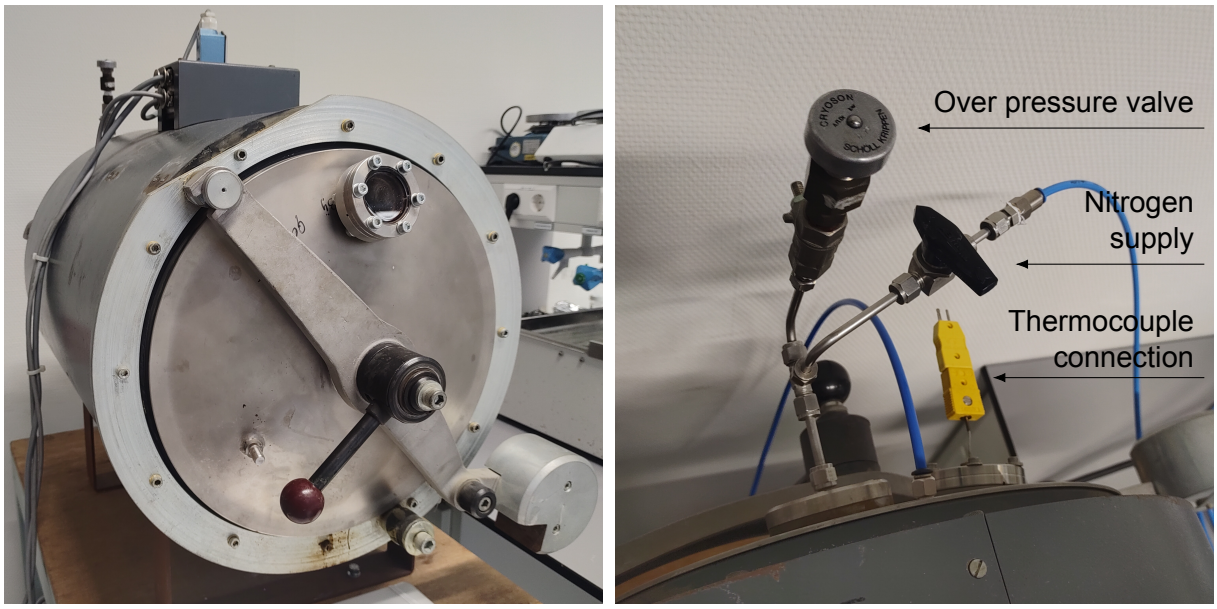

(a) The front of the oven.

(b) The back of the oven.

Figure 4.6: The front (Figure 4.6a) and back (Figure 4.6b) of the vacuum oven used for ageing.

full after approximately 31 days. The thermocouple is built into the oven: the wire sticks straight into the middle of the oven and can be connected via a plug on the back side of the oven (see Figure 4.6b).

Procedure for preparing the oven The procedure of insertion and retrieval of samples, and the preparation of the nitrogen atmosphere in the oven.

1. The oven is opened.
2. Samples are retrieved and/or inserted.
3. The oven is closed.
4. The oven atmosphere is cycled to make sure no oxygen remains in the oven:
   (a) Vacuum is pulled, the pressure is reduced to below 0.01 bar.
   (b) The oven is flooded with nitrogen gas until the pressure is 1 bar.
   (c) Vacuum is pulled, the pressure is reduced to below 0.01 bar.
   (d) The oven is flooded with nitrogen gas to 1 bar.

4.3.2 Sample preparation

The grease samples are placed into small glass bottles, a picture of one of those bottles can be found in Figure 4.7.

To ensure homogeneity between samples, the bottles should be filled to the same mass or volume. Considering that evaporation also plays a part in ageing, it should be noted that evaporation is a function of exposed surface area. The geometry of the sample is therefore important: the exposed surface area should be as flat as possible. The grease puck should also be pressed together to remove as many air pockets as possible. These things are easiest to enforce with a consistent sample volume.

The samples are prepared in pairs so that of every ageing interval there will be two samples. This ensures enough sample is aged to perform all experiments, evaporation can be averaged for a more accurate result and each individual sample is small enough to ensure small temperature gradients within the grease.

Figure 4.7: The sample bottle.

Figure 4.8: Grease tool.

The desired volume per sample is chosen to be 25 mL. With the bottle having an approximate inner diameter of 33 mm, the cross-sectional area is

$$A_c = \frac{1}{2}\pi d_b^2 = 8.55 \cdot 10^{-4}\,\mathrm{m}^2. \tag{4.7}$$

A_c is the cross sectional area of the bottle and d_b is the bottle diameter. This results in a desired puck height of

$$V_g = A_c h_b \rightarrow\ h_b = \frac{V_g}{A_c} = 29.2 \cdot 10^{-3}\,\mathrm{m} \tag{4.8}$$

or 30 mm rounded up. Grease is a very sticky substance and therefore difficult to work with sometimes. To aid in consistently creating grease samples, a tool was 3D printed. A picture of this tool can be found in Figure 4.8. This tool has a large disc, meaning the bottom of the tool is a consistent distance from the bottom of the bottle. The end of the tool has a flat bottom, for flattening the surface of the sample, and a ramp for scooping out excess grease.

During ageing, some base oil and volatile additives will evaporate. The amount evaporated can be easily obtained by comparing the mass of grease before and after ageing.

Procedure for preparing samples The procedure of preparing a sample for insertion into the oven.

1. Record the mass of the empty sample bottle.
2. Add an excess grease to the sample bottle.
3. Use the grease tool (or other means) to create a compact puck of grease with a smooth surface while removing the excess grease.
4. Use paper towel to remove excess grease stuck to the sides of the bottle.
5. Record the mass of the filled sample bottle. Subtract the mass of the empty bottle to obtain the mass of the grease sample.
6. Insert the sample into the oven and retrieve again after ageing.
7. Record the mass of the filled sample bottle after ageing. Subtract the mass of the filled bottle before ageing to obtain the mass evaporated.

4.3.3 Ageing intervals and temperature

The grease samples will be aged for three intervals: 10 days, 20 days and 30 days. The greases will be aged in two batches: first Li/M and Li/SS together, followed by PU/E.

Because the time intervals are quite large, it is not that relevant to retrieve the samples at the exact time they were inserted. The clock-time at which samples are inserted and retrieved is recorded to the minute. These clock-times then determine the range of temperature data, which is recorded on the temperature logger, that is used for the sample.

The oven makes use of a controller to set the temperature. The controller switches the heating element on when the temperature crosses a low threshold and switches the heating element off when it crosses the high threshold. This makes the temperature fluctuate at $\pm 1.5°$C of the set value. The controller's thermometer is, however, located at the heating mesh, located in the wall of the oven. So the controller allows the inside of the oven to be between 130°C and 133°C (403 K – 406 K), depending on the amount of samples in the oven and the lab temperature.

Chapter 5

Experimental results

5.1 Ageing

In this chapter, the recorded oven temperatures and measured grease properties will be presented. All samples are collected and visually compared to identify discolourations. The mass of each was sample also measured, for use in estimating the evaporation mechanism to be characterised.

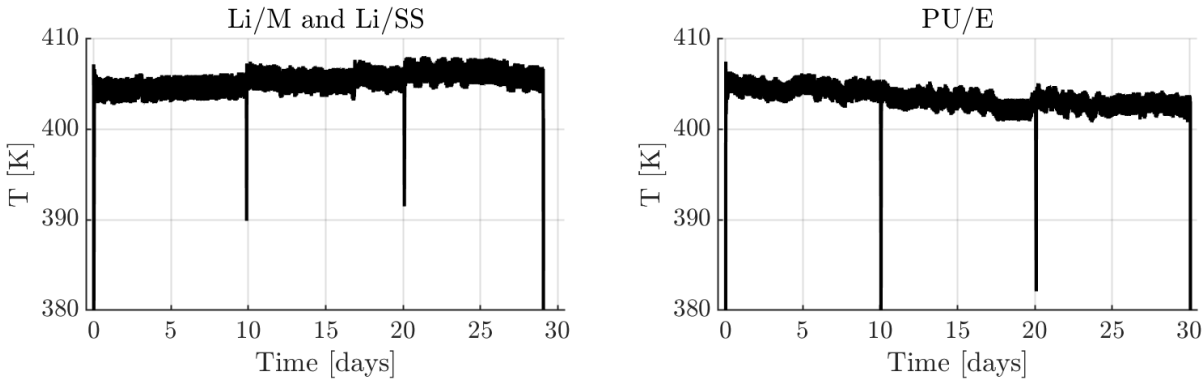

Figure 5.1: The temperature measured during ageing, without any processing. Li/M and Li/SS were aged at the same time and therefore share their temperature profile. PU/E was aged separately. The spikes coincide with when the oven was opened, where the temperature drops sharply for a handful of minutes.

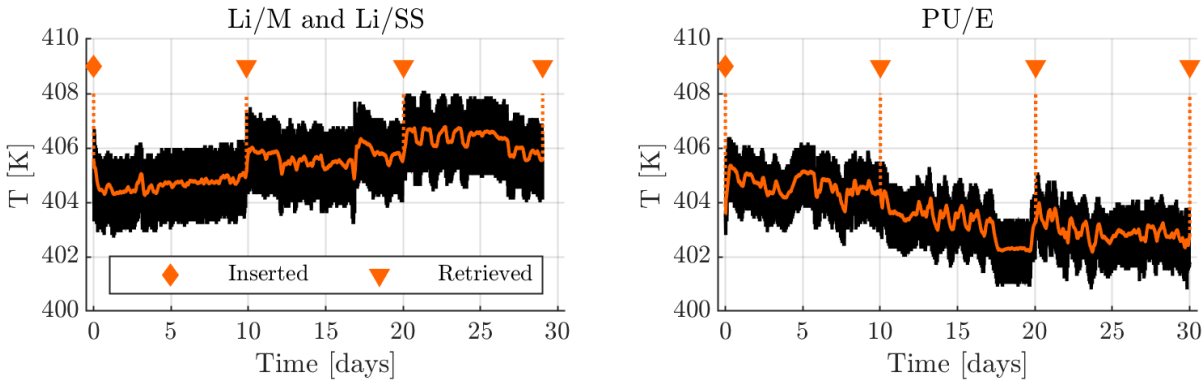

Figure 5.2: The temperature profiles during ageing, after limiting them to the time samples were in the oven and smoothing over the spikes. The orange line shows the 120 samples moving average; the temperature trend over a window with a width of 3 hours. The points where samples are inserted and retrieved are denoted with the orange symbols.

5.1.1 Oven temperature profiles and time intervals

The temperatures measured during the ageing procedure are plotted against time in Figure 5.1. Li/M and Li/SS were aged at the same time, meaning they share a temperature profile. PU/E was aged separately after that.

Notable are the spikes in the temperature profile. These correspond to when the oven was opened to insert and/or retrieve samples, as the hot oven atmosphere is replaced with cold ambient air. This only lasted for an instant however, as the oven was quickly closed and flushed with nitrogen. Therefore, the assumption is made that the impact on the grease samples is minimal and the spikes can be smoothed over.

The three greases were kept at approximately 405 K or 132°C, with the oven temperature fluctuating at 0.71 K about its 1 hour moving average. However, the average difference between the highest and lowest temperature measured during ageing is 5.5 K. The hourly fluctuations are small, but over the complete ageing procedure, the temperature changes considerably.

The temperature profile is limited to the relevant time span: from when the first samples are inserted to when the last samples are removed. This is presented in Figure 5.2 and will be the temperature used for all further analyses. The orange lines in Figure 5.2 are the moving averages of the temperature profiles to show the trends during ageing.

The times at which the samples were retrieved from the oven are presented in Table 5.1. The samples were removed after approximately after 10 days, 20 days and 30 days have passed, though it was not considered necessary to retrieve them at the exact same minute or hour at each interval. The time is simply recorded and converted to seconds as necessary.

It is important to note that, when the time axis is denoted with *Time [days]*, it concerns instantaneous time spent in the oven, and when it is denoted with *Age [days]*, it concerns the discrete time intervals of 10 days, 20 days and 30 days.

Table 5.1: The time and date when grease samples were inserted into or retrieved from the oven. Note that due to properties measurement equipment scheduling issues, Li/M and Li/SS samples, set to age for 30 days, were removed from the oven a day early.

	Li/SS & Li/M					PU/E				
Age	Date	Time	Time in oven			Date	Time	Time in oven		
t_0	10-10-2023	15:32				14-11-2023	14:47			
t_{10}	20-10-2023	12:33	9 d	21 h	1 m	24-11-2023	15:15	10 d	0 h	27 m
t_{20}	30-10-2023	16:13	20 d	0 h	42 m	04-12-2023	16:03	20 d	1 h	15 m
t_{30}	08-11-2023	15:59	29 d	0 h	27 m	14-12-2023	15:07	30 d	0 h	19 m

5.1.2 Visual inspection of the samples

Pictures were taken of the grease samples before and after ageing. These are shown in Figure 5.3. Every sample shows some amount of discolouration.

Li/M is observed to darken in colour, going from a light to a dark brown. The change is most pronounced in the first 10 days; after 20 days the darkening seemed to have stopped. Li/SS appears to follow the same pattern, where the discolouration reached its fullest extent at 20 days with the most drastic change being between 0 and 10 days. The colour, however, became more grey-ish. PU/E changes colour over the full 30 days. Every interval, the colour moved towards a darker orange, compared to the light yellow at the start.

For all samples, the discolouration seemed to mainly affect the top layer of the grease. This could suggest that evaporation is the primary cause of discolouration visible in Figure 5.3. The bulk of the grease also experiences colour changes, though less drastically than the top layer. To ensure homogeneity in grease samples used to measure properties, the samples were mildly

stirred. This issue is not considered critical, but if necessary, a thin slice of grease could be used in the ageing test to enhance homogeneity without manual stirring.

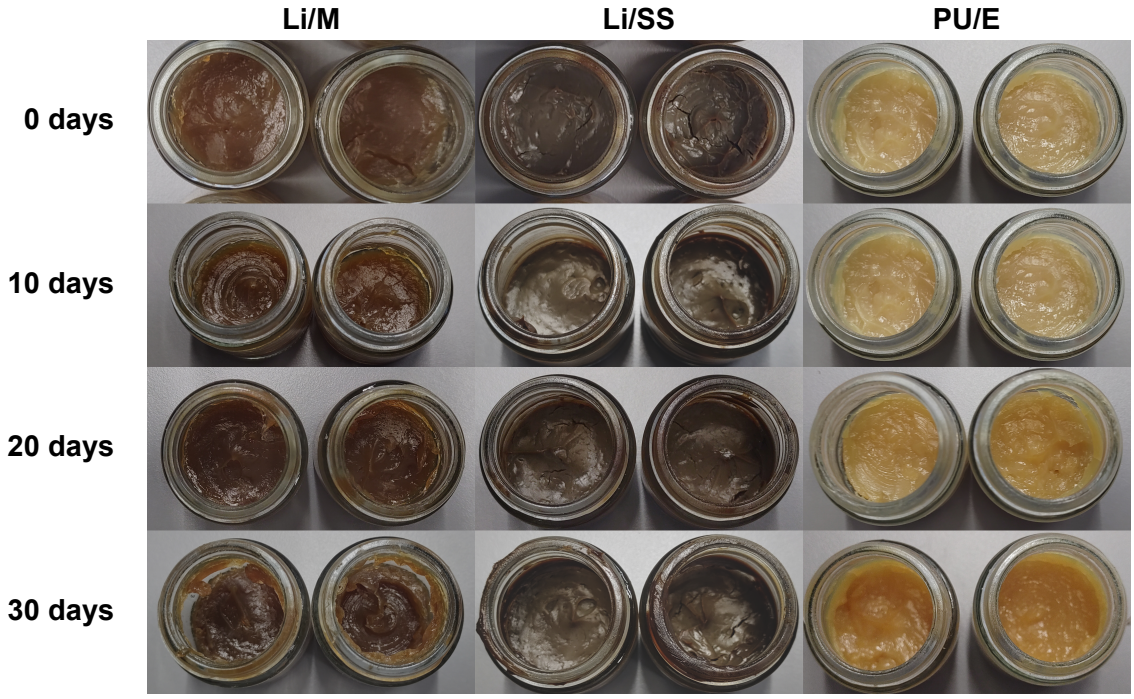

Figure 5.3: The samples of Li/M, Li/SS and PU/E at various stages during ageing in the oven. All samples experienced some form of discolouration in their top layer, along with some lesser discolouration of the bulk of the samples.

5.1.3 Mass change due to evaporation

The mass of each sample was recorded before and after ageing. Each sample has a different starting mass. The evaporation will therefore be characterised by calculating the fraction of the total mass remaining after oven ageing. The fraction remaining, dubbed the relative mass m_r, is

$$m_r = \frac{m_f}{m_s}, \tag{5.1}$$

where m_f is the final mass and m_s is the starting mass.

The relative mass (averaged over the 2 samples) of each grease is calculated per ageing interval and presented in Figure 5.4. To get a ”characteristic” sample mass, this ratio is multiplied with the average starting mass of the samples of each grease.

Figure 5.4 shows that evaporation significantly slowed down after 10 days. This suggests that the base oil and volatile additives near the surface have evaporated. Subsequently, volatiles and base oil need to move from the bottom layers toward the surface, possibly slowing down the evaporation process.

Li/M and Li/SS show similar levels of evaporation, ending at 95.5% and 94.9% of their starting masses, respectively. PU/E experiences significantly less evaporation, only reducing to 99.5% of its starting mass.

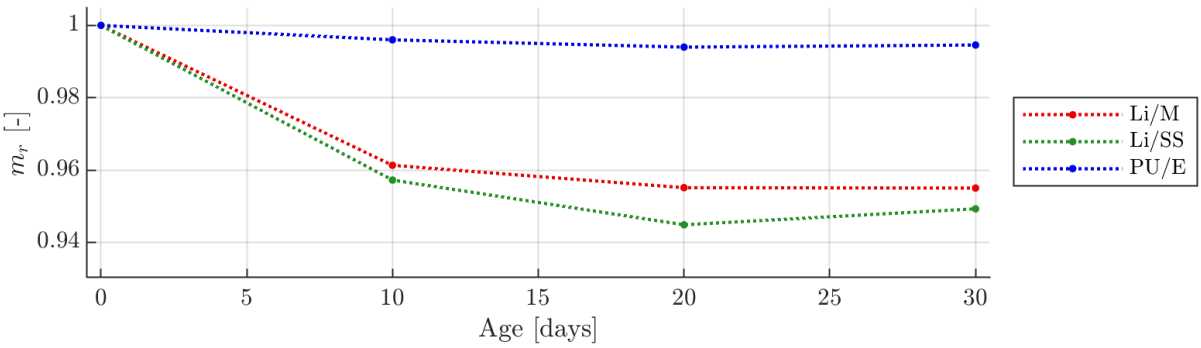

Figure 5.4: The relative masses of the grease samples for 0 days, 10 days, 20 days and 30 days. Li/M and Li/SS experience similar levels of evaporation. PU/E experiences a very low level of evaporation. All samples seem to have little evaporation after 10 days, suggesting most of the volatiles have evaporated.

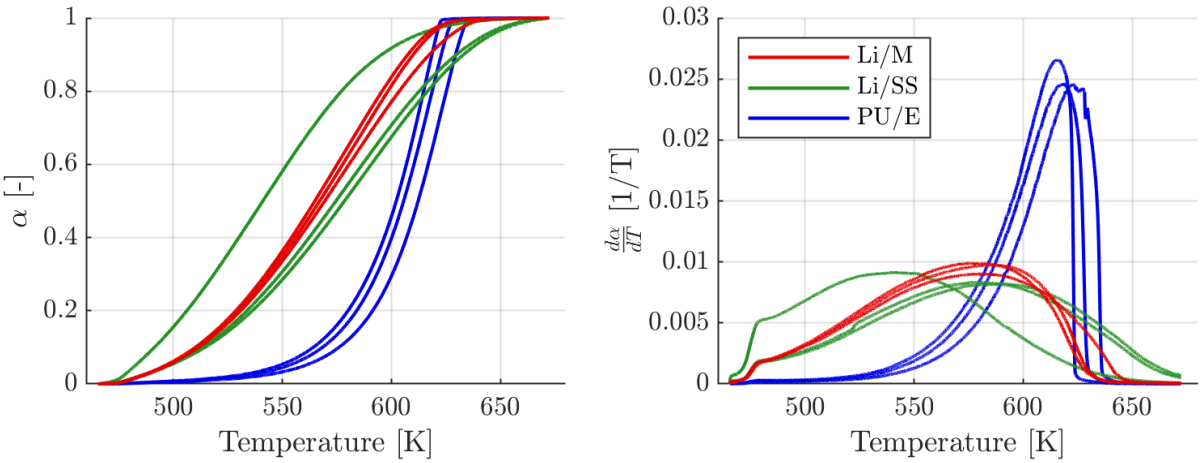

Figure 5.5: The fraction of mass evaporated α and its derivative with respect to temperature $d\alpha/dT$. Each grease type was tested thrice.

5.2 Latent heat of evaporation (LHE) of base oil

To properly characterise the evaporation of the grease samples, the LHE must be determined. This is done by means of non-isothermal thermogravimetric analysis [51–53]. Appendix A explains the process of determining the LHE in more detail.

As the temperature of the sample is raised, mass evaporates from the sample. This is characterised using the fraction evaporated

$$\alpha = \frac{m_i - m(t)}{m_i - m_f}, \tag{5.2}$$

where $m(t)$ is the instantaneous mass at time t, m_i the initial mass and m_f the final mass. Because the heating rate is constant, causing temperature to increase linearly with time, the instantaneous mass can also be considered a function of temperature $m(T)$.

The fractions evaporated α are plotted in Figure 5.5, together with their derivatives with respect to temperature ($d\alpha/dT$). This shows that the mass loss rate increases as the temperature increases. However, at some point, the process decelerates due to a reduction in available mass. For the analysis, only the rising portion of the $d\alpha/dT$-curve is needed. The measurements were repeated thrice, hence the 3 plots shown for each grease.

For PU/E, the evaporation process ends quite abruptly, while Li/M and Li/SS slow down more gradually before reaching $\alpha = 1.0$. This is likely due to Li/M and Li/SS containing a wider

Table 5.2: The LHE measured for Li/M, Li/SS and PU/E greases. All values are found with R^2 higher than 0.98.

Grease	Latent heat of evaporation
Li/M	154.0 kJ/kg
Li/SS	128.9 kJ/kg
PU/E	337.9 kJ/kg

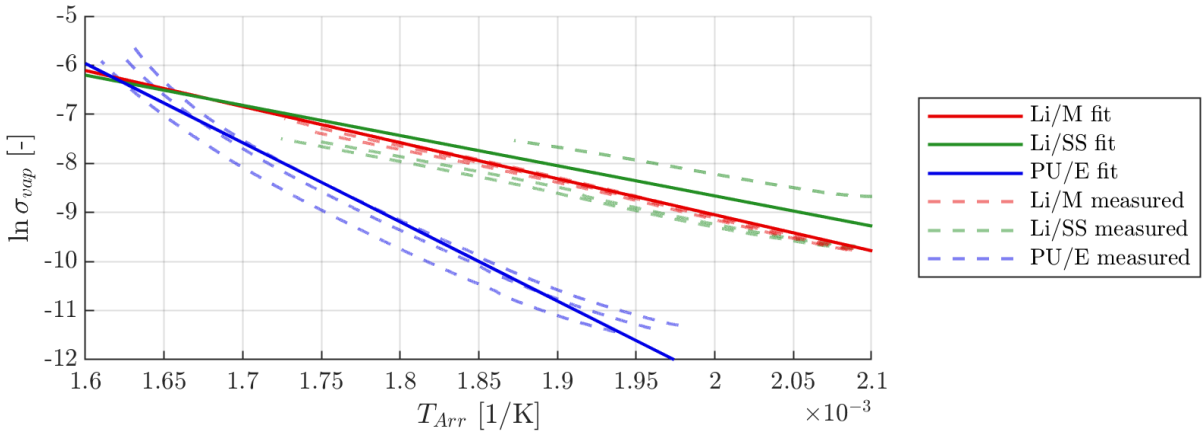

Figure 5.6: The evaporation coefficient plotted over the Arrhenius temperature (which is $T_{Arr} = 1/T$). The dashed lines show the individual measurements and the solid lines show the linear fits, the slopes of which are equal to $-L/R_s$.

spread of compounds, meaning at higher temperatures heavier compounds can start evaporating. PU/E has a more defined composition, meaning compounds that can evaporate are more quickly exhausted.

The rising portion of the $d\alpha/dT$-curve is then plotted in Arrhenius space. This plot can be found in Figure 5.6. The coefficient of evaporation σ_{vap} has an Arrhenius relationship with temperature [52]:

$$\sigma_{vap}(T) = \ln A_{Arr} - \frac{L}{R_s T}. \tag{5.3}$$

A_{Arr} is the Arrhenius constant, L is the LHE and T is the temperature. R_s is the specific gas constant for base oil vapour, equal to the universal gas constant divided by the molecular mass. However, the molecular weights of Li/M, Li/SS and PU/E could not be measured. Instead, a value is estimated from literature: a molecular weight of 397 g/mol is estimated for all three greases [56, 57].

Linear fits can be made to the data plotted in Figure 5.6, the slopes of which are equal to $-L/R_s$. The results of this analysis are in Table 5.2.

5.3 Oxidation check via IR-spectra

Figure 5.7 shows the measured IR spectra of the three greases, for the fresh samples and after the three ageing intervals. Between the fresh sample and the aged samples, there is no significant difference in IR-spectra. Note that the IR-spectra are overlaid, to aid visual and qualitative comparison of peaks.

Figure 5.7 therefore shows that no new peaks are created or removed due to ageing, meaning there is no chemical change in the grease. This rules out oxidation, meaning the ageing procedure was successful in thermally ageing grease without oxidation.

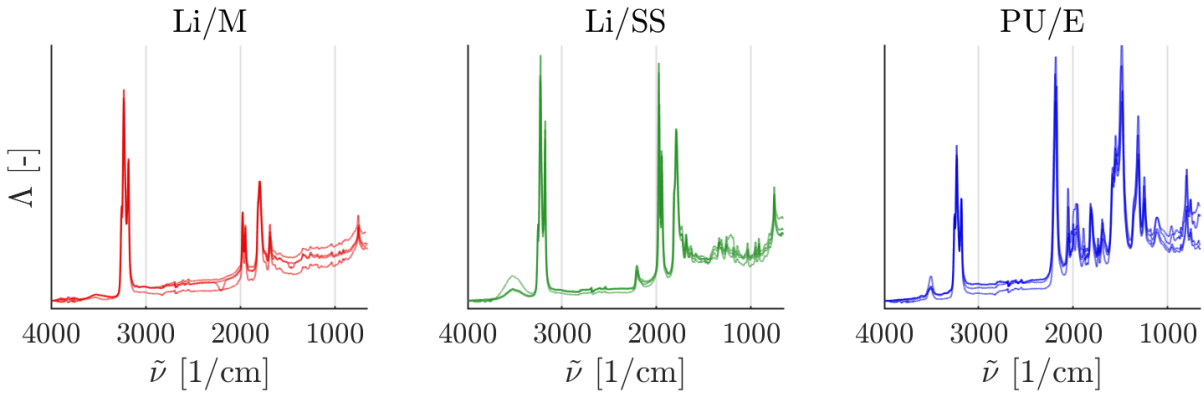

Figure 5.7: The IR-spectra for the three greases, with the fresh and after three ageing intervals overlaid on one another. Λ is the absorbance and $\bar{\nu}$ is the wavenumber. The spectra show no significant deviation.

5.4 Grease properties/degradation measures

The five degradation parameters were experimentally measured for the three grease samples. These properties were measured for fresh samples, 10 days, 20 days and 30 days aged greases. A table of all the measured values can be found in Appendix C, Table C.1.

5.4.1 Bleed capacity measure d_b

The measured bleed capacity parameter is presented in Figure 5.8. The stain diameters measured for fresh grease samples corroborate the stain diameters measured by Hogenberk et al. [10].

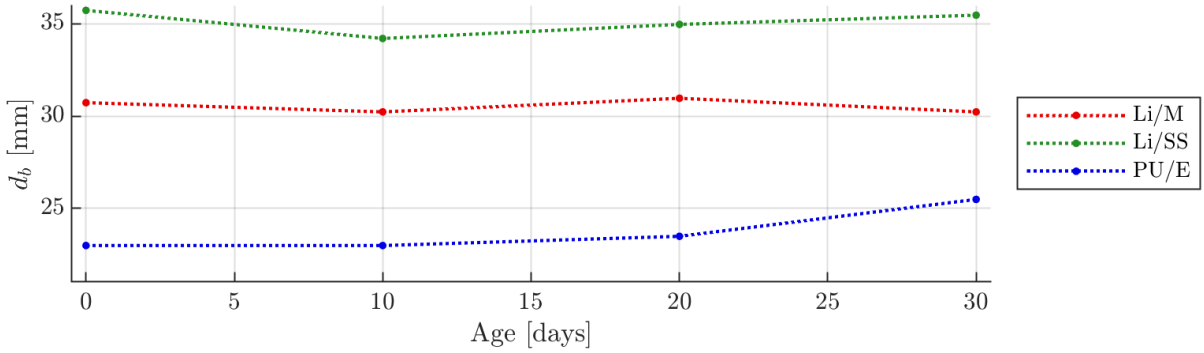

Figure 5.8: The bleed capacity measure, measured for fresh grease, as well as 10 days, 20 days and 30 days aged grease.

The bleed capacity measure can be seen to vary slightly for both Li/M and Li/SS. The former varies between 30.2 mm (10 & 30 days) and 31.0 mm (20 days), and the latter varies between 34.2 mm (10 days) and 35.7 mm (fresh). The changes in PU/E's bleed capacity seem to have a more monotonous trend, where the lowest measured value is 22.0 mm (fresh and 10 days) and it increases to 25.5 mm (30 days).

Similar to the results observed by Hogenberk et al. [10] who investigated the effect of mechanical degradation on the bleed capacity measure and permeability, no strong trends can be observed in the bleed capacity measure.

5.4.2 Specific heat capacity c

The specific heat capacity measurements are plotted in Figure 5.9.

The specific heat capacity of Li/M shows a sharp increase from its fresh grease value of 1680 J/kgK to a value of 2220 J/kgK at 10 days. After this peak, it drops consistently to a value of 1810 J/kgK at 30 days. Li/SS starts out with the highest specific heat capacity of the three greases, at 2660 J/kgK. As it ages, the specific heat capacity declines until 20 days. After 20 days, it increases again as it reaches 30 days. PU/E starts with the second highest specific heat capacity, at 2430 J/kgK, but ends with the lowest heat capacity, at 1660 J/kgK. The decline of the specific heat capacity seems steady, slowing down between 10 and 20 days.

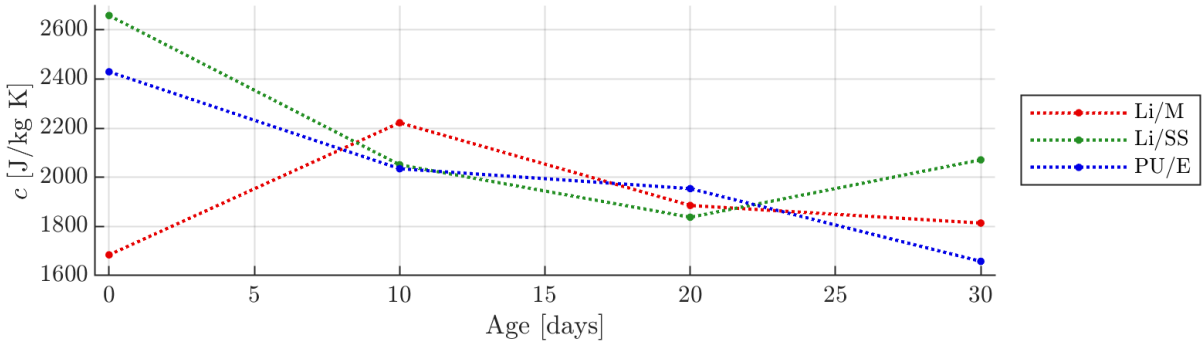

Figure 5.9: The specific heat capacity, measured for fresh grease, and after ageing for 10 days, 20 days and 30 days.

5.4.3 Storage modulus G'

The storage modulus can be found in Figure 5.10.

The storage modulus of Li/M seems little affected between 0 and 10 days. The most drastic change is between 10 and 20 days, when the storage modulus reduces by 12%. At 30 days, the storage modulus is within 2 kPa of the initial value. Li/SS shows a clear increase in its storage modulus. Overall, the storage modulus increases by 54%, or by 28.5 kPa. PU/E shows the most interesting behaviour, where the storage modulus starts at 46.5 kPa and increases to 151.8 kPa in 10 days. This is an increase by a factor of 3.3. This behaviour could be described as the grease ”stiffening”. The storage modulus at 20 days is 46.1 kPa for PU/E, within 0.5 kPa of its fresh grease value.

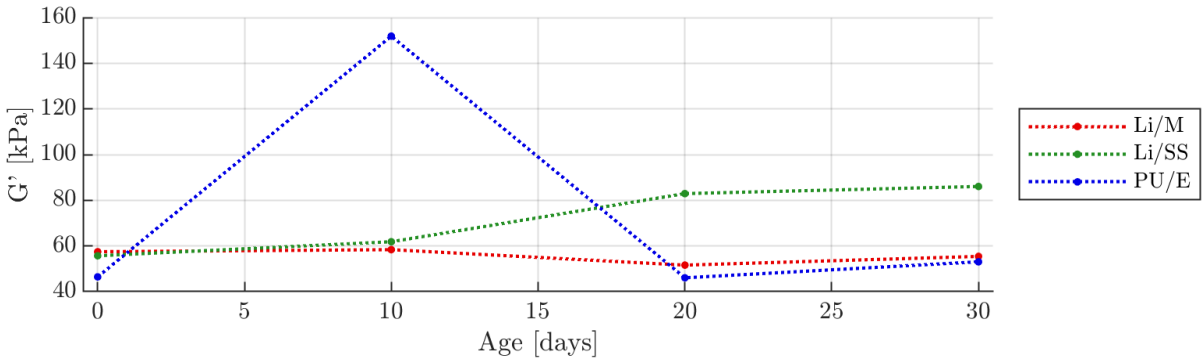

Figure 5.10: The storage modulus, measured for fresh grease, and after ageing for 10 days, 20 days and 30 days.

5.4.4 Thermal strain coefficient α_γ

The thermal strain coefficient measurements are presented in Figure 5.11.

Li/M has the highest thermal strain coefficient of all tested greases. The thermal strain coefficient increases by about 64% between 0 and 20 days. At 30 days, the thermal strain coefficient returns to 1.4 $1/\text{kK}$. Li/SS slightly increases at 10 days, but overall slowly reduces by 10% until 30 days. PU/E first reduces by 45%. After 10 days, it slowly recovers again to end up within 0.2 $1/\text{kK}$ of its original value.

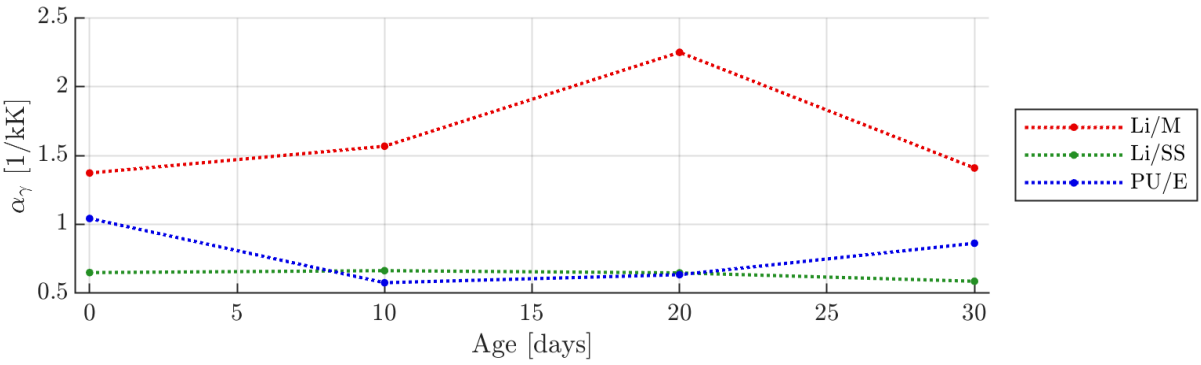

Figure 5.11: The thermal strain coefficient α_γ, measured for fresh grease, and after ageing for 10 days, 20 days and 30 days.

5.4.5 Yield stress τ_y

The yield stress measurements can be found in Figure 5.12.

Li/M's yield stress changes slightly in the first 10 days of ageing, after which it increases by 42% at 30 days. Li/SS initially rises by a factor of 3.1 at 10 days. Then it levels off between 10 and 20 days. At 30 days, it reduces again by 25.3 Pa compared to 20 days. PU/E shows the most interesting behaviour: it increases by a factor of 6.2 at 10 days. Then it reduces by 68.4 Pa between 10 and 20 days, and then increases by 73.0 Pa between 20 and 30 days. This makes for very erratic behaviour.

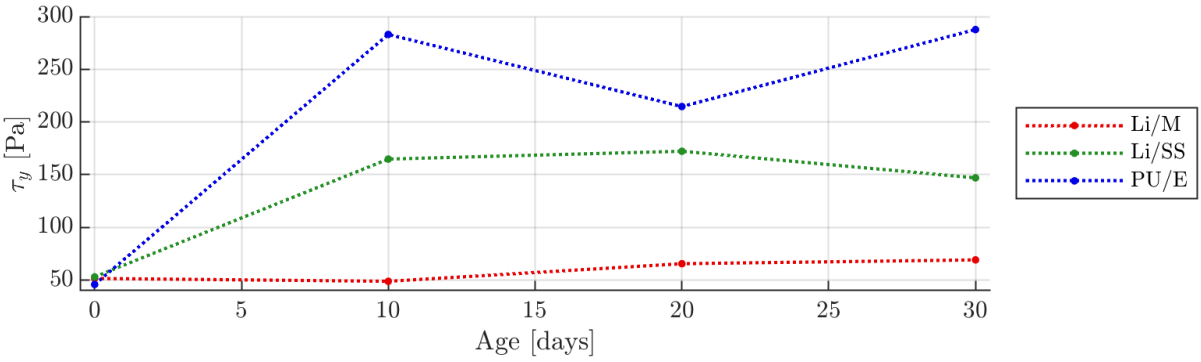

Figure 5.12: The yield stress, measured for fresh grease, and after ageing for 10 days, 20 days and 30 days.

Chapter 6

Thermal model of grease heating in an oven

Most studies involving oven heating of materials use oven temperature and time in the oven as independent variables which are correlated with observed degradation/changes in the materials. However, these studies yield qualitative results, without quantities for precise characterisation. In this study, grease temperature, which was not measured, is needed to compute the energy and entropy terms. In the absence of any known existing work detailing the heat transfer between the oven and the heated sample, this chapter develops a thermal model of oven heating.

The thermodynamic model for total entropy generation is first presented in Equation 2.23:

$$S' = \int_0^t \frac{cm}{T}\dot{T}\,dt - \int_0^t \frac{T_\infty - T}{TR_\theta}\,dt + \int_0^t \frac{L}{T}\dot{m}\,dt. \tag{6.1}$$

This model will be applied to the thermal degradation of grease ageing in the oven. The next challenge is to characterise all its components: time t, specific heat capacity c, sample mass m, sample temperature T, oven temperature T_∞, equivalent thermal resistance R_θ and the LHE L. A summary of how and where these properties are characterised can be found in Table 6.1.

The time t follows from when samples are inserted into or removed from the oven and the temperature of the oven (T_∞) is measured with 90 s intervals, see Section 5.1.1). The LHE L is assumed constant and its value can be found in Section 5.2.

A heat transfer model of the sample in the oven will be built to define R_θ. Similar to Section 3.3.1.2, the equivalent thermal resistance is a function of oven temperature and grease temperature. The grease temperature T is not measured, so the heat transfer model is used, in conjunction with the energy balance of Equation 2.10, to model the sample temperature during ageing.

As grease degrades, some of its material properties will change. This suggests the specific heat capacity c will change over time. The mass and mass derivative, m and $\dot{m}$ respectively, likewise change over time. These three properties will therefore be considered transient.

6.1 Transient material properties

Throughout the ageing procedure, the specific heat capacity and mass of the sample will change. These kinds of transient behaviours are often omitted. However, to create a more accurate characterisation of entropy generation, an effort is made to model these transient material properties.

Table 6.1: A summary of the environmental and system properties that need to be characterised to complete the thermodynamic model, along with the origin of their characterisation and where the characterisation can be found in more detail.

Property		Characterisation	Found in...
Time	t	Measured	Section 5.1.1.
Specific heat capacity	c	Interpolated using measurements	Section 6.1.1
Mass	m, $\dot{m}$	Interpolated using measurements	Section 6.1.2
Grease temperature	T	Modelled using energy balance	Section 6.3
Oven temperature	T_∞	Measured	Section 5.1.1
Thermal resistance	R_θ	Modelled using heat transfer	Section 6.2
Latent heat of evap.	L	Measured	Section 5.2

6.1.1 Transient specific heat capacity

The specific heat capacity sees quite drastic changes, exemplified by Figure 5.9. These are taken into account by interpolating between the measurement points.

Heat capacity is primarily a function of entropy generation/degradation. As entropy generated is also a function of time, it is proposed that the heat capacity can be interpolated over time. The exact shape of the specific heat capacity between the measurement points is impossible to know at this point. It is therefore assumed that the heat capacity can be described by a smooth, continuous function, differentiable in time, that passes through the measurement points.

This is done with the Matlab [49] function `makima`. This is a modified Akima fit, which provides cubic interpolation with continuous first-order derivatives. A function is created to evaluate the specific heat capacity for any time t (within the ageing period), with the four measured values as control points. The resulting function is plotted in Figure 6.1.

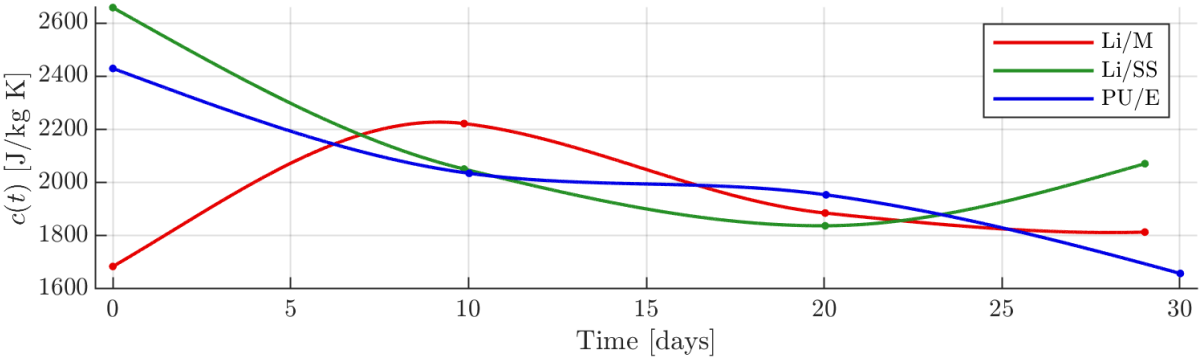

Figure 6.1: The interpolation of the specific heat capacity using Matlab's [49] `makima` function. The points denote the measured values at each ageing interval.

6.1.2 Transient mass and mass change

The mass is interpolated using methods that correlate closely with the evaporation kinetics. At the basis of finding the latent heat of evaporation, lies the single-step kinematic equation [51,58]:

$$\frac{d\alpha}{dt} = k(T)f(\alpha) \tag{6.2}$$

where, based on the earlier employed non-isothermal analyses [51–53]:

$$f(\alpha) = (1-\alpha), \qquad k(T) = A_{Arr}e^{-\frac{L}{R_s T}}. \tag{6.3}$$

Tarrío-Saavedra et al. [58] introduced a generalised logistics curve,

$$\alpha(t) = \frac{1}{\left(1 + ae^{-b(t+t_0)}\right)^{1/a}}, \tag{6.4}$$

where a, b and t_0 are coefficients that control the shape of the logistics curve. This function is able to model first-order thermal decomposition reactions with high accuracy [58]. The time derivative of the logistics curve is:

$$\frac{d\alpha}{dt} = \frac{be^{-b(t+t_0)}}{\left(1 + ae^{-b(t+t_0)}\right)^{1/a+1}}. \tag{6.5}$$

Burnham [59] studied the application of logistics curves in modelling chemical reactions. They conclude only simplest reaction can be modelled with the logistics curve approach. They suggest the logistics curve is too inflexible to accurately model more complex reactions and is therefore inferior to the extended Prout-Tompskins model. Burnham [59] names auto-catalytic and nucleation growth to be cases where it could be applied. For further analysis, results presented by Tarrío-Saavedra et al. [58] provide confidence that evaporation modelled by a first-order reaction (in accordance with Chatterjee et al. [52]), is sufficiently accurately modelled by a logistics curve.

The function α is introduced, which ranges from zero, meaning nothing has evaporated, to one, meaning everything that can evaporate has evaporated. When base oil evaporates, the heavier compounds in base oil will remain. The mass measurements will be normalised to the initial mass, so that the relative mass m_r is

$$m_r(t) = m(t)/m_i. \tag{6.6}$$

Where m_i is the initial mass. From this follows, after defining the final mass as $m_f = m_r(t_f) = m_{rf}$,

$$\alpha(t) = \frac{m_i - m(t)}{m_i - m_f} = \frac{1 - m_r(t)}{1 - m_{rf}}. \tag{6.7}$$

Here, m_r is the relative mass of the sample and m_{rf} is the final relative mass. The general logistics curve in Equation 6.4 can then be fitted to the discrete data points calculated using Equation 6.7. The fitted $\alpha(t)$ curve can then be used to calculate the relative mass at any time according to

$$m_r(t) = 1 - (1 - m_{rf})\alpha(t), \tag{6.8}$$

and the true mass can be calculated by multiplying $m_r(t)$ with the (characteristic) initial mass,

$$m(t) = m_i - (m_i - m_f)\alpha(t). \tag{6.9}$$

Finally, the mass loss rate is

$$\frac{dm}{dt}(t) = -(m_i - m_f)\frac{d\alpha}{dt}(t) \tag{6.10}$$

The resulting mass and the mass change rate are plotted in Figure 6.2. The characteristic mass, that is the average starting sample mass of the sample, is 7.8 g for Li/M, 7.3 g for Li/SS and 8.7 g for PU/E.

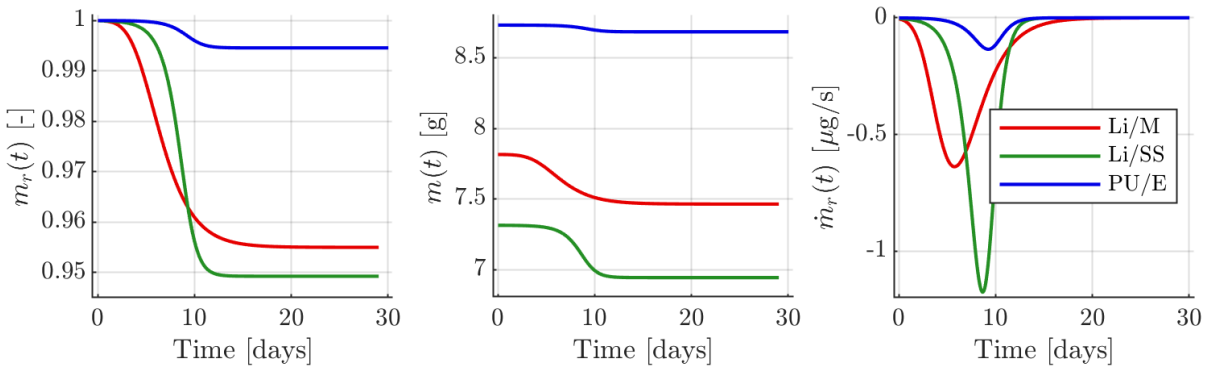

Figure 6.2: The interpolation of mass and mass loss rate during ageing. The left-hand plot shows the relative mass, the middle plot shows the total mass and the right-hand plot shows the mass loss rate. The dots represent the measured sample masses.

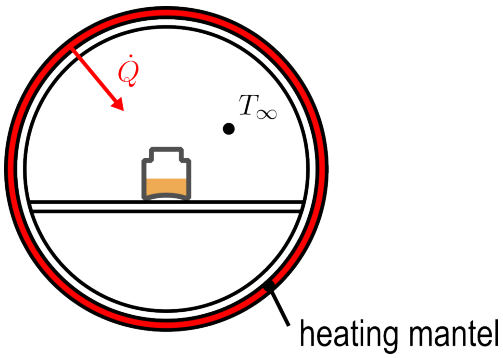

Figure 6.3: A simple diagram of the oven situation. Samples are placed on a metal plate in the oven. Heat is supplied by a heating mantel, which surrounds the oven.

6.2 Heat transfer model

The grease samples are aged in borosilicate glass bottles. These are then placed on a plate in the oven. Figure 6.3 shows a simple schematic of how the oven is set up and how heat is supplied to the oven.

Figure 6.4 shows the sample conditions in more detail. It is assumed the bottom of the glass bottle is insulated. Heat can then enter the sample via two pathways: through the wall of the bottle and the top of the sample. The resulting thermal resistance network can be found in the middle of Figure 6.4. It is assumed that only one-dimensional heat transfer occurs. The right-hand figure of Figure 6.4 shows the geometry of the simplified sample.

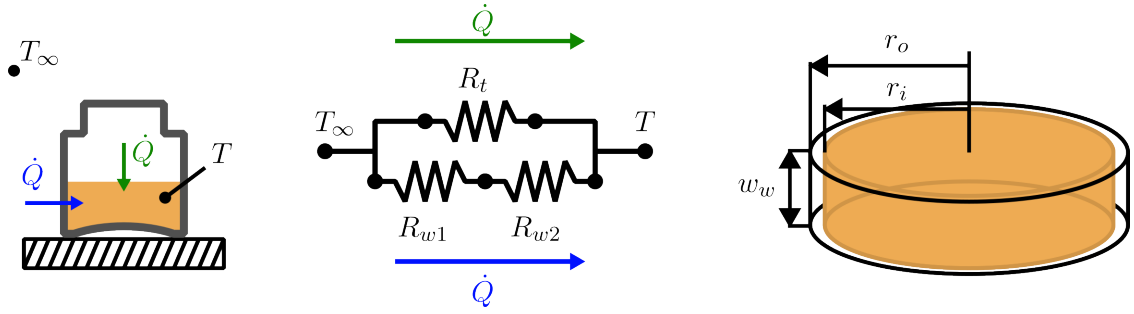

Figure 6.4: A diagram of the heat flows entering the greases sample (left), the thermal resistance network that results from it (middle) and a simple diagram of the grease puck (right).

The atmosphere of the oven is assumed stagnant: the oven is closed off airtight without any active circulation. Therefore, the dominant convection type is natural convection. The thermal resistance of the top of the sample is

$$R_t = \frac{1}{A_t h_t}. \tag{6.11}$$

where the top surface of the grease sample is $A_t = 2\pi r_i^2$. The thermal resistance of the wall of the sample exposed to the oven atmosphere is

$$R_{w1} = \frac{1}{h_w A_w}, \tag{6.12}$$

where the surface area of the wall of the bottle enclosing the grease is $A_w = 2\pi r_o w_w$. The conduction through the glass of the bottle is characterised by heat conduction through a multi-layered cylinder:

$$R_{w2} = \frac{\ln r_o/r_i}{2\pi w_w k_b}. \tag{6.13}$$

The thermal conductivity of borosilicate glass k_b is 1.2 W/mK [48]. The total thermal resistance of the wall is then the sum of the two thermal resistances:

$$R_w = R_{w1} + R_{w2}. \tag{6.14}$$

The equivalent thermal resistance of the sample is then

$$R_\theta = \frac{R_t R_w}{R_t + R_w}. \tag{6.15}$$

The next step is to characterise the convective heat transfer coefficient. First, a relation for the Nusselt number has to be found. For the top of the sample, the relation for a horizontal flat plate seems most appropriate, and for walls of the bottle, the relation for a vertical flat plate seems most appropriate [48]. The corresponding relations are

$$\mathrm{Nu}_{t\,\mathrm{HM}} = 0.59\mathrm{Ra}_{r_i/2}^{1/4}, \qquad \mathrm{Nu}_{w\,\mathrm{HM}} = 0.59\mathrm{Ra}_{w_w}^{1/4}, \tag{6.16}$$

for the top and walls of the sample respectively. These relations are only applicable for Rayleigh numbers larger than 10^4. The Nusselt number formulation will be extended to far lower values using the experimental work by Suriano and Yang [60]. Alongside data they collected from literature, they performed their own experiments, finding Nusselt numbers all the way down to a Rayleigh number of zero. The data starts to deviate at higher Rayleigh numbers, so, to ensure continuity, the assumption is made that the Nusselt number at low Rayleigh numbers should be continuous with the Nusselt number at "high" ($> 10^4$) Rayleigh numbers (provided in Equation 6.16).

A similar function was chosen to those presented in Equation 6.16, with an added constant to allow for non-zero Nusselt numbers at $\mathrm{Ra} = 0$:

$$\mathrm{Nu} = c_1 + c_2\mathrm{Ra}^n. \tag{6.17}$$

An initial fit is made to the data provided in Suriano and Yang [60], which results in

$$\mathrm{Nu}_{ti} = 1.07 + 0.168\mathrm{Ra}^{0.492}, \qquad \mathrm{Nu}_{wi} = 0.856 + 0.315\mathrm{Ra}^{0.356}. \tag{6.18}$$

These functions are plotted alongside the relevant data points in Figure 6.5. The R^2 of this fit is considered to be sufficient.

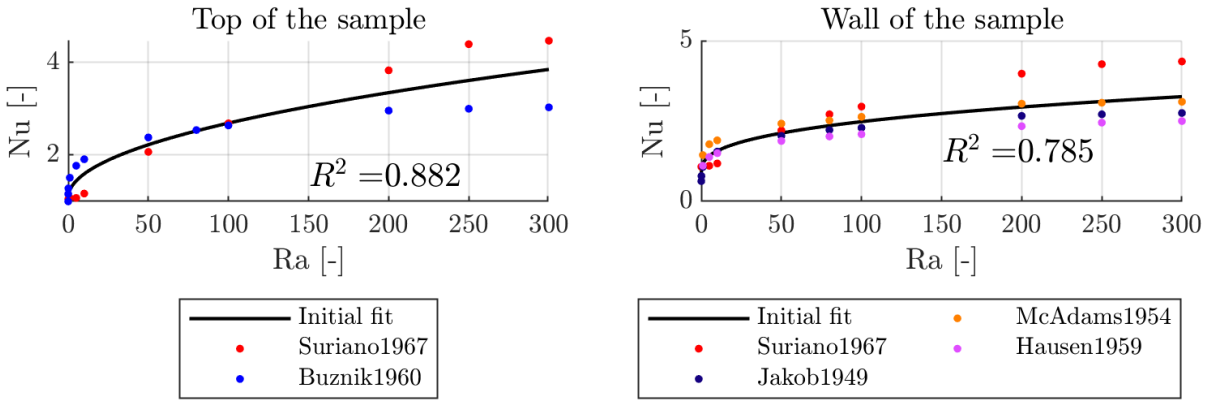

Figure 6.5: The initial fit of the Nusselt number for low-range Rayleigh numbers, based on the data provided by Suriano and Yang [60].

The relations of Equation 6.18 are then sampled for 100 points in the range $0 \leq \text{Ra} \leq 300$, where 300 is the highest Rayleigh number found in the data set. Likewise, Equation 6.16 is sampled 100 times in the range of $10^4 \leq \text{Ra} \leq 10^5$. This "resampling" method should mean both datasets should have about an equal effect on the final fit. Earlier attempts found the resulting fit depended heavily on the number of data points chosen for the higher Nusselt numbers. Equation 6.17 is fit to the 200 data points. To ensure the (near) zero behaviour is close to that of the initial fit, the first coefficient c_1 is set equal to its value in the initial fit. This results in

$$\text{Nu}_t = 1.07 + 0.567\text{Ra}^{0.242}, \qquad \text{Nu}_w = 0.856 + 0.515\text{Ra}^{0.253}, \tag{6.19}$$

for the top of the sample and the wall of the sample respectively. These new fits are plotted, alongside the initial fit to the data provided by Suriano and Yang [60] and the relations presented in Equation 6.16 [48], in Figure 6.6.

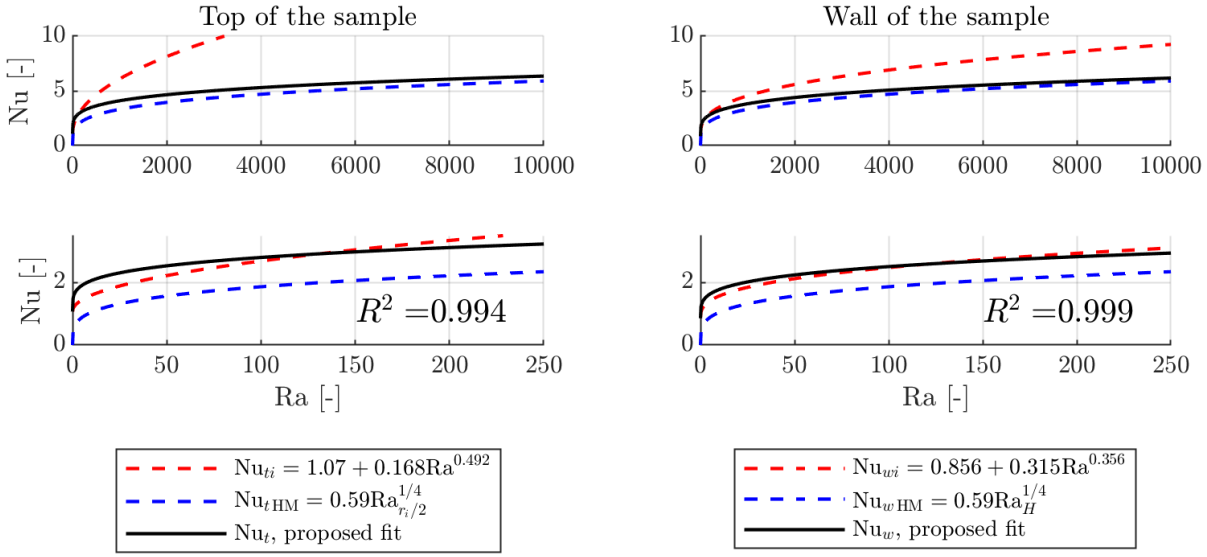

Figure 6.6: The proposed fit for the Nusselt number, plotted alongside the relations on which the fit is based. The R^2 norm for both combined fits is larger than 0.99, so the fit is considered of sufficient quality.

The properties of the oven atmosphere — which is nitrogen gas — are regarded as functions of temperature. This means the dimensionless numbers are also implicitly a function of temperatures. The material properties are plotted in Figure 6.7, where the properties are interpolated between tabulated values [48].

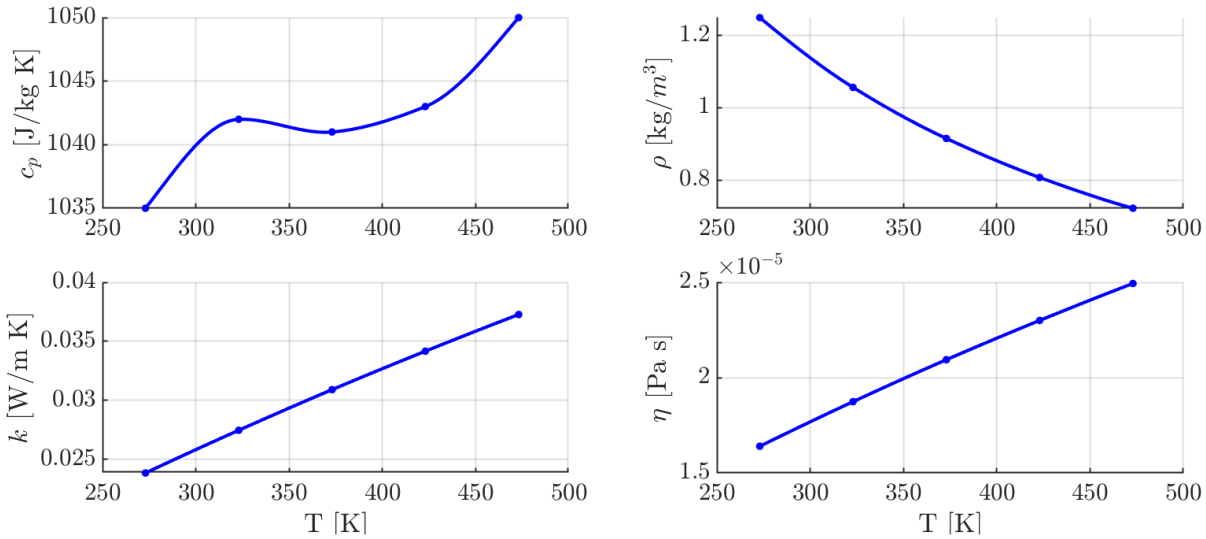

Figure 6.7: The temperature-dependent material properties of nitrogen gas. The values of nitrogen gas are tabulated [48] and interpolated using Matlab's [49] `makima` function.

The Nusselt number can now be evaluated for every temperature combination of the grease sample T and the oven atmosphere temperature T_∞. The result is plotted in Figure 6.8 for the top of the sample and Figure 6.9 for the sides. From the Nusselt numbers, the convective heat transfer coefficient can be calculated:

$$h_t(T, T_\infty) = \frac{k_{\mathsf{N_2}}(T, T_\infty)\,\mathsf{Nu}_t(T, T_\infty)}{r_i/2}, \qquad h_w(T, T_\infty) = \frac{k_{\mathsf{N_2}}(T, T_\infty)\,\mathsf{Nu}_w(T, T_\infty)}{w_w}. \tag{6.20}$$

Substitution into the equivalent thermal resistance of the network, shown in Equation 6.15, yields a temperature dependent equivalent thermal resistance $R_\theta(T, T_\infty)$. This is also plotted as a function of temperature in Figure 6.10.

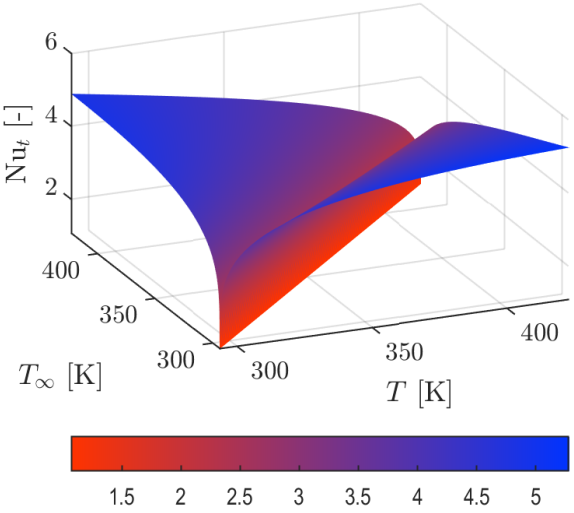

Figure 6.8: The Nusselt number for the horizontal top of the grease sample.

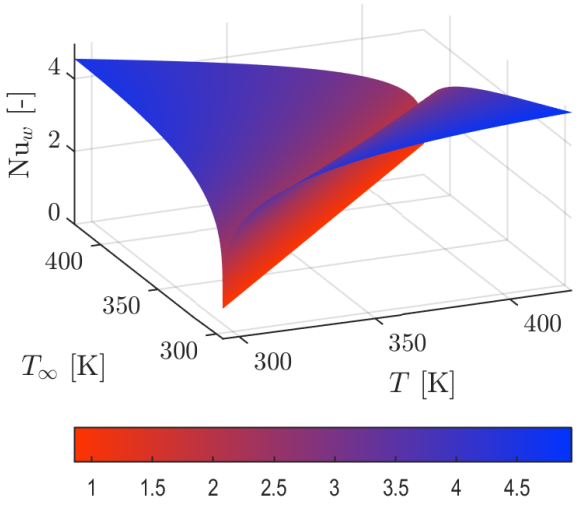

Figure 6.9: The Nusselt number for the vertical walls of the grease sample.

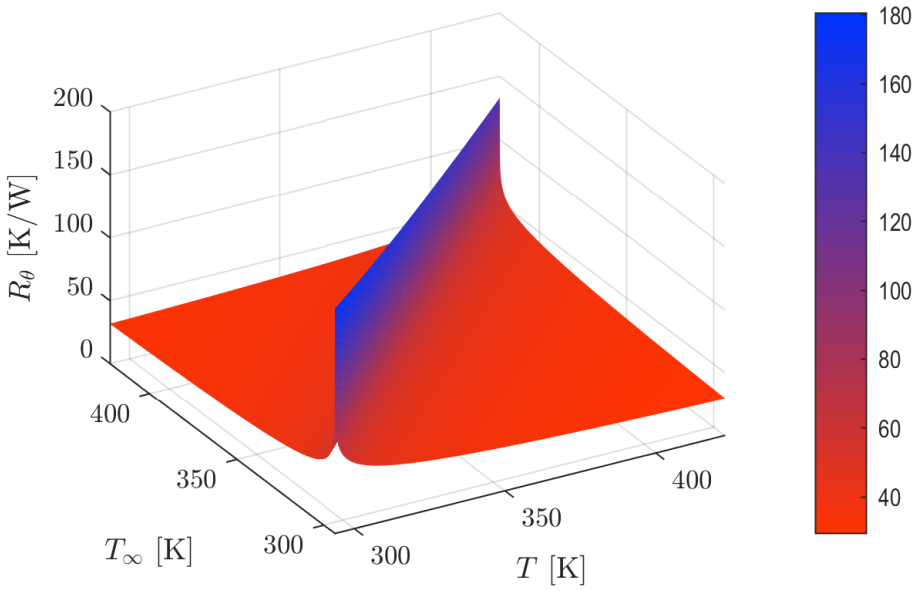

Figure 6.10: The temperature dependent total thermal resistance R_θ of the grease sample.

6.3 Estimation of grease sample temperature

The temperature of the grease was not recorded. Therefore it has been modelled using the oven temperature T_∞, equivalent thermal resistance and energy balance. The energy balance was first presented in Equation 2.10:

$$\frac{T_\infty - T}{R_\theta} = cm\dot{T} + L\dot{m} - T\dot{S}'. \tag{6.21}$$

The dissipated energy will be neglected when calculating the temperature, as the energy dissipated is expected to have little effect on the temperature of the grease in 90 second intervals.

Because of the long time step of 90 seconds between each measurement point, using a forward Euler method will not yield great results. This problem is instead approached as a transient heat conduction problem [48]. Such an approach will see the grease temperature T asymptotically reach the oven temperature T_∞ and will therefore behave better for long time steps.

This method is typically used to set initial conditions once and observe the evolution of the system temperature T. However, this application consists of changing ambient temperatures, material properties and thermal conduction. This can be solved by letting each 90 second interval be a new transient heat conduction problem. For each step, the heat capacity (c), mass (m), mass change rate ($\dot{m}$) and thermal resistance ($R_\theta(T, T_\infty)$) are updated. The ambient temperature T_∞ is set to the current oven temperature and the initial temperature of the grease is set to the previously calculated grease temperature. Then the grease temperature T is calculated after 90 seconds pass. Note that within these 90 seconds, all but the grease temperature T is constant.

This approach assumes the grease to be a lumped system. This was verified using the Biot number. The Biot number crossed the limit when the grease temperature approached the oven temperature. However, in those conditions, the temperature gradient within the grease will be small anyway.

6.3.1 Solution to the transient grease temperature

Next, a solution is going to be investigated for Equation 6.21. The derivation of the typical transient heat conduction problem is closely followed [48], but is also expanded with evaporation.

Starting from Equation 6.21, where the dissipated energy is omitted:

$$\frac{T_\infty - T(t)}{R_\theta} = cm\frac{dT}{dt}(t) + L\dot{m}. \tag{6.22}$$

One can define

$$\Theta = T(t) - T_\infty, \qquad \dot{\Theta} = \frac{dT}{dt}(t), \tag{6.23}$$

which after substitution yields

$$-\frac{\Theta}{R_\theta} = cm\dot{\Theta} + L\dot{m}. \tag{6.24}$$

Next, bring all Θ-terms to the left-hand side and free up the derivative of Θ;

$$\dot{\Theta} + \frac{\Theta}{cmR_\theta} = -\frac{L\dot{m}}{cm}. \tag{6.25}$$

An exponential function could be a solution to Θ, much like the common transient heat conduction problem [48]. So, try the following solution:

$$\Theta = ae^{-\omega t}, \qquad \dot{\Theta} = -a\omega e^{-\omega t}. \tag{6.26}$$

At time $t = 0$, one can recognise that $\Theta = T(0) - T_\infty$. Define the initial temperature as $T_i = T(0)$. Substitution yields

$$a = T_i - T_\infty. \tag{6.27}$$

Then, the substitution of Equation 6.26 into Equation 6.25 yields

$$a\left(-\omega + \frac{1}{cmR_\theta}\right)e^{-\omega t} = -\frac{L\dot{m}}{cm} \tag{6.28}$$

Because this equation should hold for $t \geq 0$, one can set $t = 0$ and obtain

$$\omega = \frac{1}{cmR_\theta} + \frac{L\dot{m}}{acm}. \tag{6.29}$$

Substitution of a (Equation 6.27) results in

$$\omega = \frac{1}{cmR_\theta} + \frac{L\dot{m}}{(T_i - T_\infty)cm} \tag{6.30}$$

for the exponent of the solution. Equations 6.23 and 6.26 results in the expression:

$$\Theta = T(t) - T_\infty = ae^{-\omega t} \tag{6.31}$$

where after dividing by a and substituting the value of a (again, Equation 6.27), one finds

$$\frac{T(t) - T_\infty}{T_i - T_\infty} = e^{-\omega t}. \tag{6.32}$$

The definition of ω will be

$$\omega \equiv \frac{1}{cmR_\theta} + \frac{L\dot{m}}{(T_i - T_\infty)cm}. \tag{6.33}$$

This function describes the temperature of the grease as a function of time. This function is constrained for the range of $0 \leq t \leq 90$.

6.3.2 Numerical simulation of the grease temperature

Equations 6.32 and 6.33 show how the grease temperature can be calculated within the time step of 90 seconds. To make use of these functions for the whole temperature range, an algorithm is constructed to calculate the grease temperature. For reference, a typical data set would contain about 29000 data points, of which each point must be evaluated sequentially.

As mentioned at the beginning of this chapter, the specific heat capacity, mass, mass change rate, ambient temperature and thermal resistance have to be retrieved at every time step. For specific heat capacity, mass and mass change rate this is an easy task, as the interpolation functions can be simply called with the current time. Ambient temperature can also be read from the measurement data for the corresponding time.

Thermal resistance is more difficult to retrieve quickly, as it was made a function of temperature. One could calculate the long chain of functions all the way down to the temperature dependent dimensionless numbers. There is a more efficient method. The grease starts at room temperature and will never pass the maximum temperature of the oven. Therefore, all possible combinations of grease temperatures and ambient temperatures can be used to precalculating all values of the thermal resistance. During execution of the algorithm, the correct value can be looked up using the current grease and ambient temperature.

The last thing to define is the initial conditions of the simulation; the starting temperature of the grease. This was assumed to be 20.5°C, equal to the lab temperature displayed on the climate control unit.

Equations 6.32 and 6.33 are adapted to be evaluated in using discrete values. To this end, the index p is defined, which starts at $p = 1$ and ends at the final data point $p = m$. Evaluating the interpolation functions for time t_p, yields c_p, m_p and $\dot{m}_p$. The ambient temperature is retrieved for time t_p, as well as the grease temperature, yielding $T_{\infty p}$ and T_p respectively. These are used to look up the appropriate thermal resistance, yielding $R_{\Theta p} = R_{\Theta}(T_p, T_{\infty p})$.

Substituting these discrete values into Equation 6.33 allows the exponent to be calculated

$$\omega_p = \frac{1}{c_p m_p R_{\theta p}} + \frac{L\dot{m}_p}{(T_{ip} - T_{\infty p}) c_p m_p}. \tag{6.34}$$

With this exponent, Equation 6.32 is evaluated after the constant time step of $\Delta t = 90$ s, to obtain the grease temperature for the next time step:

$$T_{p+1} = (T_{ip} - T_{\infty p})\, e^{-\omega_p \Delta t} + T_{\infty p}. \tag{6.35}$$

Figure 6.11 shows the temperature of the greases in colour, superimposed on the oven temperature in black. With these temperatures, the entropies are calculated in Chapter 7. Figure 6.12 shows the used algorithm visually.

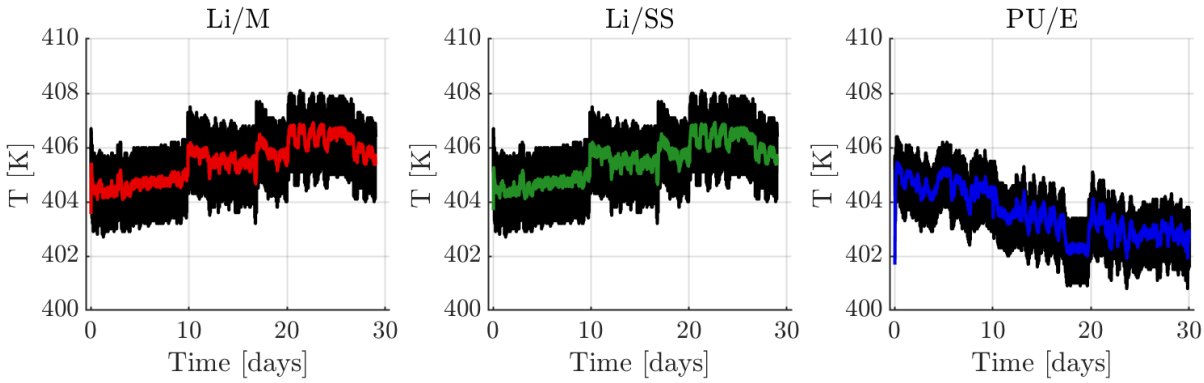

Figure 6.11: The calculated grease temperature T in colour, plotted over the measured temperature T_∞ of the oven in black. The estimated temperature behaves akin to a moving average, where the sample temperature follows the low-frequency behaviour of the temperature.

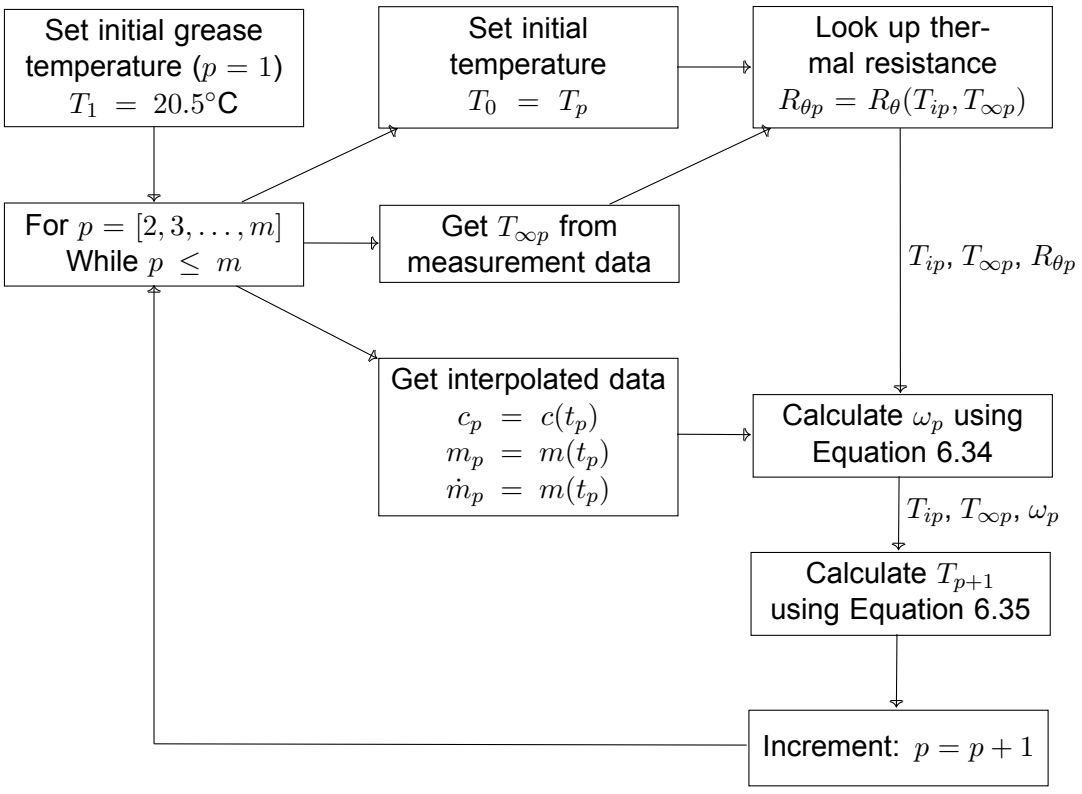

Figure 6.12: The algorithm designed to calculate the grease temperature based on measurement data, interpolated material properties and temperature dependent thermal resistance. The typical execution time of this algorithm for one grease is sub 100 ms.

Chapter 7

Grease degradation model

In this chapter, the active mechanisms during thermal ageing are discussed using energies and entropies, followed by correlation with the degradation measures to describe the effects of the thermal mechanisms on grease degradation.

7.1 Thermal energy dissipated during ageing

The energy balance is presented in Equation 2.15, rendering dissipated energy $E_d = E_T + E_m - Q$. The dissipated energy is expected to be small compared to the other terms in the energy balance.

7.1.1 Energy by mechanism/source

The energy contributions from the different mechanisms/sources are plotted in Figure 7.1. One behaviour all three greases share is the initial jump in both the heat flux Q and the heat storage energy E_T. Though this jump appears practically instant on these time scales, it takes about an hour and a half. They indicate the energy needed to bring the greases to the oven temperature.

The Li/SS and Li/M greases show two phases in their energy profile: from 0 days to 10 days and from 10 days to 30 days. This first phase, from 0 days to 10 days, sees a steady accumulation of heat flux and almost all of the evaporation energy. The accumulation of heat flux Q facilitates evaporation of material, in addition to holding samples at near oven temperature.

After evaporation completes, the evaporation energy remains constant. There are still changes in the heat storage energy. These changes can be explained via two phenomena: the changes in temperature profiles and the changes in grease heat capacities. For context, refer to Figure 6.1 for the specific heat capacities of Li/SS and Li/M. The temperatures of the oven and the greases increase throughout the ageing process, as shown in Figure 6.11. This means more heat is added to the grease (via Q) and more heat is stored (via E_T), which results in a slight upward trend in the accumulated heat flux and stored heat energy. Because both greases have similar temperature profiles, the deviation in energy stored can be mostly attributed to the difference in behaviour of the specific heat capacities and slight differences in their transient masses m_t. However, the differences in both greases' Q and E_T profiles are small, with the effect of temperature dominant on the trends.

For PU/E grease, the energy profiles are very different. This grease experiences far less evaporation compared to Li/SS and Li/M. The effect of evaporation on PU/E's accumulated heat flux (Q) and heat storage energy (E_T) is therefore less visible compared to the effects on the other greases. Again, there are two reasons for the steady decrease of the heat flux and heat storage energy: the tendencies of the grease temperature and the change in heat capacity (again, refer to Figure 6.1 for the specific heat capacity and Figure 6.11 for the grease temperatures). For both, the trend is downwards. Interestingly, because the temperature and

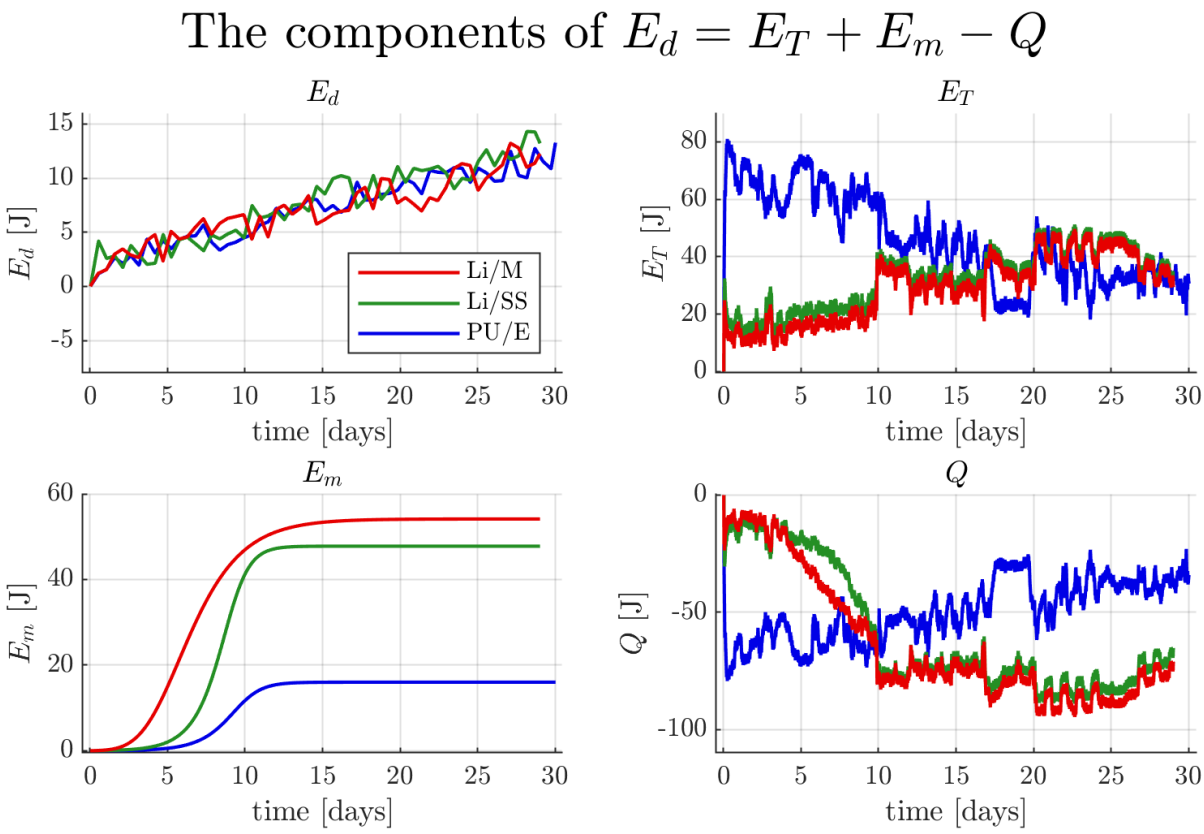

Figure 7.1: The individual thermal mechanisms in the energy balance $E_d = E_T + E_m - Q$. Both heat storage energy (E_T) and evaporation energy (E_m) contribute positively to the dissipated energy, while heat transfer contributes negatively. The instantaneous dissipated energy E_d is quite noisy, so it is filtered here: every 500$^{\text{th}}$ point is plotted.

specific heat capacity of the grease are both on a downwards trend, the heat storage energy E_T reduces. This is likely due to the unsteady heating controls of the oven.

7.1.2 Dissipated energy

It is supposed that the microstructural changes the greases undergo during ageing, which then results in degradation, take some small amount of energy. The energy dissipated is plotted again in Figure 7.2, to allow for closer inspection. Figure 7.2 shows a constantly rising trend in the amount of energy dissipated. This is expected for the imperfect (irreversible) process of thermal ageing.

7.2 Entropy generation during thermal ageing

After defining the thermal model of the grease experiencing ageing, the generated entropy can be calculated using Equation 2.23:

$$S'(t) = S_T(t) - S_Q(t) + S_m(t). \tag{7.1}$$

and each source contributes according to Equations 2.20, 2.21 and 2.22:

$$S_T(t) = \int_0^t \frac{cm}{T}\dot{T}\,dt, \qquad S_Q(t) = \int_0^t \frac{T_\infty - T}{TR_\theta}\,dt, \qquad S_m(t) = \int_0^t \frac{L}{T}\dot{m}\,dt. \tag{7.2}$$

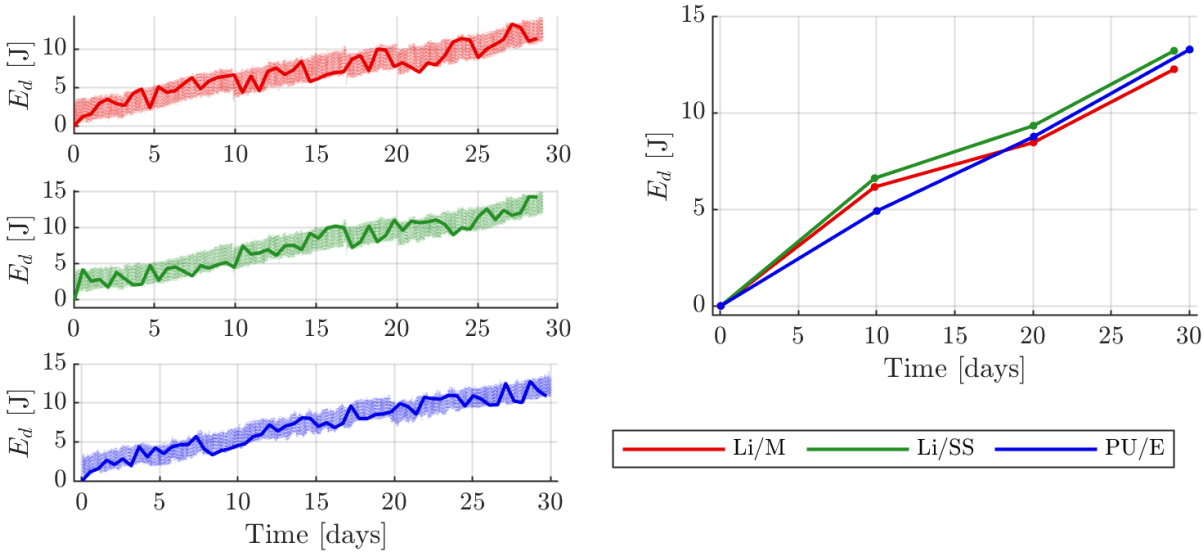

Figure 7.2: The energy dissipated in the grease samples during ageing. The left-hand figures show the dissipation for each grease separately, where the filtered instantaneous profile is plotted over the low-opacity unfiltered instantaneous dissipated energy. The right-hand plot shows the discrete energy dissipated; at 10 days, 20 days and 30 days. Both plots show there is a clear increasing trend in the dissipated energy as anticipated by theoretical formulations.

As in the case of energy dissipation, note that due to the rearrangement (in Chapter 2) which rendered the unknown entropy generation as the subject of Equation 7.1, S_Q is here negative for heat flow into the grease and S_m is positive for evaporation out of the grease, respectively. With the values for temperatures, specific heat capacity, mass and LHE established in Chapter 6, the entropies will be calculated.

7.2.1 Entropy by mechanism/source

The first step is investigating the entropy contributions of each of the three mechanisms: heat storage entropy (S_T), heat transfer/flux entropy (S_Q) and evaporation entropy (S_m). These are plotted in Figure 7.3. The tabulated values can be found in Appendix C, Table C.2.

Before discussing the entropy contributed by each source, it should be noted that the source entropies are not generated. That is, the three mechanisms mentioned are either entropy flows (S_Q and S_m) or changes (S_T). The generated entropy (S'), which follows from Equation 7.1, is the sum of these three active mechanisms, which will result in a non-negative monotonous value, per the second law of thermodynamics.

The entropy contributions follow the respective energies, so the behaviours can be explained by the same phenomena. For all the greases, the heat storage entropy S_T appears to spike almost instantaneously when the grease rapidly heats up to the oven temperature. After this initial rise, the heat storage entropy changes due to trends in the grease temperature and changes in heat capacity. A clear separation between Li/SS, Li/M and PU/E profiles indicate that the temperature profiles of the greases is the dominant factor. Note that with entropy, the energies are further divided by instantaneous temperature, magnifying the temperature effects on the observed profiles.

For Li/SS and Li/M, after the initial spike, the heat storage entropy slowly climbs until dropping at approximately 25 days. This drop is considered to be mostly driven by the temperatures of the oven and specific heat capacity reducing at 25 days. PU/E shows a constant and relatively steady drop in heat storage entropy after the initial spike. This is also the combined effect of heat capacity and grease temperature, both declining over the ageing procedure.

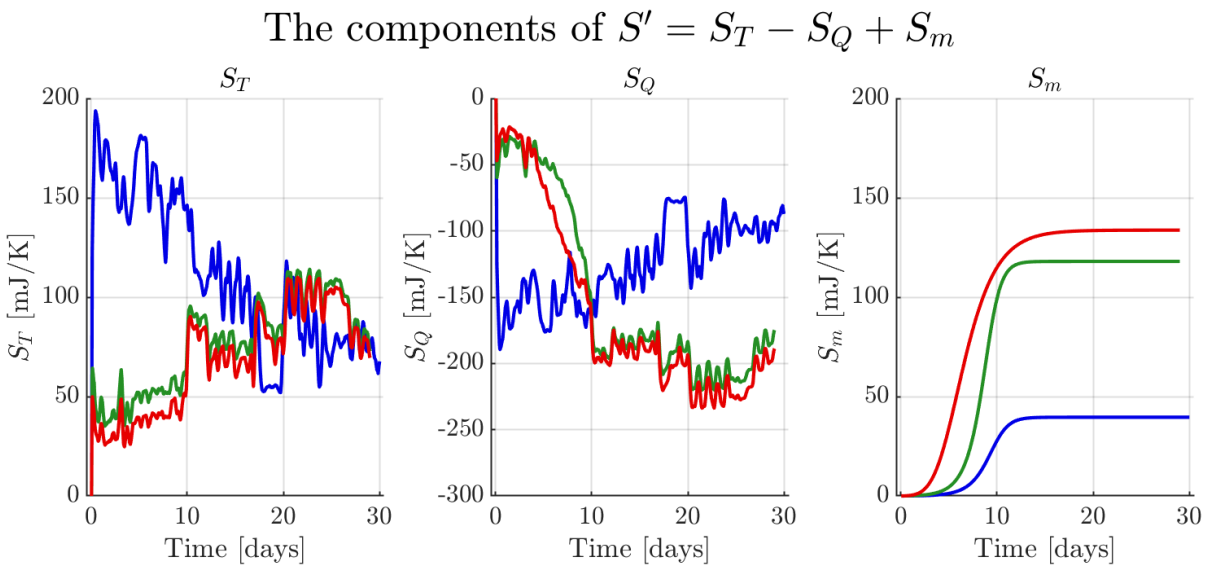

Figure 7.3: The entropy contributions by source. From left to right: the heat storage entropy S_T, heat transfer entropy S_Q and evaporation entropy S_m. The entropy contributions are plotted as they appear in the entropy balance with S_Q negative, see Equations 7.1 and 7.2.

The heat transfer entropy S_Q shows behaviour similar to the heat transfer Q in the energy balance. The heat transfer entropy rapidly increases in magnitude when evaporation is dominant, as this takes significant amounts of thermal energy. Therefore, a high heat flux is expected and, as a result, a large amount of entropy transfers into the grease via heat flux. The heat transfer entropy reduces in magnitude when evaporation ceases. After evaporation, the heat transfer entropy varies with the oven and grease temperatures.

The last source, evaporation entropy S_m, shows a rapid increase as material evaporates. As the evaporation process slows down, the accumulated entropy S_m also approaches a steady value.

7.2.2 Entropy generated

With the various contributing sources of entropy discussed, these mechanisms can be summed to obtain the generated entropy according to Equation 7.1. The result is presented in Figure 7.1. The tabulated values of the calculated entropies can be found in Appendix C, Table C.2.

First thing to note is the magnitude of the entropy contributions. All mechanisms are of the order of magnitude of 250 mJ/K. The generated entropy is an order of magnitude smaller; below 25 mJ/K. It is expected that for amounts of energy supplied to the greases discussed in Section 7.1, the amount of entropy generated should indeed be very small. With that in mind, the magnitude of the entropy generated is considered sufficiently accurate.

Furthermore, the total entropy generation of a system, like the thermally aged grease, should increase over time. Besides from the noisiness of the instantaneous entropy generation, the fact that the entropy generation overall increases leads to the conclusion that entropy generation is modelled to a satisfactory extent.

The entropy generation of Li/M and Li/SS level off between 10 and 20 days. This could be due to a steady state behaviour wherein the low evaporation during this period balanced the heat transfer entropy with the heat storage entropy.

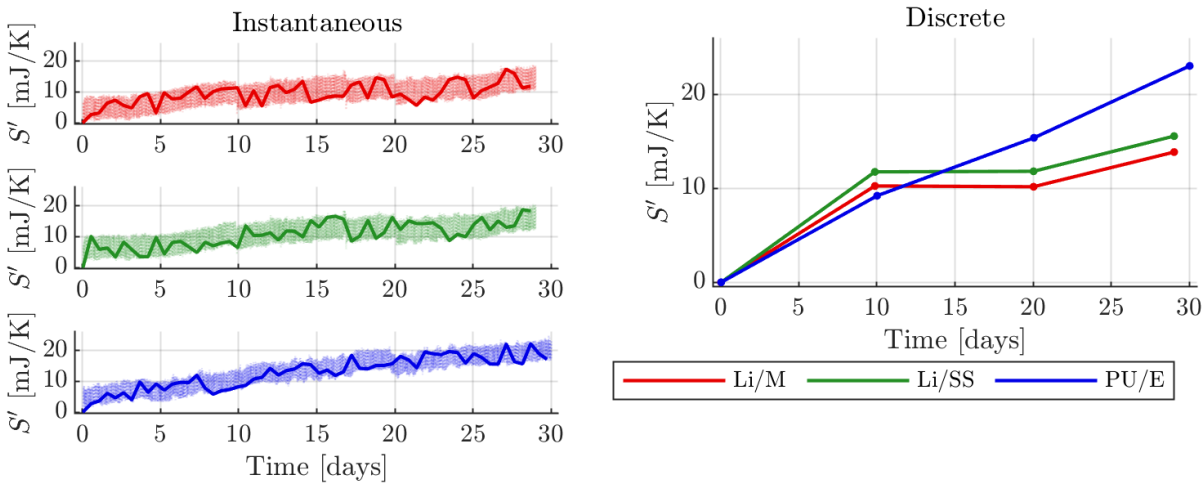

Figure 7.4: The entropy generated according to Equation 7.1. The left-hand side of the figure shows the filtered instantaneous entropy overlaid on the lower-opacity unfiltered instantaneous profile. The right-hand side shows the entropy generated for the three discrete data points; 10 days, 20 days and 30 days.

7.3 The Degradation-Entropy Generation (DEG) model

With the entropy generation characterised and the degradation measures determined for all ageing intervals, the next step is applying the DEG method. The application is already discussed in Section 2.1.5, where Equation 2.32 is presented:

$$w(S_T, S_Q, S_m) = B_T S_T + B_Q(-S_Q) + B_m S_m + w_0 \tag{7.3}$$

7.3.1 Degradation impact of active mechanisms: the DEG coefficients

As described in Section 2.1.5, the degradation coefficients can be found by solving Equation 2.34:

$$B_i = S_{ki}^{-1}(w_k - w_0 I_{k\times 1}). \tag{7.4}$$

where index i represents the entropy sources or degradation mechanisms ($i = \{T, Q, m\}$), index k represents the ageing intervals ($k = \{10, 20, 30\}$) and w_0 is the degradation measure's value for fresh grease. Matlab's [49] `mldivide` function is used to find a numerical solution to the inverse matrix problem. The calculated degradation coefficients are plotted in Figure 7.5 and tabulated in Appendix C, Table C.3.

In Figure 7.5, the red bars, like the previous red plots, represent degradation coefficients for Li/M; the green bars, like the previous green plots, are for Li/SS; and the blue, like previous blue plots, are for PU/E. For each grease, the first bar is heat storage coefficient B_T, the second is heat transfer coefficient B_Q and the third is evaporation coefficient B_m.

The first notable aspect of the degradation coefficients is the sign. For every grease-degradation measure pair, all three degradation coefficients have the same sign, for example, for Li/SS-bleed capacity, all the degradation coefficients B_T, B_Q and B_m are negative. This means that since S_Q is negative while S_T and S_m are positive, the heat transfer mechanism has an opposite effect on the degradation measures to the other two mechanisms. This accords with the relationship between heat transfer (or heat transfer entropy) and the other two mechanisms, in their contributions to energy dissipation (or entropy generation), shown in Equation 2.15 (or Equation 2.23).

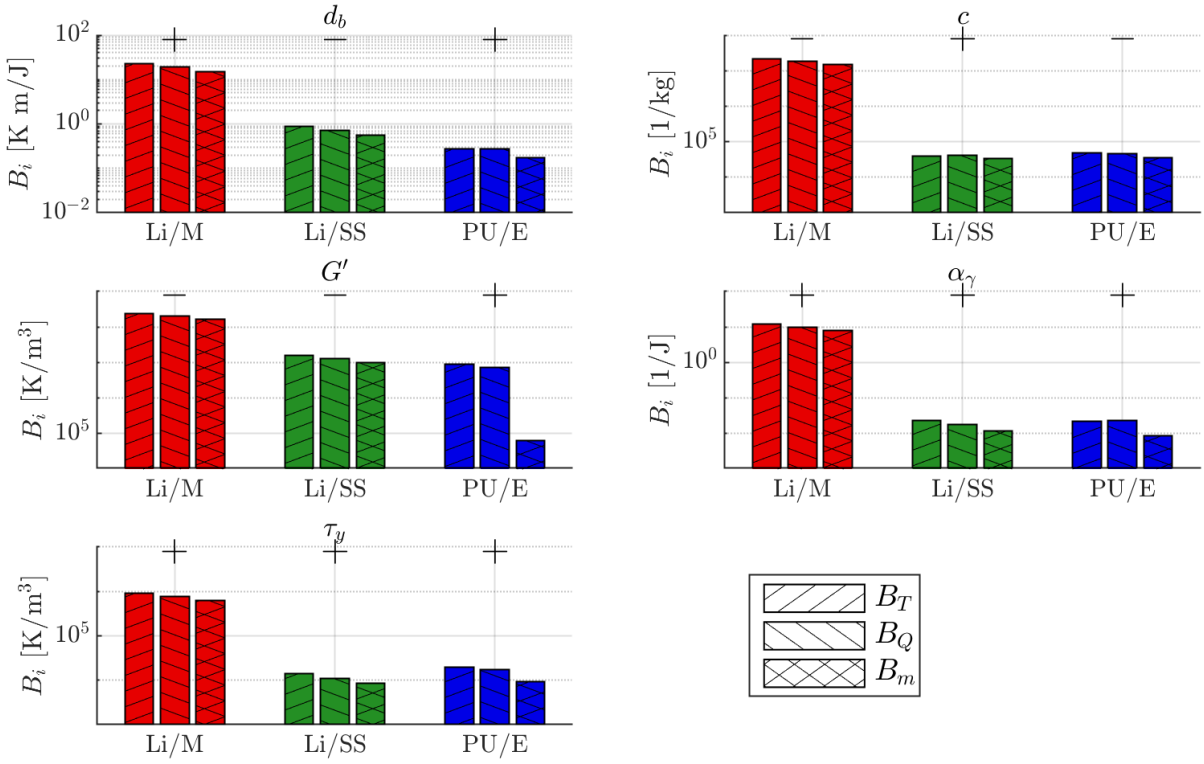

Figure 7.5: The magnitude and sign plots of the degradation coefficients corresponding to the bleed capacity measure (d_b), specific heat capacity (c), storage modulus (G'), thermal strain coefficient (α_γ) and yield stress (τ_y).

Another notable observation is that the Li/M grease consistently has the highest magnitude, meaning Li/M is the most sensitive to thermal ageing of all three greases. This is the least pronounced for the storage modulus G'. The degradation coefficients are one order of magnitude or more higher for Li/M than the other 2 greases. Li/SS is slightly more sensitive to thermal degradation of some properties than PU/E (d_b, G') and vice versa (c, α_γ, τ_y).

Another interesting pattern is the relative size of B_T, B_Q and B_m for all the greases. B_T is consistently the largest, followed by B_Q and then B_m. The exceptions are PU/E in the bleed capacity measure and thermal strain coefficient, and Li/SS in the specific heat capacity, for which B_Q is slightly higher than B_T. This indicates that the entropy resulting from increasing the temperature of the grease has the largest effect on the degradation of the grease. The entropy resulting from heat transfer has the second largest effect. Evaporation entropy has the smallest effect on degradation.

It should be noted that the difference between the mechanisms of B is relatively small. Each mechanism therefore contributes on the same scale given the entropies are also of the same order. This means that, although evaporation has the smallest coefficient, it could contribute a lot of degradation if it were to continue past 10 days. Also, the entropy generation, plotted in Figure 7.3, shows that the heat transfer entropy is opposite in sign to the heat storage and evaporation entropy. This means, with all the coefficients having the same sign, the degradation induced by heat storage and evaporation will be balanced to some extent by the heat transfer. This leads to the proposition that all three degradation mechanisms — heat storage, heat transfer and evaporation — are critical to fully characterise the ageing procedure. This proposition is further explored in Section 7.3.2.

These findings accord with the known sensitivity of mineral oil, the base oil in Li/M grease to thermal effects, restricting its use to a narrower temperature range than Li/SS and PU/E. Of all three greases, the evaporation coefficient B_m of Li/M and Li/SS is consistently closer to

the other two coefficients than it is for PU/E grease, indicating the effect of evaporation to be stronger in the lithium greases. This is in accordance with the higher percentages of volatiles in both lithium greases than the PU/E grease.

7.3.2 Mechanism significance analysis

As mentioned in Section 7.3, the similarity of the magnitudes of the three degradation coefficients suggests all the degradation mechanisms are critical to accurately model the thermal degradation of grease based on the physics of the active mechanisms.

This can be tested further. If one or two of the degradation mechanisms are not needed to describe the degradation, one could find a smaller set of degradation coefficients that can predict the degradation measure with a small error. As was proposed in Section 2.1.5, a model with the same number of entropy sources as the number of ageing intervals will always yield a (near) perfect fit. The comparison between various reduced models will therefore not demand a fit to be near perfect to show whether an entropy source is superfluous. The limits are set at $R^2 \geq 0.95$ and NRMSD ≤ 0.01, where models meeting these conditions are considered good enough.

Whether an entropy source is superfluous is calculated by setting a column of the entropy matrix to zero and then performing the fit as described in Section 2.1.5 numerically. Matlab's [49] `mldivide` does not need the entropy matrix to be square, as it automatically decides on the best numerical method to use. The error between the measured degradation measures and the value predicted by the degradation model is used. The result of this analysis can be found in Figure 7.6.

The mechanisms significance analysis shows that only when all three degradation mechanisms — heat storage, heat transfer and evaporation entropies — are taken into account is the error small for all degradation measures. Apart from this, there is no strong pattern to discern suggesting any mechanism can be dropped. This leads to the conclusion that all three degradation mechanisms studied are important and required for accurate characterisation as stipulated by the DEG theorem.

When the evaporation entropy is dropped, the performance of the model gets worse. If evaporation did not matter, or matters very little, in characterising degradation, the errors for models without evaporation entropy should be small. This is not the case however.

A more prevalent pattern seems to be, that the number of mechanisms have a larger influence on the quality of fit. The models taking two mechanisms into account perform better than those only taking one into account. This is also anticipated by the DEG theorem that requires accounting for all active dissipative mechanisms. The fewer the mechanisms taken into account, the worse the fit gets.

Some reduced models being able to model a specific degradation measure with low error is considered too random to warrant further exploration in this study. This is mainly because this pattern is limited to only one grease type and a select set of properties (c and τ_y for Li/SS for example).

7.3.3 Thermal degradation resistance: Grease ranking

The higher a degradation coefficient is, the more a degradation measure changes due to entropy contribution by the respective mechanism. Therefore, the degradation coefficients give insight into the thermal degradation resistance of the three greases as measured by the various grease properties.

A qualitative ranking of each grease based on the degradation coefficients is proposed. This is done by taking the absolute value of the average of the three degradation coefficients. These are then ranked by magnitude, from lowest (best) to highest (worst), for each degradation measure. The ranking is presented in Table 7.1.

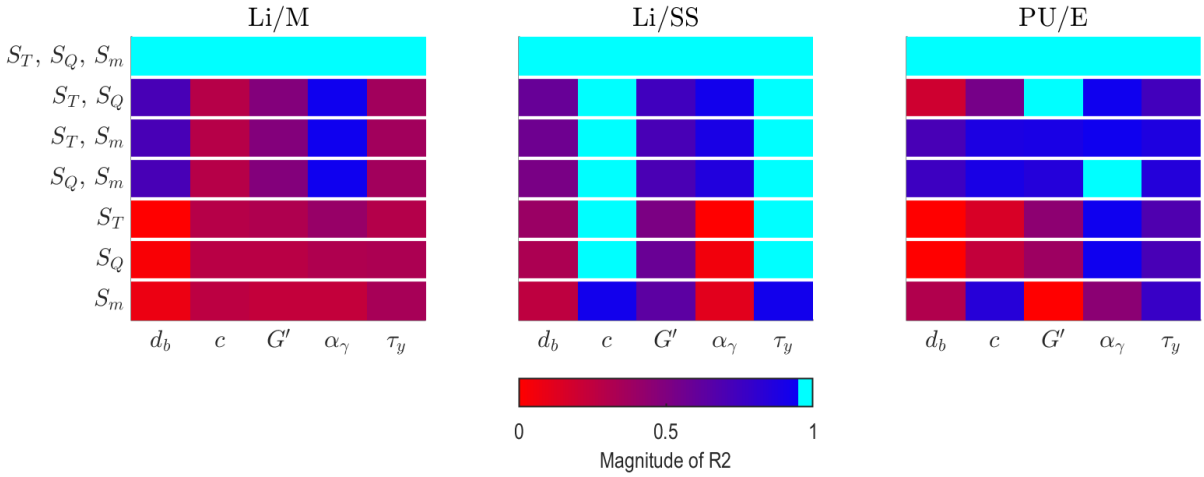

(a) The R^2 norm for the various combinations of degradation mechanisms. $R^2 \geq 0.95$ are denoted with the cyan (bright) colour.

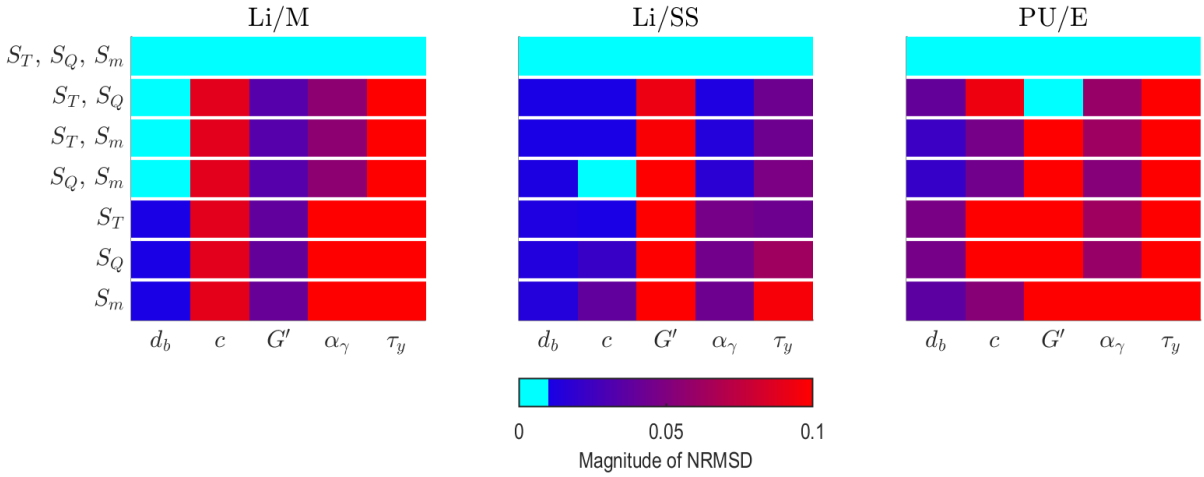

(b) The NRMSD norm for the various combinations of degradation mechanisms. NRMSD ≤ 0.01 are denoted with the cyan (bright) colour.

Figure 7.6: The R^2 (Figure 7.6a) and NRMSD (Figure 7.6b) for various combinations of degradation mechanisms, plotted per row, and degradation measures, plotted per column. The colour moves from red, which denotes a poor fit, to blue, which denotes a good fit. The brightest (cyan) colour presents the best fits. Note that only when all degradation mechanisms are taken into account is the error low for all degradation measures. This leads to the conclusion that the most complete model uses heat storage, heat transfer and evaporation entropy.

Table 7.1: Grease ranking, with greases ranked from best thermal degradation resistance (**+**) to average (**o**) to worst (**–**).

Grease	Overall	Bleed capacity measure d_b	Specific heat capacity c	Storage modulus G'	Thermal strain coefficient α_γ	Yield stress τ_y
Li/M	–	–	–	–	–	–
Li/SS	+	o	+	o	+	+
PU/E	o	+	o	+	o	o

Li/SS grease, with a Lithium-thickened semi-synthetic base oil, shows the highest resistance to thermal degradation measured by specific heat capacity, thermal strain coefficient and yield stress. PU/E grease, with a polyurea-thickened ester base oil, shows the highest resistance to thermal degradation measured by bleed capacity and storage modulus. Li/M grease, with a Lithium-thickened mineral base oil, shows the least resistance to thermal degradation. These findings accord with the established behaviours of these three greases. The choice of grease for a specific application depends on which degradation measure(s)/grease property(ies) is/are most significant.

Chapter 8

Summary, conclusions and recommendations

8.1 Thermal degradation of grease

This study has attempted to develop a physics-based model to quantify the effects of active thermal mechanisms on grease degradation. At the basis of the analysis of churning and temperature-only thermal degradation, lies the same thermodynamic model based on first principles. This model relates the entropy generation to three mechanisms: heat storage, heat transfer and evaporation. The derived model is a natural extension of the temperature-only model derived by Osara and Bryant [18] (which excluded evaporation). At its core, the proposed thermal model has heat storage and heat transfer entropies, and it has been expanded to include evaporation entropy.

8.1.1 During churning in a bearing

For its application to churning, evaporation has been omitted from the thermodynamic model. The model was used to characterise the heat storage and heat transfer entropies based on the time-temperature data from Chatra et al. [28]. The current approach expands on the work by Chatra et al. [26], adding heat storage entropy to the heat transfer entropy. However, the magnitude of the heat storage entropy is negligibly small compared to the heat transfer entropy.

The churning sub-phase categorisation was done using the heat storage entropy to separate the churning behaviour into three phases: initiation phase (phase I), continuation phase (phase II) and termination phase (phase III). Phase I represents the grease heating to the churning temperature, which ends when the heat storage entropy reaches its maximum. Phase II then commences at the steady elevated temperature where heat storage entropy is also steady until it starts to drop. Phase III was found not needed for further characterisation. The ratio of phase II to phase I total entropy generation in these two phases was defined as the churning measure $\phi = S'_{\text{II}}/S'_{\text{I}}$. When the churning measure tends to zero, the churning behaviour tends to peak-type.

The churning measure allows the churning behaviour to be characterised on a continuous scale. When applied to the data from Chatra et al. [28], it allowed for a quantified characterisation of the greases. The churning measure mostly agreed with the churning type designations by Chatra and Lugt [7], where LM3C and LM2L (designated as peak-types) had a lower churning measure than LM3L (designated as plateau-type). LCP2.5C was designated as plateau type but had a churning measure closer to LM3C and LM2L. This was also more in line with the observations from the temperature profiles, where LCP2.5C showed temperature behaviour close to that of LM2L. The same method was also applied to data provided by Shetty et al. [50], which showed little churning happened for low fill levels (7.5% and 15%), resulting in a low

churning measure. For normal fill levels (30%), the churning behaviour was better defined and the churning measure was high. This placed it at a level similar to LM3L, which is a comparable grease. Though the size of the dataset to which it was applied is still somewhat limited, this method seems promising for further application.

8.1.2 In an oven: the DEG model

To study the degradation of grease due to temperature effects only, grease samples were heated for extended periods of time. The three greases, Li/M, Li/SS and PU/E, were aged at a temperature of 130°C–133°C, for 10 days, 20 days and 30 days. Oxidation was successfully avoided by ageing in a nitrogen atmosphere, as IR-spectra of the samples indicated no change in chemical makeup.

By leaving the samples uncovered during ageing, evaporation was promoted. This evaporation is assumed to be mainly of base oil and volatiles present in the base oil. It was found that Li/M and Li/SS lost about 4.5% and 5.0% respectively of their mass, which corresponds to a base oil content of 84.4% and 84.3% respectively (assuming a starting base oil content of 85.0%). On the other hand, PU/E lost about 0.5% of its base oil, which corresponds to a base oil content of 84.9%. The fully synthetic grease, PU/E, experienced far less evaporation than the mineral oil or semi-synthetic greases. Synthetic greases have a well-defined composition, compared to mineral oil based greases, suggesting mineral oil based greases contain more volatiles than synthetic greases.

During the ageing process, all three samples experienced some extent of discolouration in the bulk of the material. This discolouration was more pronounced in the top millimetre. It is proposed that this can, to some extent, be attributed to the evaporation primarily of base oil, as the colour seemed to change the most from 0 to 10 days. However, PU/E seems to consistently darken in colour over the 30 days, suggesting other mechanisms are also in play.

To ensure homogeneity, the grease samples were stirred before measuring the properties. This is done carefully and very mildly, to avoid breaking down the thickener structure considerably. A similar method is used when folding egg foams: to preserve as much as the structure, fold the material over on itself. However, a small loss of consistency is to be expected when working with grease. The effect of this mild stirring on the experimental results is considered insignificant. If necessary, to avoid stirring, thinner samples of grease could be aged which would better retain homogeneity throughout.

The degradation of grease is characterised using the DEG theorem by Bryant et al. [37]. The first step is selecting the degradation measures. The properties chosen are mechanical, rheological and thermal properties critical to the operation of the grease [41]. The chosen properties include the bleed capacity measure, specific heat capacity, storage modulus, thermal strain coefficient and yield stress.

The degradation measures were measured for fresh and aged samples. Each measurement was done twice to ensure the accuracy of the results. The accuracy of all the measurements was verified. The specific heat capacity proved the hardest to get consistent results for and in the end some measurement points had a higher-than-ideal variation, though the vast majority were within acceptable bounds. The issues seemed to stem from the contamination of the DSC oven.

The measurements did not show any easily discernible trends, seemingly increasing and decreasing at random throughout the ageing procedure. The bleed capacity measure, in particular, showed little change over 30 days. This seems in line with the findings by Hogenberk et al. [10]. The seeming randomness of the results required a characterisation based on the active physical mechanisms as the measured properties themselves and time in the oven — which is often the basis of experimental thermal studies — bore no useful and consistent trends.

A significant challenge was quantifying the heat transfer into the grease samples from the

oven. As no existing works were found tackling this issue, a thermal model of oven heating had to be developed. To characterise the conditions in the oven, an extensive heat transfer model was built of the grease sample during ageing. This model calculated the equivalent thermal resistance of the samples based on the temperatures of the sample and oven. Due to hardware limitations, the grease temperature was not measured. This heat transfer model was used, in conjunction with the energy balance, to numerically model the grease temperature during ageing. The results of this oven heating model were deemed consistently accurate considering the magnitude of the other energy terms. In particular, the dissipated energy proved to rise steadily and maintained a magnitude of approximately 0.2 times the supplied heat.

The derived grease temperature from the above model was then used to estimate the three entropy contributions: heat storage entropy, heat transfer entropy and evaporation entropy. The heat storage entropy and evaporation entropy contributed positively to the generated entropy, while the heat transfer entropy contributed negatively. The entropy generation was found to be positive, increasing and of a small enough magnitude (below 25 mJ$/$K) to be considered realistic. The greases saw similar amounts of entropy generation, where Li/M and Li/SS were very close, as they were aged at the same time and had relatively similar evaporation profiles. Entropy generation is then used to derive a set of three degradation coefficients by correlating the entropy-generating mechanisms to changes in degradation measures. The fit was found to have an accuracy of $R^2 > 0.99$. However, the matrix formulation used led to the observation that a problem with equal numbers of ageing intervals as degradation mechanisms has an exact solution. This is critical for studies like this, where the number of measurement points is limited. It should also be notable that the DEG methods consistently result in very high R^2-s [4, 18, 39].

To see if all the degradation mechanisms were needed to accurately model the thermal degradation, mechanisms were removed from the model and the R^2 and NRMSD were compared. No combination of one or two degradation mechanisms found rivalled the combination of all three mechanisms (heat storage, heat transfer and evaporation) considered. This resulted in the conclusion that every active entropy source is critical for accurate physics-based modelling of degradation. Furthermore, evaporation is therefore critical in modelling thermal degradation, when evaporation can occur.

The degradation coefficients showed two trends of particular note. Firstly, all degradation coefficients of a grease-degradation measure pair have the same sign. Combined with the heat transfer entropy being negative for this system yields a bound system: if heat storage and evaporation entropies go up, heat transfer entropy goes down and the result is a relatively small amount of dissipation and degradation. It is a self-mediating system of sorts. Secondly, the heat storage entropy has the highest coefficient, followed by heat transfer and then evaporation. This is corroborated by the well-established knowledge that most non-thermal systems operate optimally in a given temperature range, often requiring cooling during operation to facilitate performance.

Comparing the degradation coefficients—which determine the resistances of the greases to thermal degradation—of the greases, Li/M, with mineral base oil, consistently had the largest coefficient. This led to the ranking of the greases based on the magnitude of their degradation coefficients. Lower coefficients mean higher degradation resistance and a better rating, as active mechanisms introduce smaller changes to the degradation measures. The higher the coefficient, the lower the degradation resistance and the worse the rating. Based on the properties tested, Li/SS was found to be the most resistant to thermal degradation, closely followed by PU/E, and Li/M was found to react poorly to thermal degradation.

8.2 Conclusion

A thermodynamic model has been derived from first principles to expand the existing formulations [18] with evaporation entropy. The resulting model considered temperature-only effects:

heat storage, heat transfer and evaporation entropy.

The first part of this research applied the derived thermodynamic model, excluding evaporation, to churning temperature data provided by Chatra et al. [28]. Heat storage entropy was used to define three phases in a typical churning process: the initiation phase (phase I), continuation phase (phase II) and termination phase (phase III). It was observed that churning processes with large amounts of entropy generation in the continuation phase behave plateau-like, while short continuation phases behave peak-like.

The churning measure ϕ was introduced to quantify this observation. It characterises the churning behaviour using the ratio of phase II to phase I entropy generation. The magnitude of the churning measure represents the churning behaviour, wherein the closer the churning measure is to zero, the more the churning process represents peak-like behaviour.

Application of the churning measure to churning data provided by Chatra et al. [28] and Shetty et al. [50] showed the churning measure is able to characterise the churning behaviour on a continuous scale. The low and high churning measures mostly agreed with their respective qualitative designation of peak and plateau type [7], meaning the churning measure was able to quantitatively describe the designation.

As a second part of this research work, the thermal degradation of grease was studied by thermally ageing three different greases at 130°C for 10 days, 20 days and 30 days. These three greases are commonly used: Li/M (lithium soap/mineral base oil), Li/SS (lithium soap/semi-synthetic base oil) and PU/E (polyurea/synthetic ester base oil). Oxidation was prevented by ageing in a nitrogen atmosphere, which was verified by measuring IR-spectra.

The inert atmosphere allowed samples to remain uncovered in the oven, promoting evaporation. Mass measurements showed evaporation was most significant in the first 10 days, after which little to no evaporation occurred. It was found that PU/E lost about 0.54% of its initial mass, whereas Li/M lost 4.5% and Li/SS lost 5.1%. To quantify evaporation energy and entropy, the latent heat of evaporation for Li/M, Li/SS and PU/E base oil was found using non-isothermal thermogravimetric analysis.

The grease degradation was measured by selecting five thermo-physical, rheological and mechanical grease properties, critical for the performance of grease. The selected degradation parameters were bleed capacity measure, specific heat capacity, storage modulus, thermal strain coefficient and yield stress. Altogether, a total of 60 measurement points were created for the degradation measures alone. All measures but the bleed capacity measure showed inconsistent behaviour over 30 days. The bleed capacity measure showed little variation over time.

An extensive oven-heating thermal model was created to model the heat transfer and grease temperature of the samples aged in the oven. This model was constructed based on and verified with the energy balance. It showed sufficiently small energy magnitudes and energy dissipation, as anticipated by the theory.

The same model was then used to calculate heat storage, heat transfer and evaporation entropies. These entropies were found to each remain below 250 mJ/K. It was found that heat storage entropy and evaporation entropy had positive contributions to the entropy generation, while heat transfer entropy contributed negatively, due to the sample being externally heated. The total entropy generation was found to be positive and rising during ageing, with a magnitude below 25 mJ/K, according to the second law of thermodynamics that requires entropy generation to be positively monotonic.

The DEG method was applied to the data from three ageing intervals, with a coefficient of determination of $R^2 > 0.99$. The degradation coefficients were found to always have the same sign for any grease-degradation measure pair. With a few exceptions, the heat storage coefficient was the largest, followed by the heat transfer coefficient and evaporation coefficient, though all coefficients were of the same order of magnitude for every grease and degradation measure (with only one exception). Further analysis to check whether one or two degradation

Table 8.1: The grease ranking, where the greases are ranked from best thermal degradation resistance (**+**) to average (**o**) to worst (**–**).

Grease	Overall	Bleed capacity measure d_b	Specific heat capacity c	Storage modulus G'	Thermal strain coefficient α_γ	Yield stress τ_y
Li/M	–	–	–	–	–	–
Li/SS	+	o	+	o	+	+
PU/E	o	+	o	+	o	o

mechanisms were superfluous found that all three mechanisms are needed to properly characterise the degradation. From this follows evaporation should be considered significant when considering temperature-only degradation in an open (unsealed) application.

The degradation coefficients were used to rank each of the three greases on their resistance to thermal ageing, as shown in Table 8.1.

8.3 Recommendations

Based on the current study, the following recommendations are made for further research:

- The data to which the churning measure has been applied is still somewhat limited. To truly understand its applicability, the churning measure can be applied to experimental data with various combinations of RPM, radial load and grease filling level. This can further the understanding of how the churning measure reacts to different experimental setups and further explore its applicability.

- Temperature-only entropy generation has been characterised for churning in bearings. However, these entropies have not been studied in the context of degradation. Further research can be done into the temperature-only thermal degradation experienced by grease during churning and the extend of this degradation can be compared to the mechanical degradation.

- Entropy generation has been calculated based on a derived oven-heating model of the grease samples during ageing. This model which yielded the thermal resistance and grease temperature, relied intensely on existing, general formulations. It is therefore recommended to experimentally determine the thermal resistance of a sample and directly measure the grease temperature for future analyses.

- Evaporation was characterised using first-order kinetics. It was found that little evaporation occurs after 10 days of ageing. However, there is little known about the evaporation behaviour of grease between 0 days and 10 days. It is therefore recommended to further study the evaporation behaviour of greases in this period. By creating thinner, flatter samples, more evaporation can be induced via a greater surface area, keeping grease samples homogeneous. Further validation of the latent heat of evaporation of base oil should be done and the molecular weight of base oil should be directly measured to properly characterise the latent heat of evaporation.

- The DEG theorem produced a model correlating three degradation mechanisms to five degradation measures. The degradation coefficients were based on three ageing intervals, which produced a fit with a $R^2 > 0.99$. The thermal degradation can be further investigated with shorter ageing intervals, yielding a more granular dataset. It could be

interesting to see if the DEG could be used to predict future temperature-only degradation of a material when provided with phenomenological properties.

REFERENCES

[1] P. M. Lugt. *Grease lubrication in rolling bearings*. John Wiley & Sons, 2013.

[2] G. W. Stachowiak and A. W. Batchelor. *Engineering Tribology*. Butterworth–Heinemann, fourth edition, 2014.

[3] R. M. Mortier and S. T. Orszulik. *Chemistry and Technology of Lubricants*. Glasgow: Blackie, 1992.

[4] Jude A. Osara and Michael D. Bryant. Thermodynamics of grease degradation. *Tribology International*, 137, 2019.

[5] A. Rezasoltani and M. M. Khonsari. On Monitoring Physical and Chemical Degradation and Life Estimation Models for Lubricating Greases. *Lubricants*, 4, 2016.

[6] Y. Zhou, R. Bosman, and P. M. Lugt. A Model for Shear Degradation of Lithium Soap Grease at Ambient Temperature. *Tribology Transaction*, 61, 2018.

[7] S. K. R. Chatra and P. M. Lugt. Channeling behavior of lubricating greases in rolling bearings: Identification and characterization. *Tribology International*, 143, 2020.

[8] A. Akchurin, D. van den Ende, and P. M. Lugt. Modeling impact of grease mechanical ageing on bleed and permeability in rolling bearings. *Tribology International*, 170, 2022.

[9] A. Rezasoltani and M. M. Khonsari. An engineering model to estimate consistency reduction of lubricating grease subjected to mechanical degradation under shear. *Tribology International*, 103, 2016.

[10] F. Hogenberk, J. A. Osara, D. Ende, and P. M. Lugt. On the evolution of oil-separation properties of lubricating greases under shear degradation. *Tribology International*, 179, 2023.

[11] In-Sik Rhee. Decomposition Kinetic of Greases by Thermal Analysis. Technical report, US ARMY TACOM 6501 E. 11 Mile Road Warren, MI 48397-5000, 2007.

[12] In-Sik Rhee. Prediction of High Temperature Grease Life Using a Decomposition Kinetic Model. Technical report, US Army RDECOM-TARDEC 6501 E 11 Mile Rd Warren, MI 48397-5000, 2009.

[13] A. Rezasoltani and M. M. Khonsari. Experimental investigation of the chemical degradation of lubricating grease from an energy point of view. *Tribology International*, 137, 2019.

[14] Jude A. Osara, P. M. Lugt, Michael D. Bryant, and Micheal M. Khonsari. Thermodynamic Characterization of Grease Oxidation–Thermal Stability via Pressure Differential Scanning Calorimetry. *Triology Transactions*, 65, 2022.

[15] S. K. Naldu, E. E. Klaus, and J. L. Duda. Kinetic Model for High-Temperature Oxidation of Lubricants. *Industrial and Engineering Chemistry Product Research and Development*, 25, 1986.

[16] S. Hurley, P. M. Cann, and H. A. Spikes. Thermal Degradation of Greases and the Effect on Lubrication Performance. *Tribology Series*, 34, 1998.

[17] S. Hurley, P. M. Cann, and H. A. Spikes. Lubrication and Reflow Properties of Thermally Aged Greases. *Tribology Transaction*, 43, 2000.

[18] J. A. Osara and Michael D. Bryant. A temperature-only system degradation analysis based on thermal entropy and the degradation-entropy generation methodology. *International Journal of Heat and Mass Transfer*, 158, 2020.

[19] P. Jiabao, Y. Guangxin, and W. Jianping. Effect of thermorheological properties on tribological behaviors of lubricating grease. *Materials Research Express*, 7, 2020.

[20] M. A. Delgado, C. Valencia, M. C. Sánchez, J. M. Franco, and C. Gallegos. Thermorheological behaviour of a lithium lubricating grease. *Tribology Letters*, 23, 2006.

[21] I Cournonne and P. Vergne. Rheological Behavior of Greases: Part II–Effect of Thermal Aging, Correlation with Physico-Chemical Changes. *Tribology Transaction*, 43, 2000.

[22] Y. Zhou, R. Bosman, and P. M. Lugt. A Master Curve for the Shear Degradation of Lubricating Greases with a Fibrous Structure. *Tribology Transaction*, 61, 2019.

[23] P. Shetty, R. J. Meijer, and P. M Lugt. An Evaporation Model for Base Oil from Grease-Lubricated Rolling Bearings including Breathing. *Tribology Transaction*, 64, 2021.

[24] S. K. R. Chatra and P. M. Lugt. The process of churning in a grease lubricated rolling bearing: Channeling and clearing. *Tribology International*, 153, 2021.

[25] S. K. R. Chatra, J. A. Osara, and P. M. Lugt. The lubrication mechanism behind the transition from churning to bleeding in grease lubricated bearings – Experimental characterization. *Tribology International*, 183, 2023.

[26] S. K. R. Chatra, J. A. Osara, and P. M. Lugt. Thermo-mechanical aging during churning in grease lubricated bearings and its impact on grease life. *Tribology International*, 181, 2023.

[27] R. J. Meijer and P. M. Lugt. The Grease Worker and Its Applicability to Study Mechanical Aging of Lubricating Greases for Rolling Bearings. *Tribology Transaction*, 65, 2022.

[28] S. K. R. Chatra, J. A. Osara, and P. M. Lugt. Impact of grease churning on grease leakage, oil bleeding and grease rheology. *Tribology International*, 176, 2022.

[29] J. Lundberg and E. Höglund. A new method for determining the mechanical stability of lubricating greases. *Tribology International*, 33, 2000.

[30] E. Kuhn. Description of the energy level of tribologically stressed greases. *Wear*, 188, 1995.

[31] E. Kuhn. Investigations into the Degradation of the Structure of Lubricating Greases. *Tribology Transaction*, 41, 1998.

[32] E. J. Kuhn. Energetical Investigations of the Tribology of Lubricating Greases. *SAE Technical Papers*, 2000.

[33] E. Kuhn. Analysis of a grease-lubricated contact from an energy point of view. *Int. J. Materials and Product Technology*, 38, 2010.

[34] E. Kuhn. Correlation between System Entropy and Structural Changes in Lubricating Grease. *Lubricants*, 3, 2015.

[35] N. Acar, J. M. Franco, and E. Kuhn. On the shear-induced structural degradation of lubricating greases and associated activation energy: An experimental rheological study. *Tribology International*, 144, 2020.

[36] L. Ahme, E. Kuhn, and M. A. D. Canto. Experimental Study on the Expended Energy on Structural Degradation of Lubricating Greases. *Tribology Letters*, 70, 2022.

[37] M. D. Bryant, M. M. Khonsari, and F. F. Ling. On the thermodynamics of degradation. *Proceedings of the Royal Society A*, 464, 2012.

[38] A. Gurt and M. M. Khonsari. The Use of Entropy in Modeling the Mechanical Degradation of Grease. *Lubricants*, 7, 2019.

[39] Jude A. Osara and Michael D. Bryant. Thermodynamics of Fatigue: Degradation-Entropy Generation Methodology for System and Process Characterization and Failure Analysis. *Entropy*, 21, 2019.

[40] E. Kuhn. Aspects of Self-Organization of Tribological Stressed Lubricating Greases. *Lubricants*, 8, 2020.

[41] J. A. Osara, S. K. R. Chatra, and P. M. Lugt. Grease material properties from first principles thermodynamics. *Lubrication Science*, n/a, 2023.

[42] L. Huang, D. Guo, P. M. Cann, G. T. Y. Wan, and S. Wen. Thermal Oxidation Mechanism of Polyalphaolefin Greases with Lithium Soap and Diurea Thickeners: Effects of the Thickener. *Tribology Transaction*, 59, 2016.

[43] K. P. Lijesh and M. M. Khonsari. On the Assessment of Mechanical Degradation of Grease Using Entropy Generation Rate. *Tribology Letters*, 67, 2019.

[44] H. B. Callen. *Thermodynamics and an introduction to Thermostatistics*. John Wiley & Sons, Inc., second edition edition, 1985.

[45] I. Prigogine. *Introduction to Thermodynamics of Irreversible Processes*. Interscience Publishers, second edition edition, 1962.

[46] D. Kondepudi and I. Prigogine. *Modern Thermodynamics: From Heat Engines to Dissipative Structures*. John Wiley & Sons, Ltd, second edition edition, 2014.

[47] Selecting grease or oil. `https://www.skf.com/group/products/rolling-bearings/principles-of-rolling-bearing-selection/bearing-selection-process/lubrication/selecting-grease-or-oil`. Accessed: 18-03-2024.

[48] Y. A. Çengel and A. J. Ghajar. *Heat and Mass Transfer: Fundamentals and Applications*. McGraw-Hill Education, fifth in si units edition, 2015.

[49] The MathWorks Inc. MATLAB Version: 9.14.0.2239454 (R2023a) Update 1, 2023.

[50] P. Shetty, R. J. Meijer, J. A. Osara, R. Pasaribu, and P. M Lugt. Effect of Grease Filling on the Film Thickness in Deep-Groove Ball Bearings. *Tribology Transaction*, 2023.

[51] D. Dollimore, T. A. Evans, Y. F. Lee, and F. W. Wilburn. Correlation between the shape of a TG/DTG curve and the form of the kinetic mechanism which is applying. *Thermochimica Acta*, 198, 1992.

[52] K. Chatterjee, D. Dollimore, and K. S. Alexander. Calculation of vapor pressure curves for hydroxy benzoic acid derivatives using thermogravimetry. *Thermochimica Acta*, 392-393, 2002.

[53] L. A. Smook, S. Chatra R. K., and P. M. Lugt. Evaluating the oxidation properties of lubricants via non-isothermal thermogravimetric analysis: Estimating induction times and oxidation stability. *Tribology International*, 171, 2022.

[54] D. N. Gerasimov and E. I. Yurin. *Kinetics of Evaporation*, volume 68. Springer Cham, first edition edition, 2018.

[55] F. Cyriac, P. M. Lugt, and R. Bosman. On a New Method to Determine the Yield Stress in Lubricating Grease. *Tribology Transaction*, 58, 2015.

[56] S. L. S. Sarowha. Determination of Molecular Weights of Petroleum Products Using Gel Permeation Chromatography. *Petroleum Science and Tecnology*, 23, 2005.

[57] C. Zhou. *Unconventional Petroleum Geology*, chapter Oil Shale. Elsevier, second edition edition, 2017.

[58] J. Tarrío-Saavedra, J. López-Beceiro, S. Naya, M. Francisco-Fernández, and R. Artiaga. Simulation study for generalized logistic function in thermal data modeling. *Journal of Thermal Analysis and Calorimetry*, 118, 2014.

[59] A. K. Burnham. Use and misuse of logistics equations ofr modeling chemical kinetics. *Journal of Thermal Analysis and Calorimetry*, 127, 2017.

[60] F. J. Suriano and Kwang-Tzu Yang. Laminar free convection about vertical and horizontal plates at small and moderate grashof numbers. *International Journal of Heat and Mass Transfer*, 11, 1967.

[61] C. Tsioptsias. On the latent limit of detection of thermogravimetric analysis. *Measurement*, 204, 2022.

Appendix A

Finding the latent heat of grease base oil

A.1 Introduction

Base oils in greases consist of relatively heavy hydrocarbon compounds [1–3]. However, the exact makeup is (often) not known. Yet, to calculate the entropy generation by evaporating base oil, it is critical to know the latent heat of evaporation. The latent heat of evaporation, or latent heat of vaporisation, determines the energy needed to evaporate a unit of mass from the fluid. The LHE is denoted by L and either in J/mol or J/kg. All mass measurements will be in kg, so the latter unit will be used.

One method of finding this is supplying heat to a set mass of grease and finding the energy needed to evaporate some measurable mass of base oil. A disadvantage of this method is that high temperatures combined with exposure to oxygen will inevitably lead to oxidation [1, 11–15]. Another problem is due to the base oil being a mixture of different chemical compounds, each with its own latent heat of evaporation. Therefore, this experiment should be repeated for a large number of different temperatures.

A method proposed by Dollimore et al. [51] utilises non-isothermal thermogravimetric analysis to characterise solid-state kinetic parameters of thermal decomposition. These kinetic parameters are considered to be the unknowns of the Arrhenius relation that governs the decomposition process. In the current case, the decomposition process can be considered the evaporation of material. Chatterjee et al. [52] applied the aforementioned method to find the latent heat of evaporation as a step to find the vapour pressure curves of hydroxy benzoic acid derivatives. Smook et al. [53] applied the same non-isothermal method to study the oxidation stability of grease to great effect. All in all, the non-isothermal thermogravimetric analysis methodology will be used to find the LHE for the base oils of these greases.

A.2 Analysis

The methodology is adapted from Chatterjee et al. [52] and Smook et al. [53].

A.2.1 Compensation for changing gas density

As the TGA heats up, the purge gas will heat as well. This results in a reduction of density and therefore the buoyant forces on the TGA crucible, increasing the apparent weight of the crucible [61]. The method of compensation is partially adapted from the study by Tsioptsias. A

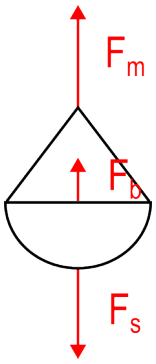

Figure A.1: The Free Body Diagram (FBD) of a TGA basket.

free body diagram of the TGA crucible can be seen in Figure A.1. The sum of forces is

$$\sum F_y = F_m + F_b - F_s = 0 \tag{A.1}$$

$$\rightarrow F_s = F_m + F_b \tag{A.2}$$

The subscript s denotes the real properties of the sample and m denotes the measured properties. F_b is the buoyant force. By expanding the forces,

$$m_s g = m_m g + \rho_{\mathsf{N}_2}(T) V_s g. \tag{A.3}$$

where the subscript N_2 notes the properties of the purge gas. Note that the density of the fluid is temperature dependent. The volume of the sample is equal to $V_s = m_s/\rho_s$. Substitution and division by the gravitational acceleration yields

$$m_s = m_m + m_s \frac{\rho_{\mathsf{N}_2}(T)}{\rho_s}. \tag{A.4}$$

The density of the samples could also be considered temperature dependent, however, this relation is not known and not expected to have much influence on liquids. Continue by gathering the terms for the real mass,

$$m_s \left(1 - \frac{\rho_{\mathsf{N}_2}(T)}{\rho_s}\right) = m_m, \tag{A.5}$$

and then isolating the real mass,

$$m_s = \frac{m_m}{\left(1 - \frac{\rho_{\mathsf{N}_2}(T)}{\rho_s}\right)}, \tag{A.6}$$

the measured mass is corrected. The function describing the changing density of the fluid is made using the ideal gas law. The ideal gas law becomes:

$$p_\infty V = \frac{m_{\mathsf{N}_2}}{M_{\mathsf{N}_2}} RT. \tag{A.7}$$

The atmospheric pressure is denoted by p_∞, as the gas pressure inside the TGA crucible is approximately that of the atmosphere. Rewriting to yield the density results in

$$\frac{m}{V} = \rho_{\mathsf{N}_2}(T) = \frac{p_\infty M_{\mathsf{N}_2}}{RT}. \tag{A.8}$$

Equation A.8 is combined with Equation A.6 to find the true mass of the sample.

A.2.2 Non-isothermal evaporation

This analysis will be primarily based on those non-isothermal thermogravimetric analyses by Dollimore et al. [51], Chatterjee et al. [52] and Smook et al. [53]. These analyses start by defining the mass fraction evaporated

$$\alpha = \frac{m_i - m(t)}{m_i - m_f}, \tag{A.9}$$

where m_i is the initial mass and m_f the final mass. The rate of evaporation is equal to

$$\frac{d\alpha}{dt} = k(T)f(\alpha) \tag{A.10}$$

where $k(T)$ is the temperature dependent reaction rate and $f(\alpha)$ the conversion function, which is determined by the mechanics of the function. Evaporation behaves as a first-order reaction, meaning $f(\alpha) = 1 - \alpha$ [52]. As the temperature is the main drive behind the mass change, one can rewrite the reaction rate as a function of temperature:

$$\frac{d\alpha}{dT} = \frac{d\alpha}{dt}\frac{dt}{dT} = \frac{1}{\dot{T}}\frac{d\alpha}{dt}. \tag{A.11}$$

Note that $(dt/dT) = (dT/dt)^{-1}$, in other words, the inverse of the heating rate. This can be denoted by $\dot{T}$. The heating rate remains constant throughout the experiment. Substituting the heating rate and Equation A.10 into Equation A.11 yields

$$\frac{d\alpha}{dT} = \frac{k(T)f(\alpha)}{\dot{T}} \tag{A.12}$$

Rewriting to yield the reaction rate yields

$$k(T) = \frac{\dot{T}}{f(\alpha)}\frac{d\alpha}{dT} \tag{A.13}$$

and substituting $f(\alpha) = 1 - \alpha$ results in

$$k(T) = \frac{\dot{T}}{1-\alpha}\frac{d\alpha}{dT} \tag{A.14}$$

Considering the reaction rate, the coefficient of evaporation characterises the rate of evaporation [54]. Furthermore, evaporation is commonly thought of as having an Arrhenius relation with temperature [23, 52]. Therefore, considering that the coefficient of evaporation is

$$k(T) = \sigma_{vap}(T) = A_{Arr}e^{-\frac{E_a}{R_sT}}. \tag{A.15}$$

Recall that for evaporation, the activation energy is the latent heat of evaporation, i.e. $E_a = L$ [23, 52]. This results in

$$\sigma_{vap}(T) = A_{Arr}e^{-\frac{L}{R_sT}} \tag{A.16}$$

and taking the natural logarithm results in

$$\ln \sigma_{vap}(T) = \ln A_{Arr} - \frac{L}{R_sT}. \tag{A.17}$$

By substituting Equation A.14 one gets a way of calculating the latent heat of evaporation

$$\ln\left(\frac{\dot{T}}{(1-\alpha)}\frac{d\alpha}{dT}\right) = \ln A_{Arr} - \frac{L}{R_sT} \tag{A.18}$$

R_s is the specific gas constant for base oil vapour, equal to the universal gas constant divided by the molecular mass. However, the molecular weights of Li/M, Li/SS and PU/E could not be measured. Instead, a value is estimated from literature.

Sarowha found molecular weights between 221 (for HSD gas oil) to 582 (for Brightsstock lube oil) [56]. The same study describes 314 g/mol to 360 g/mol as the range in which the average molecular weight of lubricating oils reside. It was also found that the source for lubricating oils is made from crude oil with fractions in the range of C_{18}-C_{30} [57]. This would correspond to heavy neutral feed to Brightsstock lube oil, the weight of these greases are on average 397 g/mol.

Appendix B

A comparison of different ways of modelling entropy

B.1 The various ways of calculating system properties

The calculation of grease temperature and entropy is based on a few assumptions. The strongest assumptions are the interpolation functions for the mass and specific heat capacity and the temperature dependent thermal resistance. To check the validity of these assumptions and explore the other options, the entropy generated is compared for various types of interpolation functions thermal resistances.

B.1.1 Linear interpolation of material properties

Material properties are linearly interpolated based on the measured values. Consider the time points of the ageing interval t, where the samples were retrieved from the oven. Each time point has a measured value of the specific heat capacity c and mass m associated with it.

Consider the following vectors, where the subscript denotes the age in days (where 0 refers to fresh properties):

$$t = \begin{bmatrix} t_0 & t_{10} & t_{20} & t_{30} \end{bmatrix}, \tag{B.1}$$

$$c = \begin{bmatrix} c_0 & c_{10} & c_{20} & c_{30} \end{bmatrix}, \tag{B.2}$$

$$m = \begin{bmatrix} m_0 & m_{10} & m_{20} & m_{30} \end{bmatrix}. \tag{B.3}$$

For each interval, an interpolation function is made to run between values at the start and end. This yields the following piece-wise function for the heat capacity

$$c(t) = \begin{cases} c_0 + \frac{c_{10}-c_0}{t_{10}-t_0}(t-t_0) & t : [t_0, t_{10}\rangle \\ c_{10} + \frac{c_{20}-c_{10}}{t_{20}-t_{10}}(t-t_{10}) & t : [t_{10}, t_{20}\rangle \\ c_{20} + \frac{c_{30}-c_{20}}{t_{30}-t_{20}}(t-t_{20}) & t : [t_{20}, t_{30}] \end{cases} \tag{B.4}$$

and for the mass

$$m(t) = \begin{cases} m_0 + \frac{m_{10}-m_0}{t_{10}-t_0}(t-t_0) & t : [t_0, t_{10}\rangle \\ m_{10} + \frac{m_{20}-m_{10}}{t_{20}-t_{10}}(t-t_{10}) & t : [t_{10}, t_{20}\rangle \\ m_{20} + \frac{m_{30}-m_{20}}{t_{30}-t_{20}}(t-t_{20}) & t : [t_{20}, t_{30}] \end{cases} \tag{B.5}$$

respectively. The mass change rate is the derivative of the mass, $\dot{m} = dm/dt$. The mass change rate is then defined as

$$\dot{m}(t) = \begin{cases} \frac{m_{10}-m_0}{t_{10}-t_0} & t : [t_0, t_{10}\rangle \\ \frac{m_{20}-m_{10}}{t_{20}-t_{10}} & t : [t_{10}, t_{20}\rangle \\ \frac{m_{30}-m_{20}}{t_{30}-t_{20}} & t : [t_{20}, t_{30}] \end{cases} \tag{B.6}$$

For all these functions holds that they are defined for $t : [t_0, t_{30}]$.

B.1.2 Non-linear interpolation

Non-linear interpolation employs other methods to interpolate system properties over time. For the heat capacity, an interpolation function is built using Matlab's [49] `makima` with

$$t = \begin{bmatrix} t_0 & t_{10} & t_{20} & t_{30} \end{bmatrix}, \tag{B.7}$$

$$c = \begin{bmatrix} c_0 & c_{10} & c_{20} & c_{30} \end{bmatrix}, \tag{B.8}$$

$$\tag{B.9}$$

as control points. These vectors denote the measured system properties, where the subscript denotes the age in days (and 0 refers to fresh properties).

The evolution of mass is modelled using a generalised logistics curve, based on the work by Tarrío-Saavedra et al. [58]:

$$\alpha(t) = \frac{1}{\left(1 + \tau e^{-\kappa(t+t_0)}\right)^{1/\tau}}, \tag{B.10}$$

where α is the fraction reacted or evaporated. Its time derivative is

$$\frac{d\alpha}{dt} = \frac{be^{-\kappa(t+t_0)}}{\left(1 + \tau e^{-\kappa(t+t_0)}\right)^{1/\tau+1}}. \tag{B.11}$$

This allows the mass to be obtained by

$$m(t) = m_i - (m_i - m_f)\alpha(t) \tag{B.12}$$

and the mass loss rate is then

$$\frac{dm}{dt}(t) = -(m_i - m_f)\frac{d\alpha}{dt}(t). \tag{B.13}$$

Here, m_i is the initial mass and m_f is the final mass. Matlab's [49] `fit` function is used to fit Equation B.10 to the measured data t and m.

B.1.3 Thermal resistance

Thermal resistance is progressively calculated when modelling the grease temperature in the oven. For every time step, a new thermal resistance is calculated based on the grease temperature and oven temperature.

For the case a constant mean value is used, the thermal resistance is evaluated centred at the average temperature of the oven, which is 405.51 K. A range of 2 degrees of variation is taken around this temperature. By taking the mean value of this surface, a thermal resistance of 68.0 K/W. The surface in question can be found in Figure B.2.

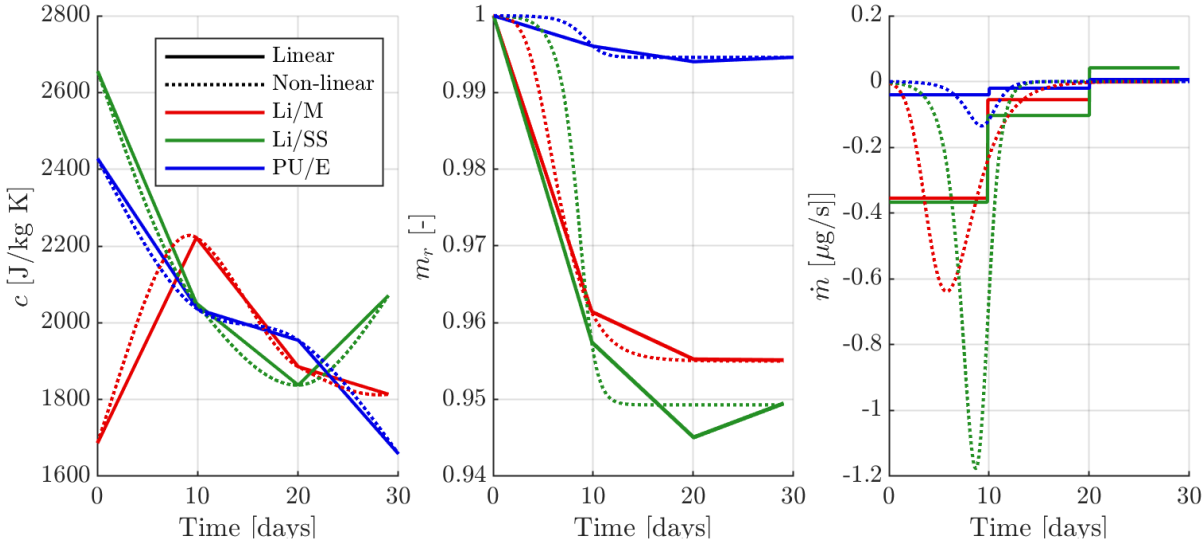

Figure B.1: The two ways the specific heat capacity, mass and mass change rate are interpolated, shown for Li/SS.

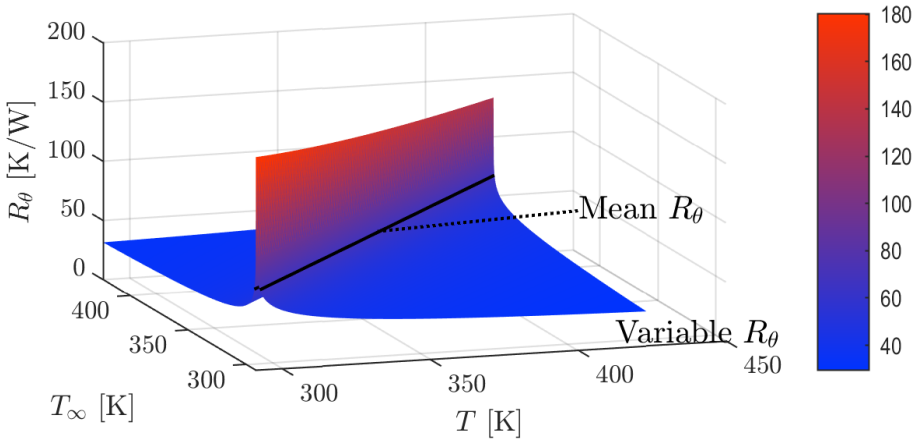

Figure B.2: Caption

Table B.1: The table containing the two-letter code representing each model setup. The first letter determines whether the material properties interpolation is linear or non-linear. The second letter represents whether the thermal resistance is either variable or constant.

Model	Interpolation	Thermal resistance
LC	Linear	Constant mean value
LV	Linear	Variable
NC	Non-linear	Constant mean value
NV	Non-linear	Variable

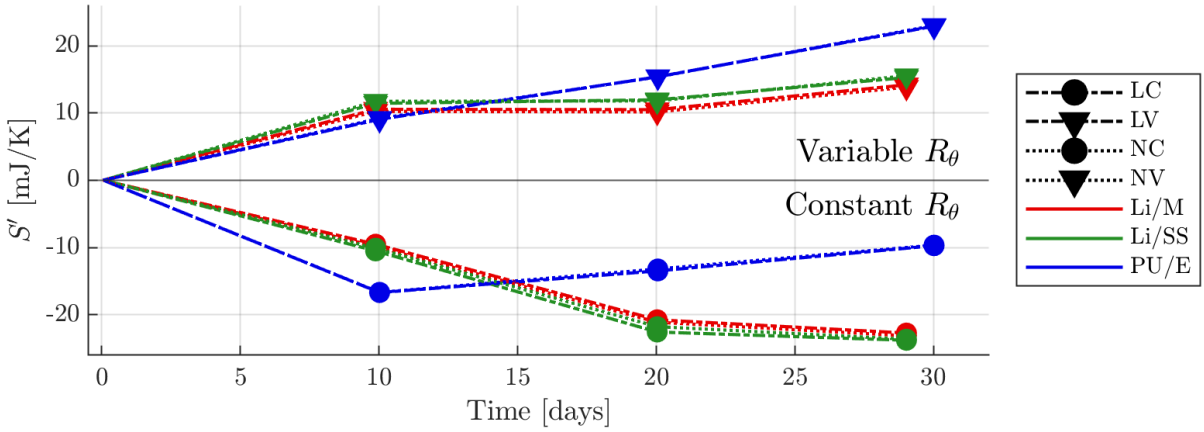

Figure B.3: The total generated entropy by the models. There is a clear distinction between the models with variable and constant thermal resistance. The former result in a positive entropy generation, while the latter results in a negative entropy generation.

B.2 Comparing system properties

The important details of each model are mentioned in Table B.1. The same script is now run, with the different combinations of material properties and thermal resistances.

B.3 Comparing the resulting entropy calculations

The entropy is then calculated for all cases. A short overview of the various cases is given in Table B.1. Figure B.3 shows the calculated entropy generation per model.

The best point of comparison for all these models is the total entropy generated, as the behaviour is the most defining and the most important for its use in the rest of this study. For an ageing procedure of sufficient length, one can expect the following:

1. Greases undergoing the same external conditions should experience approximately the same entropy generation.

2. The entropy generation should be positive and increasing as a trend.

Measuring the curves of Figure B.3 to these expectations, both the LV and NV model behave as expected. The models with constant thermal resistance perform poorly. Those models are LC and NC. It is concluded that either LV or NV models can be used, as they are consistent and increasing. When choosing either one of those models, a preference is given for the NV model (non-linear interpolation and variable thermal resistance) as smooth functions are expected to better model the material behaviour than piece-wise linear functions.

Appendix C

Tabulated values

This appendix chapter contains the tabulated values for:

- Table C.1: The experimentally determined degradation measures..
- Table C.2: The calculated discrete entropies.
- Table C.3: The degradation coefficients.

Table C.1: The degradation measures of Li/M, Li/SS and PU/E, measured over the ageing intervals.

		Li/M				
Age	Time	d_b [mm]	c [J/kgK]	G' [kPa]	α_γ [kK]	τ_y [Pa]
0 days	t_0	30.72	1684	57.48	1.372	51.59
10 days	t_{10}	30.22	2222	58.38	1.567	48.86
20 days	t_{20}	30.96	1885	51.61	2.248	65.55
30 days	t_{30}	30.22	1814	55.43	1.409	69.16
		Li/SS				
Age	Time	d_b [mm]	c [J/kgK]	G' [kPa]	α_γ [kK]	τ_y [Pa]
0 days	t_0	35.73	2658	55.07	0.6501	53.07
10 days	t_{10}	34.21	2051	61.84	0.6639	164.8
20 days	t_{20}	34.97	1837	82.92	0.6479	172.2
30 days	t_{30}	35.47	2071	86.05	0.5871	147.0
		PU/E				
Age	Time	d_b [mm]	c [J/kgK]	G' [kPa]	α_γ [kK]	τ_y [Pa]
0 days	t_0	22.98	2429	46.46	1.043	45.90
10 days	t_{10}	22.98	2035	151.8	0.5765	283.0
20 days	t_{20}	23.48	1954	46.06	0.6348	214.6
30 days	t_{30}	25.48	1658	53.06	0.8630	287.6

Table C.2: The discrete entropies of Li/M, Li/SS and PU/E: the heat storage entropy (S_T), heat transfer entropy (S_Q), evaporation entropy (S_m) and the generated entropy (S').

		Li/M			
Age	Time	S_T [mJ/K]	S_Q [mJ/K]	S_m [mJ/K]	S' [mJ/K]
0 days	t_0	0.0	0.0	0.0	0.0
10 days	t_{10}	65.48	−170.3	115.0	10.24
20 days	t_{20}	85.48	−208.7	133.5	10.16
30 days	t_{30}	65.87	−185.8	133.7	13.84
		Li/SS			
Age	Time	S_T [mJ/K]	S_Q [mJ/K]	S_m [mJ/K]	S' [mJ/K]
0 days	t_0	0.0	0.0	0.0	0.0
10 days	t_{10}	74.19	−162.0	99.52	11.74
20 days	t_{20}	91.35	−197.5	118.0	11.80
30 days	t_{30}	69.18	−171.6	118.0	15.54
		PU/E			
Age	Time	S_T [mJ/K]	S_Q [mJ/K]	S_m [mJ/K]	S' [mJ/K]
0 days	t_0	0.0	0.0	0.0	0.0
10 days	t_{10}	141.5	−161.4	29.10	9.199
20 days	t_{20}	100.4	−124.7	39.59	15.36
30 days	t_{30}	73.06	−89.66	39.59	23.00

Table C.3: The degradation coefficients, calculated according to the method outlined in Chapter 2. The columns show the degradation coefficients of each degradation mechanism: B_T for heat storage, B_Q for heat flux and B_m for evaporation. The rows show the degradation measure these three coefficients belong to: bleed capacity measure (d_b), specific heat capacity (c), storage modulus (G'), thermal strain coefficient (α_γ) or yield stress (τ_y).

Degradation		Li/M		
measures	Unit	B_T	B_Q	B_m
d_b	[Km/J]	22.5	18.9	15.2
c	[1/kg]	$-2.20 \cdot 10^7$	$-1.85 \cdot 10^7$	$-1.49 \cdot 10^7$
G'	[K/m^3]	$-2.44 \cdot 10^8$	$-2.06 \cdot 10^8$	$-1.65 \cdot 10^8$
α_γ	[1/J]	12.0	10.1	8.07
τ_y	[K/m^3]	$9.05 \cdot 10^5$	$7.63 \cdot 10^5$	$6.14 \cdot 10^5$
Degradation		Li/SS		
measures	Unit	B_T	B_Q	B_m
d_b	[Km/J]	−0.870	−0.725	−0.547
c	[1/kg]	$3.86 \cdot 10^4$	$4.20 \cdot 10^4$	$3.35 \cdot 10^4$
G'	[K/m^3]	$-1.56 \cdot 10^7$	$-1.32 \cdot 10^7$	$-9.82 \cdot 10^6$
α_γ	[1/J]	$2.38 \cdot 10^{-2}$	$1.80 \cdot 10^{-2}$	$1.17 \cdot 10^{-2}$
τ_y	[K/m^3]	$1.41 \cdot 10^4$	$1.11 \cdot 10^4$	$8.66 \cdot 10^3$
Degradation		PU/E		
measures	Unit	B_T	B_Q	B_m
d_b	[Km/J]	0.276	0.273	0.172
c	[1/kg]	$-4.83 \cdot 10^4$	$-4.62 \cdot 10^4$	$-3.50 \cdot 10^4$
G'	[K/m^3]	$9.10 \cdot 10^6$	$7.31 \cdot 10^6$	$-6.45 \cdot 10^4$
α_γ	[1/J]	$2.20 \cdot 10^{-2}$	$2.37 \cdot 10^{-2}$	$8.58 \cdot 10^{-3}$
τ_y	[K/m^3]	$1.97 \cdot 10^4$	$1.75 \cdot 10^4$	$9.35 \cdot 10^3$